Biomarker discovery and drug testing in Idiopathic Pulmonary Fibrosis

Isis Enlil Fernandez Buelvas

2018

Aus dem Comprehensive Pneumology Center / Institut für Experimentelle Pneumologie der Ludwig-Maximilians-Universität München

komm. Interim Direktorin und Direktor: Dr.rer.nat. Antje Brand, PD Dr.med. Anne Hilgendorff, Dr.vet.med. Ali Önder Yildirim

Biomarker discovery and drug testing in Idiopathic Pulmonary Fibrosis

Dissertation

zum Erwerb des Doctor of Philosophy (Ph.D.)

an der Medizinischen Fakultät der Ludwig-Maximilians-Universität München

vorgelegt von

Isis Enlil Fernandez Buelvas

aus Cartagena, Colombia

München

2018

Mit Genehmigung der Medizinischen Fakultät der Ludwig-Maximilians-Universität München

Berichterstatter:

Prof. Dr.med. Oliver Eickelberg

Mitberichterstatter:

Prof. Dr.med. Jürgen Behr

Dekan:

Prof. Dr. dent. med. Reinhard Hickel

Tag der mündlichen Prüfung:

27.11.2018

Eidesstattliche Versicherung

Ich, Isis Enlil Fernandez Buelvas, erkläre hiermit an Eides statt, dass ich die vorliegende Dissertation mit dem Thema

„Biomarker discovery and drug testing in Idiopathic Pulmonary Fibrosis“

selbstständig verfasst, mich außer der angegebenen keiner weiteren Hilfsmittel bedient und alle Erkenntnisse, die aus dem Schrifttum ganz oder annähernd übernommen sind, als solche kenntlich gemacht und nach ihrer Herkunft unter Bezeichnung der Fundstelle einzeln nachgewiesen habe.

Ich erkläre des Weiteren, dass die hier vorgelegte Dissertation nicht in gleicher oder in ähnlicher Form bei einer anderen Stelle zur Erlangung eines akademischen Grades eingereicht wurde.

München, 10.12.18	Isis E. Fernandez
Ort, Datum	Unterschrift

Table of contents

List of Abbreviations

α-SMA	α-smooth muscle actin
ABCA-3	ATP-binding cassette sub-family A member 3
ASCEND IPF	Assessment of Pirfenidone to Confirm Efficacy and Safety in
BALF	Broncho-alveolar lavage fluid
CAPACITY	Clinical Studies Assessing Pirfenidone in IPF: Research of Efficacy and Safety Outcomes
CCL18	Chemokine (C-C motif) ligand 18
DPLP	Diffuse parenchymal lung disease
DLco	Diffusing capacity of the lung for carbon monoxide
DNA	Deoxyribonucleic acid
ECM	Extracellular matrix
FTICR	Fourier-Transform Ion Cyclotron Resonance
FVC	Forced vital capacity
GWAS	Genome-wide association studies
HRCT	High resolution computed tomography
ICAM1	Intercellular cell adhesion molecule 1
IIP	Idiopathic interstitial pneumonia

ILA	Interstitial lung abnormalities
IPF	Idiopathic pulmonary fibrosis
KL-6	Krebs von den Lungen-6
MALDI	Matrix-assisted laser desorption/ionization
MMP7	Matrix metalloproteinase 7
MUC5B	Mucin 5B
MSI	Mass spectrometry imaging
PANTHER-IPF	Prednisone, Azathioprine, and N-Acetylcysteine: A Study That Evaluates Response in Idiopathic Pulmonary Fibrosis
SNP	Single-nucleotide polymorphisms
SP-A	Surfactant protein A
SP-D	Surfactant protein D
TCL	Total lung capacity
TGF-β	Transforming growth factor beta
TOLLIP	Toll-interacting protein
UIP	Usual interstitial pneumonia

Publications included in this thesis

Peer-reviewed publications

Systematic phenotyping and correlation of biomarkers with lung function and histology in lung fibrosis

Fernandez IE, Amarie OV, Mutze K, Königshoff M, Yildirim AÖ, Eickelberg O. Am J Physiol Lung Cell Mol Physiol 2016 May 15;310(10):L919-27.

Pharmacokinetic and pharmacometabolomic study of pirfenidone in normal mouse tissues using high mass resolution MALDI-FTICR-mass spectrometry imaging

Sun N, Fernandez IE, Wei M, Wu Y, Aichler M, Eickelberg O, Walch A. Histochem Cell Biol. 2016 Feb;145(2):201-11.

Publications not included in this thesis

Peer-reviewed publications

Pharmacometabolic response to pirfenidone in pulmonary fibrosis detected by MALDI-FTICR-MSI

Sun N*, Fernandez IE*, Wei M, Witting M, Aichler M, Feuchtinger A, Burgstaller G, Verleden SE, Schmitt-Kopplin P, Eickelberg O, Walch A. Eur Respir J. 2018 Aug 2. pii: 1702314. doi: 10.1183/13993003.02314-2017. [Epub ahead of print]

Time- and compartment-resolved proteome profiling of the extracellular niche in lung injury and repair

Schiller HB, Fernandez IE, Burgstaller G, Schaab C, Scheltema RA, Schwarzmayr T, Strom TM, Eickelberg O, Mann M. Mol Syst Biol. 2015 Jul 14;11(7):819.

New cellular and molecular mechanisms of lung injury and fibrosis in idiopathic pulmonary fibrosis

Fernandez IE, Eickelberg O. Lancet. 2012 Aug 18;380(9842):680-8.

The impact of TGF-β on lung fibrosis: from targeting to biomarkers

Fernandez IE, Eickelberg O. Proc Am Thorac Soc. 2012 Jul;9(3):111-6.

Summary

Idiopathic pulmonary fibrosis (IPF) is a devastating and lethal disease, with a median survival of 2-3 years after diagnosis. It is chronic, progressive and occurs predominantly in middle-age and older adults. Multiple working hypotheses speak of possible triggers of IPF development, e.g. multiple microinjuries of the alveolar epithelium, aberrant fibroblast activation, and immune deregulation. Currently, there are two drugs approved for the treatment of mild-to-moderate IPF worldwide, neither Pirfenidone or Nintedanib provide a definitive cure for disease, but slow in disease progression. Thus, animal models of pulmonary fibrosis are a critical tool for disease understanding, drug development and pre-clinical intervention.

In **chapter 2.1**, the first study included in this thesis (Fernandez et al., 2016a), we comprehensively analyzed IPF-relevant peripheral biomarkers, histological compromise along with physiological parameters, to determine disease onset, progression and resolution in preclinical models of fibrosis. We observed and validated that the bleomycin-induced pulmonary fibrosis model reached its peak of fibrosis 14 days after treatment and from there on, resolution started. Furthermore, we created a semi-automatized histologic scoring system to quantify the degree of fibrosis, and correlated histology score with lung function decline during the initiation, peak and resolution phase of the model. Interestingly, we observed that at day 28 and 56 although histological compromise was still present, lung function was close to normal. Furthermore, we determine that plasma levels of ICAM-1 strongly correlate with the extent of fibrosis. We complemented and extended our characterization of the model further. In a following study, we performed multi-compartmental deep

proteomics in lung tissue and bronchoalveolar lavage (Schiller, Fernandez et al., 2015), with emphasis on characterizing the matrisome, from the initiation to the resolution of bleomycin-induced fibrosis, in where we could determine the initial signatures of injury, as well as the ones that drive lung repair.

In **chapter 2.2**, we highlighted the second study of this thesis (Sun et al., 2015), that goes along with a complementary publication of our authorship. We use the ability of matrix-assisted laser desorption/ionization mass spectrometry imaging (MALDI-MSI) to simultaneously record the distribution of hundreds of molecules, in a highly multiplexed and unbiased manner. After oral administration of pirfenidone, we could detect, visualize, and quantify the pharmacokinetics and in-situ distribution of pirfenidone in lung, liver and kidney from unchallenged mice. Furthermore, we performed analysis in fibrotic mice and IPF patients, untreated and under pirfenidone therapy (Sun*, Fernandez* et al. 2018). As expected, we detected mouse and human specific and shared responses; specific alterations of metabolite pathways in fibrosis, and most importantly, metabolic recalibration following pirfenidone treatment. Taking together, bleomycin-induced pulmonary fibrosis is an extremely valuable tool for preclinical drugs evaluation, as well as for target validation and modulation of Idiopathic Pulmonary Fibrosis.

Zusammenfassung

Die idiopathische pulmonale Fibrose ist eine schwerwiegende und tödlich verlaufende Erkrankung mit einer durchschnittlichen Lebenserwartung von zwei bis drei Jahren nach Diagnosestellung. Die chronisch progressive Erkrankung tritt vorwiegend im mittleren Lebensalter sowie bei älteren Erwachsenen auf. Zahlreiche Arbeitshypothesen zeigten mögliche Auslöser der IPF auf, wie beispielsweise Mikroverletzungen des Alveolarepithels, eine gestörte Fibroblastenaktivierung sowie eine Fehlregulation des Immunsystems. Derzeit sind weltweit zwei Medikamente zur Behandlung von leichter bis mittelschwerer IPF zugelassen, Pirfenidon und Nintedanib. Beide Medikamente verlangsamen den Verlauf der Erkrankung führen jedoch zu keiner Heilung. Somit sind Tiermodelle der Lungenfibrose ein wichtiges Werkzeug für das Verständnis von Krankheiten, die Arzneimittelentwicklung und präklinische Intervention.

Kapitel 2.1 fasst die erste Publikation dieser Arbeit zusammen. In Fernandez et al. 2016 analysierten wir IPF-relevante periphere Biomarker und führten einen histologischen Vergleich mit physiologischen Parametern durch, um die Entstehung der Erkrankung, den Verlauf und die Resolution in präklinischen Modellen der Fibrose zu bestimmen. Unsere Ergebnisse zeigten, dass die Fibrose im bleomycininduzierten Modell der Fibrose ihren Höhepunkt an Tag 14 nach Belomycinbehandlung erreichte und danach die Phase der Resolution begann. Wir generierten ein semi-automatisiertes histologisches Bewertungssystem um den Grad der Fibrose zu quantifizieren und korrelierten diesen Wert mit der Abnahme der Lungenfunktion während der Initiierungsphase, der maximalen Fibrose und der Resolutionsphase des Models.

Interessanterweise beobachteten wir an Tag 28 und 56 eine nahezu normale Lungenfunktion, obwohl histologische Auffälligkeiten noch immer vorhanden waren. Wir entdeckten, dass die Plasmaspiegel von ICAM-1 stark mit dem Fibrosegrad korrelierten. Wir erweiterten die Charakterisierung des Fibrosemodells und schlossen eine weitere Studie an, in der wir eine multi-kompartmentelle tiefgehende Proteomanalyse von Lungengewebe und bronchoalveolären Lavagen durchführten. Der Fokus lag dabei auf der Charakterisierung des Matrisoms von der Initiierungs- bis zur Resolutionsphase der bleomycininduzierten Fibrose. Wir konnten die anfänglichen Signaturen der Verletzung bestimmen, sowie diejenigen, die die Lungenreparatur antreiben

Kapitel 2.2 hebt die zweite Publikation der vorliegenden Arbeit hervor, Sun et al., 2015, der eine Koautorenschaft zugrunde liegt. Hierbei nutzten wir die Methode der Matrix–Assistierten Laser–Desorptions/Ionisierungs Massenspektrometrie Bildgebung (Imaging) (MALDI-MSI), welche es ermöglicht in einem multiplexen und ungezielten Ansatz simultan die Verteilung hunderter Moleküle zu messen. Nach oraler Gabe von Pirfenidon, visualisierten und quantifizierten wir die gemessene Pharmakokinetik und in situ Verteilung von Pirfenidon in Lunge, Leber und Niere von gesunden Mäusen. Zusätzlich analysierten wir fibrotische Mäuse und IPF-Patienten, unbehandelt als auch unter Pirfenidontherapie (Sun*, Fernandez* et al. 2018). Wie erwartet entdeckten wir sowohl maus- und menschspezifische als auch gemeinsame Reaktionen, bezüglich spezifischer Änderungen metabolischer Prozesse in Fibrose und, von besonderer Bedeutung, der metabolischen Neukalibrierung nach Pirfenidonbehandlung. Zusammengefasst ist das Tiermodell der bleomycininduzierten pulmonalen Fibrose ein wichtiges Werkzeug für die präklinische Arzneimittelbewertung, sowie für die Validierung potentieller Zielmoleküle und einer Modulation der idiopathischen pulmonalen Fibrose.

1. Introduction

1.1. Idiopathic pulmonary fibrosis

"IPF is defined as a specific form of chronic, progressive fibrosing interstitial pneumonia of unknown cause, occurring primarily in older adults, limited to the lungs, and associated with the histopathologic and/or radiologic pattern of UIP."

Definition by the Official ATS/ERS/JRS/ALAT Statement on Idiopathic Pulmonary Fibrosis (Raghu et al., 2011).

1.1.1. Definition, epidemiology and clinical phenotypes

Diffuse parenchymal lung diseases (DPLP) are a diverse group of clinical entities, where reversible or irreversible scaring and interstitial fibrosis of the lungs occur. So far, more than 150 causes of DPLD are recognized. For the majority of patients it is possible to identify a cause e.g. mold, bird exposure, or an underlying autoimmune disease. However, when no cause is identified, is considered as idiopathic interstitial pneumonia (IIP). Idiopathic pulmonary fibrosis (IPF) is the most common (55%) of all idiopathic interstitial pneumonias (Travis et al., 2013).

Idiopathic pulmonary fibrosis is an orphan disease that affects subjects globally, even though its incidence varies among populations (Hutchinson et al., 2015). In Europe and North America, it is estimated conservatively around 3-9 per 100 000 per year (Raghu et al., 2006). More specifically, Raghu et al. reported in US incidence according to broad or narrow diagnostic criteria adjusted by age of 16.3, and 6.8 per 100 000 respectively. In another later study, Raghu et al.

reported an incidence up to 93.7 per 100 000 in people 65 years old or older (Raghu et al., 2014). While in Asia and South America (Brazil) IPF incidence is reported around 1.2 to 4 and 0.26 to 0.48 per 100 000 per year, respectively (Hutchinson et al., 2015). Regarding prevalence, the variability across populations persists. In North America, the estimated prevalence per 100 000 of the population for all genders fluctuates between 14.0 and 63.0 depending study, narrow or broad criteria. In Europe, it fluctuates between 1.25 and 23.4 per 100 000 (Nalysnyk et al., 2012). In several studies in North America and Europe, prevalence is reported to be increasing. Yet, is unclear whether this phenomenon is due to a true increase in incidence or to an increase in disease detection.

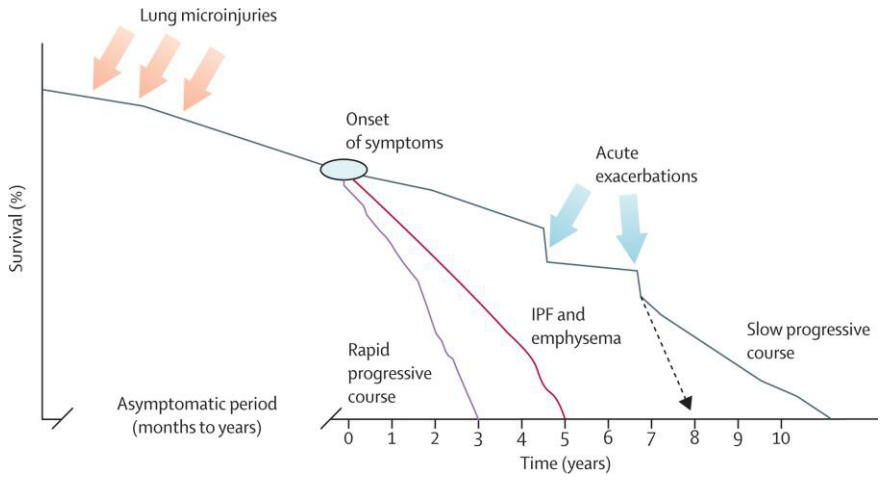

Figure 1. Heterogeneity of the natural history and clinical sub-phenotypes of IPF patients. Previous microinjuries during the asymptomatic period, contribute to disease development. At time of diagnosis and "onset of symptoms" IPF patients can take different clinical trajectories, either "rapid progressor", "slow progressor" (Taken and adapted from King et al., 2011)

IPF has a predilection for middle-aged and older subjects, largely males. The natural history of IPF is progressive, pernicious, and unpredictable with eventual death (Figure 1). It is reported that patients are diagnosed between 6 to 24 months after initiation of symptoms. When diagnosed, prognosis is uncertain and there are several clinical sub phenotypes that have being described. Some

patients have a rapid deterioration with a poor short-term prognosis, so called “rapid progressors”. Others present a slow deterioration with multiple acute exacerbation episodes, characterized by respiratory worsening, fever and infections-like symptoms due to unrecognized reasons that shorten their life expectancy (Figure 2), called “slow progressors”. And others present steady disease deterioration over years, called “stable” (Raghu et al., 2011) (King et al., 2011). Based on that, median survival is estimated 3 to 5 years from diagnosis. This estimation is based on studies performed previous to approval of currently used therapies; therefore it might not reflect the present scenario.

1.1.2. Pathobiological features

1.1.1.1. Pathophysiology, molecular features and current hypothesis

The direct cause of IPF is unknown. Subjects with genetic susceptibility and life-long exposure to risk factors that develop disease account for up to a third of all patients. To date, while the key initiating triggers are unidentified, it is known is that pulmonary fibrosis develops as an abnormal response to various lung insults, triggering aberrant wound-healing, epithelial apoptosis and senescence, uncontrolled fibroblast proliferation and activation, excessive extracellular matrix deposition, and a fibrotic-related immune reaction. Several environmental risk factors and life-long exposures contribute to initiate microinjuries in the lung. These include familial susceptibility (Kropski et al., 2015; Nogee et al., 2001), cigarette smoking (Baumgartner et al., 1997), environmental exposures (Baumgartner et al., 2000), chronic silent micro aspiration (Lee, 2014), chronic viral infection (Arase et al., 2008), mainly herpes virus infection (Lawson et al., 2008; Tang et al., 2003), among others.

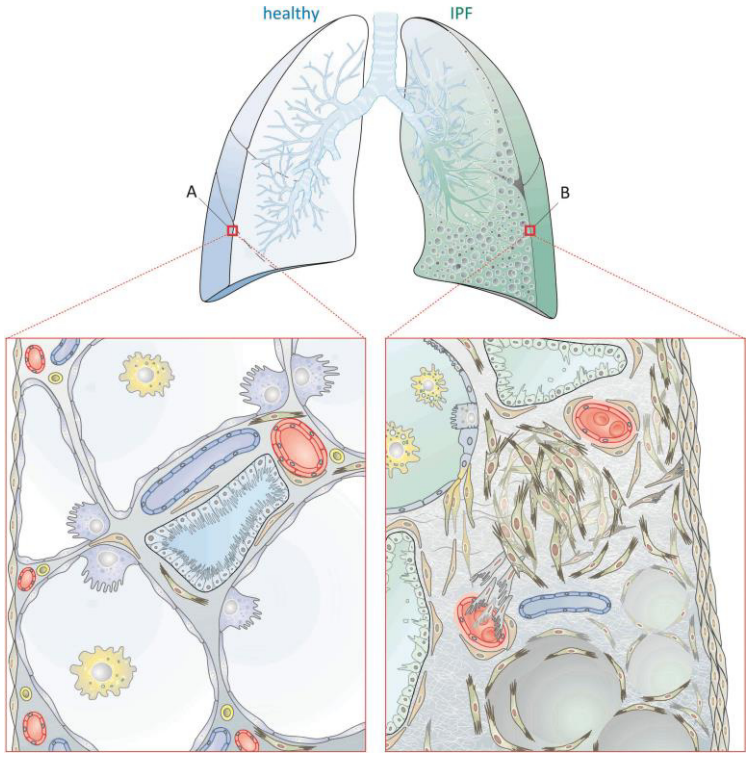

Figure 2. Lesions in idiopathic pulmonary fibrosis. A) Normal lung appearance, with functional alveoli. B) Basal, subpleural disease distribution in with altered architecture; injured apoptotic epithelium with fibroblastic foci accumulation in the lung parenchyma (Taken from Fernandez I.E. et al 2012).

IPF is a highly complex molecular disorder, where multiple lung structural players e.g. epithelial cells, fibroblast, mesenchymal cells together with innate and adaptive immune cells, interplay to impair organ function, enhance ECM deposition, and ultimately destroy the lung architecture. The epithelium and fibroblast have being the more extensively studied compartments in IPF.

The alveolar epithelium is the first barrier line of the lung; as such it receives at first hand the noxious impacts of the environment. Providing first-defense against infections (e.g. bacterial and viral), foreign particles, etc. and by itself, is able to orchestrate the initiation of innate and adaptive immune responses (Camelo et al., 2014). In biopsies from IPF patients, the alveolar epithelium is described as aberrant and hyperplastic (Cavazza et al., 2010). Thus, it raised the

hypothesis that during the asymptomatic period, silent microinjuries of the alveolar epithelium might drive disease initiation in susceptible individuals. Among the biological mechanisms in epithelial cells that have being described altered in IPF are unfolded protein response, endoplasmic reticulum stress (Korfei et al., 2008), autophagy (Araya et al., 2013; Patel et al., 2012), senescence (Lehmann et al., 2017), ultimately leading to apoptosis and necroptosis (Lee et al., 2018).

Another crucial finding in IPF histology is the co-localization of areas of hyperplastic and apoptotic alveolar epithelial cells neighboring reticular areas of α-SMA positive myofibroblast, so called “fibroblastic foci”, a pathognomonic IPF lesion (Cool et al., 2006). These findings, along with multiple studies, support that epithelial damage activates fibroblasts, and induces fibroblast differentiation into myofibroblasts (Kendall & Feghali-Bostwick, 2014). Fibroblasts are the main support cell in all connective tissues. For maintaining parenchymal organization, they produce structural ECM proteins as collagens, elastins, laminins, fibronectin, glycosaminoglycans (Kendall & Feghali-Bostwick, 2014). Fibroblast activation is key for homeostatic wound healing processes, and when activation is unrestrained it triggers myofibroblast differentiation, excessive ECM generation and deposition, inflammatory feed-back loops, bi-directional epithelial-fibroblast activation, among other phenomena. Different cell types has been proposed as sources of activated fibroblast in fibrosis (Figure 3), for instance pleural mesothelium, pericytes, resident quiescent fibroblast, fibrocytes, endothelial and epithelial cells, which upon injury would undergo epithelial- or endothelial-to-mesenchymal transition acquire mesenchymal markers, and contribute to the fibroblast pool.

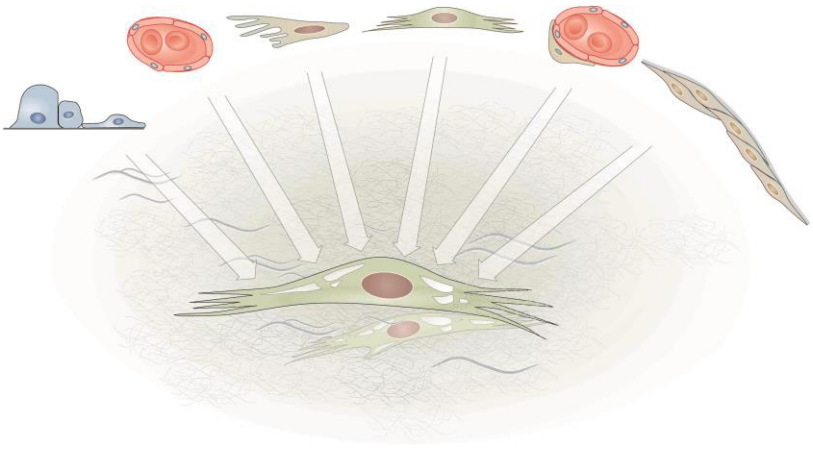

Figure 3. Possible sources of fibroblast in the fibrotic lung. In the top, from left to right: epithelial cells, endothelial cells, fibrocytes, resident fibroblast, pericyte, mesothelial cells (Modified from Fernandez IE. et al, 2012).

Growth factors, cytokines, chemokines and soluble mediators together with central pathway activation are of pivotal importance in IPF. Pathways as WNT (Konigshoff et al., 2009), Sonic Hedgehog (Bolanos et al., 2012) and Notch (Hu et al., 2015), highly active in the developmental embryo get reactivated in highly proliferative diseases, as IPF (Selman et al., 2008). Transforming growth factor-β (TGF-β) is a master regulator and by far one of the most studied growth factors in fibrosis. When activated, TGF-β plays pleiotropic functions like chemotactic and proliferation induction. While is critical for epithelial cells homeostasis, increased levels induce epithelial apoptosis and transformation of fibroblast into myofibroblast (Fernandez & Eickelberg, 2012).

It is now clear that elements of the innate and adaptive immune response participate at several cellular and sub-cellular levels to myofibroblast differentiation and fibrogenesis (Desai et al., 2018). From the adaptive immunity angle, T cell role is complex and subset-dependent. Th1, Th22 and γδ-T (Simonian et al., 2010) cells seem to attenuate lung fibrosis, while Th2 and Th17 (Simonian et al., 2009) cells to promote it. Tregs (Kotsianidis et al., 2009) and Th9 subsets are controversial, and show both anti- and pro-fibrotic effects. From the innate immune cells angle contributions from new players as myeloid

derived suppressor cells (Fernandez et al., 2016b) and ILC2 (Lai et al., 2016), has been proposed, and the widely-studied M2 macrophages and neutrophils are known to enhance pulmonary fibrosis, whereas M1 macrophages show a protective role (Wynn & Vannella, 2016). Fibrocytes represent bone marrow-derived immune cells that migrate to the lung differentiate into myofibroblasts to promote pulmonary fibrosis (Moeller et al., 2009). Altogether, these reports suggest that an immunosuppressive network affect and shift the phenotype and function of immune cells in IPF, suggesting that an immunosuppressive environment operates in the peripheral blood and lungs and might influence disease progression. Indeed, the putative downregulation of protective immune pathways could, at least partially, explain the failure of the PANTHER-IPF clinical trial, in which IPF patients who received immunosuppressive agents had worse outcomes (Idiopathic Pulmonary Fibrosis Clinical Research et al., 2012).

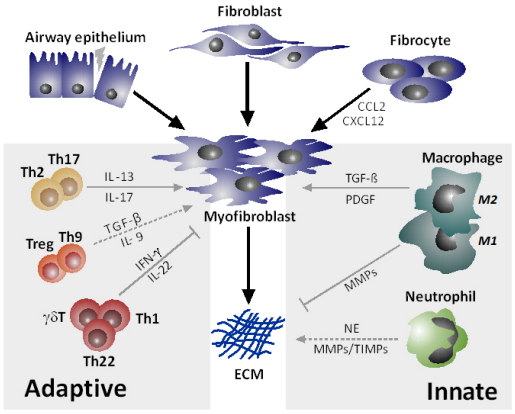

Figure 4. Innate and adaptive immune cells as fibrosis modulators. (Taken from Kolahian S. Et al, 2016)

1.1.1.2. Genetic determinants

Advances in genomic techniques have allowed major progress in unraveling the genetic landscape of IPF patients. Three key genome-wide association studies (GWAS) (Allen et al., 2017; Fingerlin et al., 2013; Noth et al., 2013) identified

single-nucleotide polymorphisms (SNPs) associated with IPF susceptibility, in the Mucin 5B (MUC5B) and toll-interacting protein (TOLLIP). Polymorphism in the promoter region of MUC5B (rs35705950) is associated with a higher likelihood of developing IPF (Peljto et al., 2013). MUC5B is localized in areas of microscopical honeycombing, and honeycomb cysts (Seibold et al., 2011). Although patients carrying this allele have higher risk of disease, they concur with milder course and longer survival. To date, the precise role of MUC5B in the pathophysiology of IPF is unclear.

Variants in TOLLIP are not only associated with susceptibility, but also with treatment responses in IPF. The SNP rs5743890 within TOLLIP gene is associated with increased mortality risk (Noth et al., 2013), and rs3750920 with better response to N-acetylcysteine therapy (Oldham et al., 2015).

Genetic variations also include an autosomal dominance inheritance that lead to familial forms of disease. In IPF telomerase mutations and shortening, show a strong relationship in relatives with Familial IPF. Recently, genetic evaluations of IPF patients and affected relatives, confirmed the relationship with telomerase mutation (Kropski et al., 2017) and shortening (Stuart et al., 2015). Other studies have reported that familial forms are associated with variances of TERT, TERC (hTR), DKC1, TINF2, RTEL1, and PARN, as well as mutations in surfactant proteins SP-A, SP-D, and ABCA3 genes (Epaud et al., 2014; Kropski et al., 2017).

1.1.3. Diagnosis and clinical features

Clinically, patients consult with non-specific symptoms and typically debut with breathlessness on exertion, which can or cannot be accompanied by dry cough. Unless IPF is suspected, this unspecific presentation delays proper and timely diagnosis. At physical examination bibasilar expiratory crackles (rales) are often found (Cottin & Cordier, 2012), together with finger clubbing in about 50% of patients (Kanematsu et al., 1994). On spirometry, a restrictive defect in lung function and abnormal gas exchange are preset. Furthermore, it is characterized

by a reduced forced vital capacity and total lung capacity, and a reduction in diffusing capacity of the lung for carbon monoxide (DLco).

IPF is associated with a specific radiological and/or histopathological pattern of usual interstitial pneumonia (UIP), consider the hallmark of IPF diagnosis. Along with the exclusion of other causes of interstitial fibrosis, e.g. connective tissue disease, adverse effect of medication, granulomatous diseases, among others, the diagnosis is made of combination of clinical diagnostic criteria, high-resolution computed tomography (HRCT) scan, and biopsy (when required), in a multidisciplinary consensus between pulmonologist, radiologist, pathologist, rheumatologist, and in some cases thoracic surgeons.

Radiologically, a HRCT pattern of UIP consists of reticular opacities, traction bronchiectasis and honeycombing, usually bibasilar and subpleural (Figure 5). Other features as reactive mediastinal and linear lymphadenopathy are also present. Ground-glass opacities are not exclusive of a UIP patter, but can be found. Based on radiological evaluation the HRCT can be classified as definite UIP, possible IPF or inconsistent.

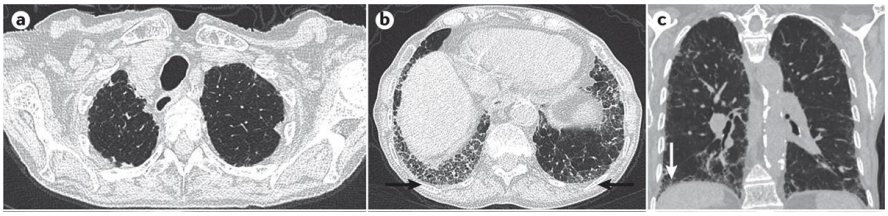

Figure 5. HRCT images from IPF. High-resolution CT (HRCT) images collected from a woman with progressive cough and dyspnea, showing her upper lung zones (panel a), lower lung zones (panel b) and the sagittal plane of the lungs (panel c). These images show lower lobe-predominant peripheral honeycomb change (panels b and c, arrows), which is typical of the usual interstitial pneumonia (UIP) pattern. (Modified from Martinez, F. J. et al. 2017)

Due to increased mortality risk, open lung biopsy is no longer gold standard for IPF diagnosis. However, when imaging is inconclusive, biopsy is recommended. Histologically, a pattern of UIP consist of patchy and heterogeneous distribution, with architectural destruction at low magnification areas, alternating between fibrosis, scaring and honeycombing, with less affected areas of "normal" appearance (Figure 6). These areas are usually sub-pleural and paraseptal. Fibrotic zones are characterized for dense accumulation of extracellular matrix, and fibroblast bundles, so called "fibroblastic foci", located in vicinity of hyperplastic type 2 epithelial cells. Honeycomb regions are composed by cystic spaces lined by hyperplastic and aberrant bronchial epithelium.

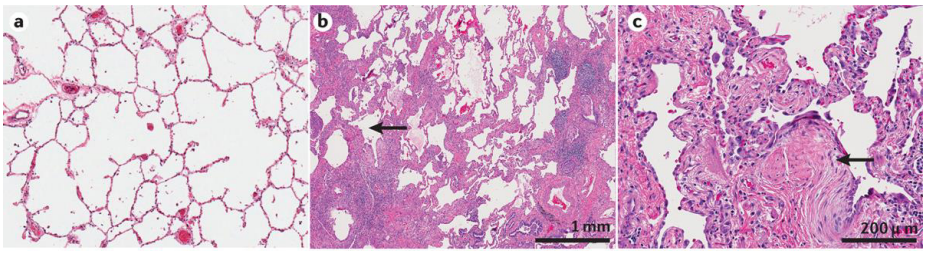

Figure 6. Histological UPI pattern from IPF. A) normal lung histology. B) Low-power H&E from a patients with UIP, revealing honeycombing, a characteristic of usual interstitial pneumonia (UIP) pattern, with of subpleural cystic airspaces, and well-defined walls. C) High-power H&E from the lung biopsy in "B", confirming the presence of fibroblastic foci (arrow) (Modified from Martinez, F. J. et al. 2017)

1.1.4. Biomarkers

To-date there is no molecular biomarkers in widespread use for IPF. There are several exciting candidates under study, yet none of them has reached clinical practice use internationally. Currently, imaging through detection of interstitial lung abnormalities (ILA) are the closest attempt of early detection of fibrosis (Sack et al., 2017; Washko et al., 2011). In IPF there a tremendous unmet need in stablishing markers for disease early diagnostics, progression and outcome (Ley et al., 2014), hence, several groups have focused their research on developing

and establishing these signatures (Table 1). KL-6 (Yokoyama et al., 2006), CCL-18 (Prasse et al., 2009), and SP-A (Greene et al., 2002) were some of the first molecules proposed as biomarkers in pulmonary fibrosis. KL-6 was analyzed retrospectively in a cohort of 27 patients, revealing that elevated serum levels (>1000U/ml) could predict survival, and acute exacerbations (Collard et al., 2010). When compared with clinical parameters (age, FVC, DLco and FVC change), high levels of KL-6 did not improve prediction of survival (Song et al., 2013). CCL18, a chemoattractant produced in alveolar macrophages, was found to predict outcome in a cohort of 72 patients, where 6-month follow-up study increased levels of CCL18 correlated with FVC and TLC decline. Recently in both CAPACITY 1 and 2, and ASCEND trials plasma concentrations of CCL18 were the most consistent predictor of progression, studied in a IPF trial to study treatment response (Neighbors et al., 2018). SP-A also showed potential of mortality prediction in the serum from 82 patients. (Song et al., 2013).

Other proposed biological markers relate to ECM turnover e.g. matrix metalloprotease 7 (MMP7) (Bauer et al., 2017; Rosas et al., 2008; Tzouvelekis et al., 2017), collagen degradation products (Jenkins et al., 2015), ECM-related autoantibodies (Li et al., 2017), epithelial signatures (Maher et al., 2017). For the focus of this thesis, is important to highlight a study by Richards et at. where combining clinical parameters and plasma protein concentrations, the authors could distinguished high and low mortality risk subgroups, an could accurately predict mortality. In this study 92 proteins were measured in plasma from 241 IPF patients (140 for derivation and 101 for validation cohort), reporting a poor overall survival prediction by elevated levels of MMP7, ICAM1, IL8, VCAM1, and S100A12 in both discovery and derivation cohort. ICAM1 was the only predictor of poor survival in the validation cohort, all five proteins were correlated with poorer transplant-free survival (Richards et al., 2012). Taken together, these data show that predicting IPF outcome might be feasible by combining clinical data

and peripheral blood biomarkers. Further studies in broader populations need to establish the reliability of these markers in routine clinical settings.

1.1.5. Treatment

In 2011, the antifibrotic agent Pirfenidone was first approved in Europe and Japan, for the treatment of IPF followed by US approval in 2014. Nintedanib, was then concomitantly approved worldwide as IPF therapy (Karimi-Shah & Chowdhury, 2015).

Nintedanib is a kinase inhibitor, initially developed as an anticancer agent. It blocks the downstream effect of growth factors implicated in fibrosis, including the receptors for vascular endothelial growth factor, fibroblast growth factor and platelet-derived growth factor (Wollin et al., 2015). Two phase 3 trials (INPULSIS-1 and INPULSIS-2) were reported in May 2014. Nintedanib-treated group had a significant reduction in FVC decline, when compared to placebo, reducing also the recurrence of acute exacerbations (Richeldi et al., 2014).

Pirfenidone was the first drug licensed specifically for IPF. To-date the exact mechanism of action of pirfenidone remains unclear. However, evidence shows that exerts anti-fibrotic, anti-inflammatory and antioxidant effects (Schaefer et al., 2011). Molecularly, treatment with pirfenidone reduces fibroblast production of fibronectin, α-SMA, collagen 1, collagen V and collagen fibril formation (Knuppel et al., 2017; Lehtonen et al., 2016). The beneficial effects of pirfenidone were first observed in 1999, and got the approval after multiple preclinical testing and four phase 3 trials (Poletti et al., 2014). The results reported by the first 3 trial were not concordant. CAPACITY 2, ASCEND, and the Japanese trial, found that pirfenidone significantly reduced FVC compared with placebo, slowing disease progression, but CAPACITY 1 study did not show similar results (Noble et al., 2011). To clarify the lack of reproducibility, a Cochrane meta-analysis of these three trials was done and showed that pirfenidone significantly reduced the risk of disease progression (Spagnolo et al., 2010). Then, in ASCEND

pirfenidone significantly improved progression-free survival, and slowed FVC decline, confirming the results from CAPACITY 2 (King et al., 2014).

Both dugs are recommended for use as IPF therapy by all worldwide thoracic societies (Raghu et al., 2015), and currently under consideration for combination therapy (Flaherty et al., 2018; Rajchgot et al., 2018). At present, treatment of IPF is transforming quickly, with the highest aim to hopefully one-day reverse disease.

1.2. Modeling pulmonary fibrosis in mice

For modeling IPF, scientist have used different approaches, substances like bleomycin, silica (Davis et al., 1998), or fluorescein isothiocyanate (FITC) (Christensen et al., 1999), irradiation (Haston & Travis, 1997), gene manipulation (Sime et al., 1997), cytokine overexpression (Kolb et al., 2001), and is still much missing to fully mimic the human scenario. It is widely accepted that the current animal models do not adequately replicate the pathophysiological features of IPF (Jenkins et al., 2017). Ideally, the perfect animal model would recreate the characteristic histological features of UIP, be progressive or at the least irreversible, applicable across mouse strains, reproducible, and if possible, be performed in a reasonably short time.

Nevertheless, these models have been extremely useful for identifying pathways leading to lung fibrosis, including those involving TGF-β, connective-tissue growth factor, fibroblast growth factor, platelet-derived growth factor, microRNAs, reactivation of developmental pathways, MMP-7, among others.

1.1.2. The bleomycin-induced pulmonary fibrosis model

Bleomycin is a chemotherapeutic agent used for cancer treatment (Evans et al., 1982). Pulmonary toxicity is one of the side effects, which can be life threatening

(Catane et al., 1979). Bleomycin induces DNA breaks that produce oxidative damage and injures the lungs due to lack of bleomycin hydrolase, an enzyme that inactivates the drug (Claussen & Long, 1999; Jules-Elysee & White, 1990).

With its advantages and disadvantages, bleomycin induced-pulmonary fibrosis is consider “the best-characterized animal model available for preclinical testing” (Jenkins et al., 2017). By far, it has being the most studied model for IPF research, from different administration routs (e.g. intratracheal, oropharyngeal, subcutaneous, intravenous) to different strains, dosage and administration frequency (Degryse et al., 2010).

The comparison between bleomycin-induced pulmonary fibrosis and IPF has been, and will always be, highly controversial. Nevertheless, many studies show strong similarities at many levels, ratifying the continuous use for preclinical testing (Bauer et al., 2015). At first, the inflammatory phase takes place within the first 7 days, followed by increased ECM deposition with a maximum at day 14, and resolution from day 21-28 onward. Largely, lung function returns to basal levels at 56 days post bleomycin treatment(Moore & Hogaboam, 2008). In mice, the lesions induced by bleomycin are heterogeneous, time-limited and self-resolving, with the disadvantage of a narrow time window for preclinical testing. From another angle, it offers the advantage of analyzing the dynamics of injury-fibrosis-resolution and assesses heterogeneity in an intraindividual manner.

To-date the most popular endpoints in pre-clinical models of IPF are histological scoring and lung collagen content (Carrington et al., 2018). However, in IPF patients the used endpoints are imaging and pulmonary function tests. Therefore, we propose that examining more clinically relevant endpoints in pre-clinical models would provide better indication of treatment efficacy, in a more clinically relevant setting.

1.3. Objectives

Despite advances in understanding the molecular mechanisms, genetic influence, and clinical features of idiopathic pulmonary fibrosis, there are several unmet needs. Currently, there is no available clinically approved biomarker that improves disease accuracy, reflects disease course, or predicts prognosis. Furthermore, the two drugs available for treatment of IPF patients, pirfenidone and nintedanib, slow down functional decline and disease progression, but are not yet curative. Remaining lung transplantation as the only curative treatment with a median survival of 5 about years and accessible only to highly selected patients.

The aims of this thesis were to comprehensively analyze the bleomycin-induced pulmonary fibrosis model in order to: first, design tools for biomarker discovery and clinical assessment of the model; second, improve preclinical drug evaluation in mice. These results may reflect in an increase knowledge in the model, and hopefully in more successful drug approvals and clinical trial performances.

2. Publications originating from this thesis

2.1. Systematic phenotyping and correlation of biomarkers with lung function and histology in lung fibrosis

Isis E Fernandez, Oana V Amarie, Kathrin Mutze, Melanie Königshoff, Ali Önder Yildirim, Oliver Eickelberg .

published first in

American Journal of Physiology - Lung Cellular and Molecular Physiology. 2016 May 15;310(10):L919-27

Am J Physiol Lung Cell Mol Physiol 310: L919–L927, 2016.
First published March 18, 2016; doi:10.1152/ajplung.00183.2015.

CALL FOR PAPERS | *Biomarkers in Lung Diseases: from Pathogenesis to Prediction to New Therapies*

Systematic phenotyping and correlation of biomarkers with lung function and histology in lung fibrosis

Isis E. Fernandez, Oana V. Amarie, Kathrin Mutze, Melanie Königshoff, Ali Önder Yildirim, and Oliver Eickelberg

Comprehensive Pneumology Center, University Hospital of the Ludwig Maximilians University and Helmholtz Zentrum München, Munich, Germany

Submitted 8 June 2015; accepted in final form 15 March 2016

Fernandez IE, Amarie OV, Mutze K, Königshoff M, Yildirim AÖ, Eickelberg O. Systematic phenotyping and correlation of biomarkers with lung function and histology in lung fibrosis. *Am J Physiol Lung Cell Mol Physiol* 310: L919–L927, 2016. First published March 18, 2016; doi:10.1152/ajplung.00183.2015.—To date, phenotyping and disease course prediction in idiopathic pulmonary fibrosis (IPF) primarily relies on lung function measures. Blood biomarkers were recently proposed for diagnostic and outcome prediction in IPF, yet their correlation with lung function and histology remains unclear. Here, we comprehensively assessed biomarkers in liquid biopsies and correlated their abundance with lung function and histology during the onset, progression, and resolution of lung fibrosis, with the aim to more precisely evaluate disease progression in the preclinical model of bleomycin-induced pulmonary fibrosis in vivo. Importantly, the strongest correlation of lung function with histological extent of fibrosis was observed at *day 14*, whereas lung function was unchanged at *days 28* and *56*, even when histological assessment showed marked fibrotic lesions. Although matrix metalloproteinase-7 (MMP-7), MMP-9, and PAI-1 were significantly elevated in broncheoalveolar lavage of fibrotic mice, only soluble ICAM-1 (sICAM-1) was elevated in the peripheral blood of fibrotic mice and was strongly correlated with the extent of fibrosis. Importantly, tissue-bound ICAM-1 was also elevated in lung homogenates, with prominent staining in hyperplastic type II alveolar epithelial and endothelial cells. In summary, we show that lung function decline is not a prerequisite for histologically evident fibrosis, particularly during the onset or resolution thereof. Plasma levels of sICAM-1 strongly correlate with the extent of lung fibrosis, and may thus be considered for the assessment of intraindividual therapeutic studies in preclinical studies of pulmonary fibrosis.

interstitial lung diseases; pulmonary fibrosis; lung injury and repair; monitoring; outcome; surveillance

REPETITIVE LUNG INJURY FREQUENTLY induces lung fibrosis (13), which leads to impairment of the alveolar-capillary units, enhances fibroblast proliferation and extracellular matrix (ECM) deposition, and aberrant repair processes. These processes ultimately cause irreversible scarring of the lung, often resulting in idiopathic pulmonary fibrosis (IPF) (3, 12). IPF is a rapidly progressive and deadly disease with a median survival of 2–3 yr after diagnosis. Although two drugs (nintedanib and pirfenidone) have been recently approved for mild-to-moderate IPF in Europe and the United States, these slow down the progression of IPF but are unable to reverse or cure it (18, 29). To date, the clinical evaluation of IPF most commonly relies on repeated physiological lung function measurements [e.g., forced vital capacity (FVC), lung CO diffusing capacity (DL_{CO})] and radiological findings on high-resolution computed tomography and, when available, histopathology (27). It is currently unclear, however, which of these parameters best correlates with disease progression in IPF (40, 41). Importantly, the survival of patients with interstitial lung disease significantly differs, even when comparing groups with a similar decline in lung function [as assessed by FVC or forced expiratory volume in 1 s (FEV_1)] (38), suggesting that the additional use of predictive biomarkers will more accurately project the disease course. As such, defining sensitive parameters that assess and predict the progression of lung fibrosis is imperative, in particular by systematically evaluating recently suggested blood biomarkers compared with lung function and histology (5). To begin to address this question, we addressed biomarker profiles in the widely used bleomycin model of lung fibrosis in an effort to adequately and precisely correlate biomarkers with physiological and pathological parameters (33).

The assessment of drug efficacy in animal models of lung fibrosis has been criticized recently, because several drugs showed efficacy in animal models but not in clinical studies in IPF. It is important to note, however, that the evaluation of animal models is, in many cases, biased by reader-dependent measurements (23). One particular challenge, for example, is the interindividual heterogeneity of fibrosis in response to bleomycin, for which it should be systematically accounted (22). Furthermore, systemic evaluation of the bleomycin model is currently limited to biochemical assays, biased selection of fibrosis-affected areas, or reader-dependent scoring of histology sections (e.g., Ashcroft score). Hence, more quantitative assessment of fibrosis or better selection criteria in preclinical testing will be critical for drug efficacy evaluation in these models.

Recently, a large prospective biomarker study showed that VCAM-1, matrix metalloproteinase-7 (MMP7), ICAM-1, and IL-8 are strong predictors of survival in IPF and might thus aid in disease monitoring. Their correlation with lung histology, however, remains unclear (28). Furthermore, a large retrospec-

Address for reprint requests and other correspondence: O. Eickelberg, Comprehensive Pneumology Center, Ludwig-Maximilians Univ. Hospital and Helmholtz Zentrum München, Max-Lebsche-Platz 31, 81377 München, Germany (e-mail: oliver.eickelberg@helmholtz-muenchen.de).

tive IPF cohort study demonstrated that all current available models and commonly measured variables (e.g., FVC, dyspnea score, and 6-min walk distance) failed to accurately predict physiological and functional progression of IPF (19). Thus we sought to assess these biomarkers in several compartments [broncheoalveolar lavage fluid (BALF), peripheral blood] during the initiation, establishment, and resolution of fibrosis, and comprehensively correlated their levels with histology and lung function to better define the disease state and severity of lung fibrosis. Finally, we performed serial blood measurements of soluble ICAM-1 (sICAM-1), the best performing biomarker in our study, and assessed its expression and localization in the lung and primary alveolar epithelial cells during injury and fibrosis.

METHODS

Animals. Pathogen-free female C57BL/6 mice (10–12 wk old) were obtained from Charles River Laboratories and maintained at constant temperature and humidity with a 12:12-h light-dark cycle. Animals were allowed food and water ad libitum. All animal experiments were conducted under strict governmental and international guidelines and were approved by the local government for the administrative region of Upper Bavaria (TVA 55.2-1-54-2532-21-12), as previously described (17).

Induction and assessment of pulmonary fibrosis. Pulmonary fibrosis was initiated by a single intratracheal instillation of 50 μl of bleomycin (3 U/kg, Sigma Aldrich, Taufkirchen, Germany) dissolved in sterile PBS, and applied using the MicroSprayer Aerosolizer (Model IA-1C; Penn-Century, Wyndmoor, PA). Control mice were instilled with 50 μl of PBS. After 7, 14, 28, or 56 days after bleomycin or PBS instillation, lung function was measured using the FlexiVent system (Sireq), and mice were sacrificed for biochemical and histological analysis. Bronchoalveolar lavage (BAL) was performed by instilling the lungs with 3 × 0.5-ml aliquots of sterile PBS to obtain BALF for biomarker analysis, and total/differential cell counts for inflammatory cell recruitment of neutrophils, macrophages, or lymphocytes were measured. Lung tissue was either snap-frozen in liquid nitrogen to determine tissue mRNA/protein expression or fixed by intratracheal instillation of 4% paraformaldehyde and embedded into paraffin for staining.

Image acquisition, processing, and analysis. At least three sections from the same lung were cut and arranged on the same paraffin block, and the slides were stained with hematoxylin-eosin (H&E). Stained sections were automatically scanned with a digital Mirax slide scanner system (3DHISTECH, Budapest, Hungary) equipped with a ×20 objective with a numerical aperture of 0.75. The actual scan resolution (effective pixel size in the sample plane) at ×20 was 0.23 μm. The accompanying software allowed the user to navigate through the captured Whole Slide Image (Zeiss, Germany).

Quantification of fibrosis using semiautomated image analysis. A minimum of three whole-lobe cuts of 500 μm from identical mice were exported in high-quality .tif files (8). All images were analyzed using an already developed macro (15), which required ImageJ v1.38 software or higher. This ImageJ macro was written to quantify the percentage of fibrosis compared with the total amount of tissue within an image. This percentage was determined by quantifying the total tissue areas occupied by dense parenchyma. The threshold was set arbitrarily after the black and white conversion to ±5 (205) for all slides. To do so, we converted the image from color to 8-bit, followed by the delimitation of the area of interest (whole lobe selection) and measurement of the selected area (Fig. 2*A*) as density percentage. The alveolar space was determined by "parenchymal-free" area quantification, which included bronchi and vessels (Fig. 2*B*). We then quantified at least three sections (2 mm approximate distant from each other in a transversal cut) from each lung; this value was averaged and assigned as the percentage of alveolar space of each individual.

Luminex multiplex assay and ELISA. A multiplex biometric ELISA-based immunoassay was performed using plasma or BALF from PBS- or bleomycin-treated mice according to the manufacturer's protocols. We used the Mouse Cardiovascular Disease (CDV) panel 1 commercially available multiplex kit from Millipore (Billerica, MA). MMP-7 and sICAM-1 ELISAs were performed using plasma, BALF, or ATII supernatants from PBS- or bleomycin-treated mice, according to the manufacturers' protocol (Uscn Life Science, Wuhan, China; Thermo-Scientific, Rockford, IL, respectively).

Immunofluorescent stainings. Lung tissue was embedded in paraffin and immunofluorescence analysis was performed as previously described (37). Briefly, sections were stained with anti-mouse ICAM-1 (Thermo Fisher Scientific) or E-cadherin (Millipore) overnight at 4°C, washed three times with PBS, and subsequently incubated with the secondary antibodies (1:250 dilutions of Alexa Fluor 568 goat anti-rabbit or Alexa Fluor 488 goat anti-mouse) and 4′,6-diamidino-2-phenylindole (DAPI, 1:2,000; Sigma-Aldrich, St Louis, MO) for 1 h at room temperature. Finally, the sections were washed three times with PBS and mounted in fluorescent mounting medium (Dako). Images were acquired with an LSM 710 microscope (Zeiss) operated in multitrack mode.

RNA isolation and real-time quantitative reverse-transcriptase PCR analysis. RNA extraction from mouse tissue was performed using the Roti Quick Kit (Carl Roth, Karlsruhe, Germany), followed by RNA purification with the peqGold RNA isolation kit (Peqlab, Erlangen, Germany), according to manufacturers' instructions. Quantitative real-time PCR (qRT-PCR) was performed using the SYBR Green PCR master mix (Roche Applied Science, Mannheim, Germany).

Immunoblotting. Pulverized mouse tissue was homogenized in Radio-Immunoprecipitation Assay (RIPA) buffer containing a protease and phosphatase inhibitor cocktail (Roche). Protein concentrations were determined using the Pierce BCA Protein Assay (Thermo Fisher Scientific). Samples were denatured in Laemmli buffer, resolved by SDS-PAGE, and transferred to polyvinylidene diflouride membranes. Nonspecific membrane binding was blocked with 5% low-fat milk in 0.1% Tween 20, TBS (TBS-T). Membranes were incubated with the primary antibodies to ICAM-1 (Thermo Fisher Scientific) or β-actin (Sigma Aldrich) overnight at 4°C. After washing with TBS-T, the membranes were incubated with secondary antibodies for 1 h at room temperature. Blots were rinsed with TBS-T and visualized with the enhanced chemiluminescence system (Thermo Fisher Scientific, Waltham, MA), followed by analysis using the ChemiDocXRS+ imaging system (Bio-Rad, Munich, Germany). Band quantification was performed using ImageJ software (version v1.38).

Primary murine ATII cell isolation and culture. Primary murine ATII (pmATII) cell isolation from PBS- or bleomycin-treated mice was performed as previously described (24). Supernatants were collected and snap-frozen; 1:2 diluted supernatants were used for the assessment of sICAM-1 levels by ELISA.

Statistical analysis. Results are presented as means ± SD and were considered statistically significant at $P < 0.05$. Data of selected groups were compared using one-way ANOVA, followed by Dunnett's post hoc test. The Pearson's correlation coefficient (r value) was used to determine the degree of association between variables and interpreted using Dancey and Reidy's categorization (9). Here, r values of ±1, ±0.7 to ±0.99, ±0.4 to ±0.69, ±0.1 to ±0.39, and 0 were interpreted as perfect, strong, moderate, weak, or no correlation, respectively. The statistical significance of the correlations was assessed by P value. A linear regression analysis between two variables was performed and the best fit curve drawn from data points.

RESULTS

The dynamics of lung injury, fibrosis, and resolution in bleomycin injury. We first sought to perform an extensive phenotypic characterization of the bleomycin-induced fibrosis model over an extended time period up to 56 days after

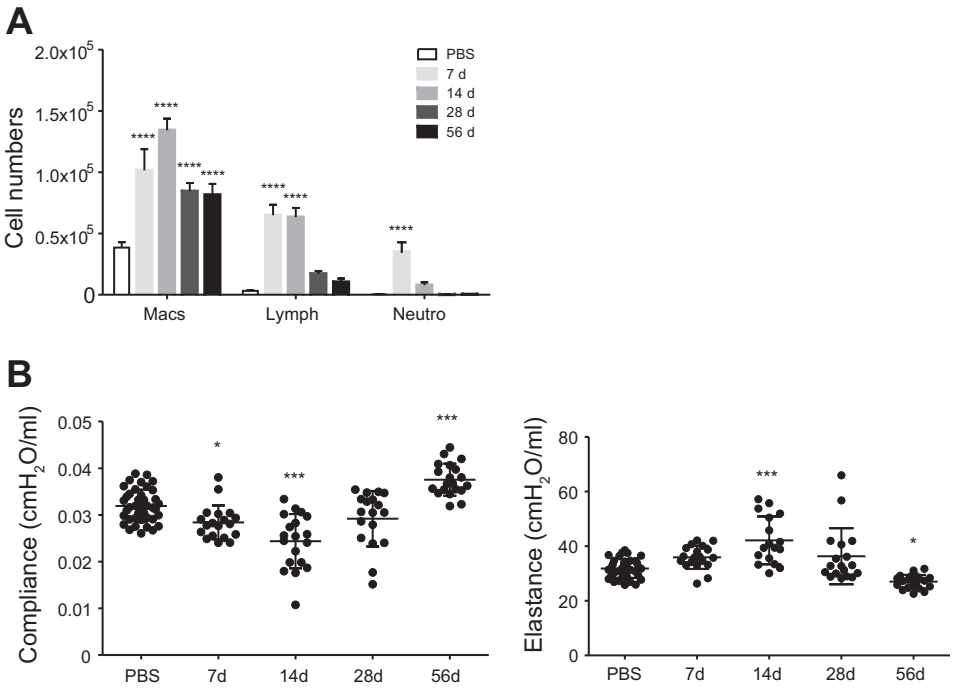

Fig. 1. Inflammatory cell recruitment and lung function during lung fibrosis. C57BL/6 mice (aged 10–12 wk, female) were treated with bleomycin or PBS and harvested at *days 7*, *14*, *28*, or *56* after treatment. PBS represents a pool of PBS-treated mice for 7, 14, 28, and 56 days. *A*: differential cell counts of inflammatory cells were assessed in bronchoalveolar lavage fluid (BALF). *B*: tissue stiffness was determined by lung function measurement of compliance and elastance. Data are presented as means ± SD; for statistical analysis, one-way ANOVA was used. For all experiments $*P < 0.05$, $**P < 0.01$, and $***P < 0.001$. Macs, macrophages; Lymph, lymphocytes; Neutro, neutrophils.

intratracheal application of bleomycin. Lymphocyte and neutrophil cell numbers significantly increased in BALF during the first 7 days after bleomycin injury and returned to baseline levels after 28 days. BALF macrophage numbers, in contrast, were significantly increased at all time points (*day 7* to *day 56)* and peaked 14 days after bleomycin injury (Fig. 1*A*). Static lung compliance, a surrogate of tissue stiffness, was significantly decreased 7 days postbleomycin, with a major decrease 14 days after bleomycin instillation. Static compliance returned to baseline levels at *day 28* and was significantly increased at *day 56* (Fig. 1*B*). Similar observations were made for tissue elastance (Fig. 1*B*). Histological analysis revealed a peak of lung fibrosis at *day 14* after injury, which regressed, but did not completely resolve, by *day 56* (Fig. 2*A*).

To avoid reader-dependent bias, we designed a semiautomatized algorithm to calculate the percentage of alveolar space (Fig. 2*B*). After measuring 39 individual mice, including 29 bleomycin-injured mice ($n = 8$, 9, 5, and 7 for *days 7*, *14*, *28*, and *56* after bleomycin application, respectively) and 10 controls (harvested from all time points, for a total of 149 images), we observed a significant drop in alveolar space at *day 7* compared with controls. The percentage of alveolar space remained reduced over the entire observation period of 56 days (Fig. 2*C*). We then assessed the correlation strength of the

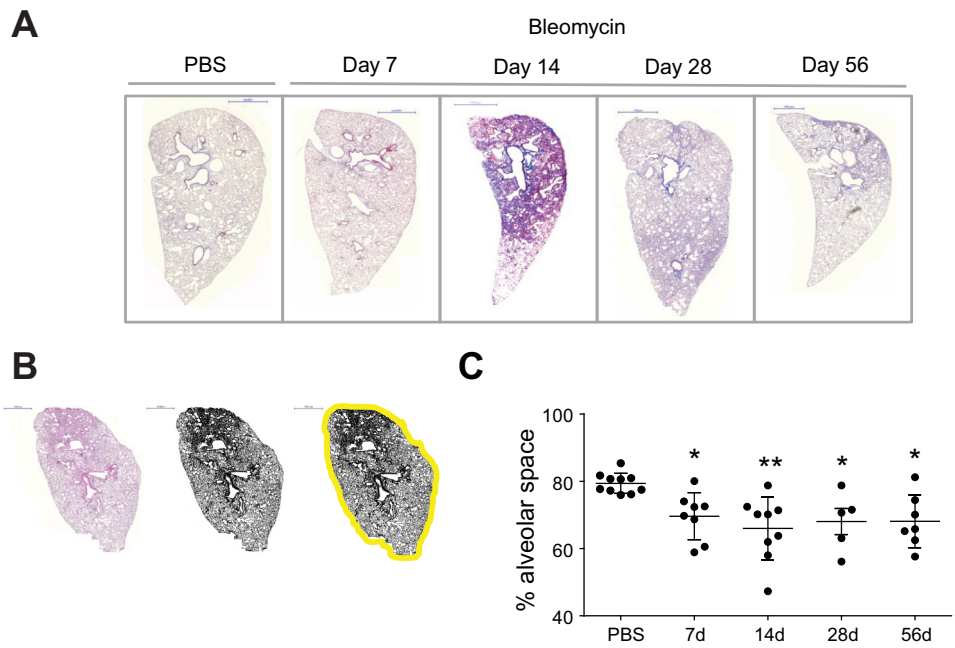

Fig. 2. Semiautomatized quantification of lung fibrosis. Hematoxylin-and-eosin (H&E) staining of mouse lung sections from *day 7*, *14*, *28*, or *56* after treatment were scanned, analyzed, and quantified with Image J software. PBS represents a pool of PBS-treated mice for 7, 14, 28, and 56 days. *A*: representative Masson trichrome stainings from PBS- or bleomycin-treated mice are depicted. *B*: threshold settings, 8-bit conversions, and area selections of H&E stainings are shown. *C*: quantification of alveolar space via Image J software throughout the bleomycin time course is shown. Each dot represents the mean quantification of at least three whole-lobe sections per subject. Statistical differences ($*P < 0.05$, $**P < 0.01$, and $***P < 0.001$) were determined by one-way ANOVA.

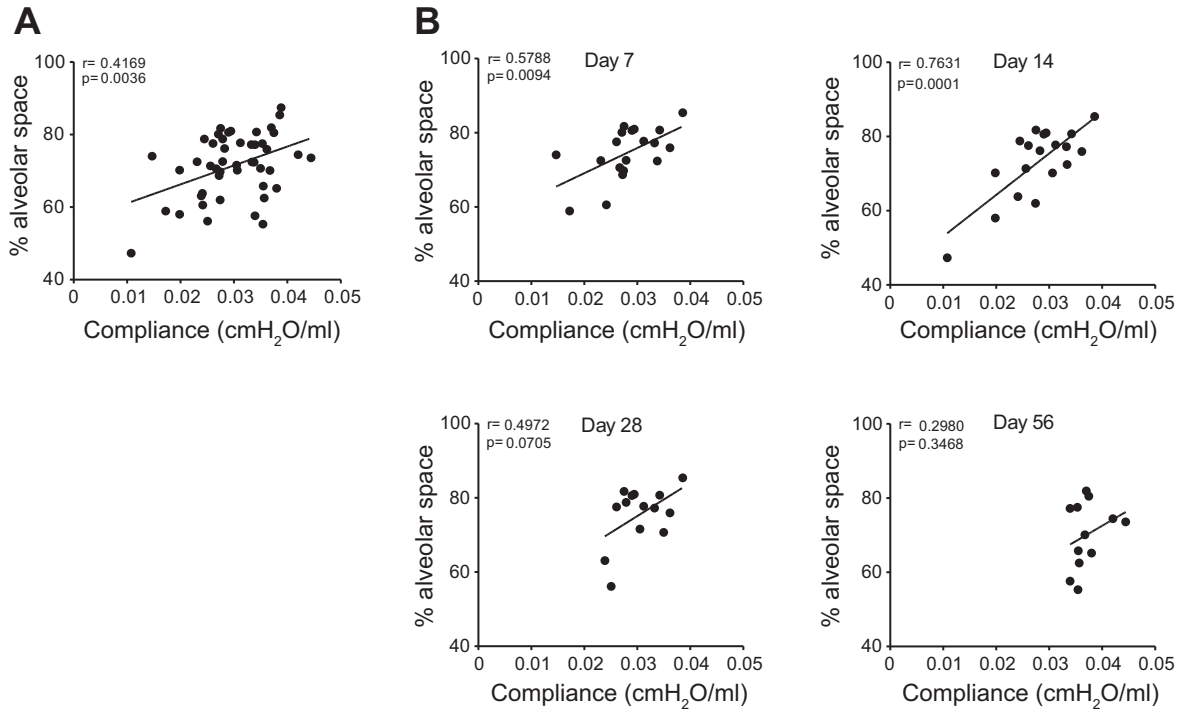

Fig. 3. Correlation of lung function and histology over time in lung fibrosis. Correlations between the percent of alveolar space and lung compliance were determined using Pearson's correlation coefficient. *A*: all-samples correlation including time point matching PBS controls and mice treated for 7, 14, 28, and 56 days. *B*: time point-specific correlations are shown.

percent of alveolar space with lung function parameters (compliance) using all samples at all time points. We observed a moderate positive correlation ($r = 0.4$) for all samples analyzed (Fig. 3*A*). When single time point correlations were performed, we observed the strongest correlation at *day 14* after treatment, followed by *day 7* (Fig. 3*B*). No significant correlations were obtained at *day 28* or *day 56*. This indicated that lung function parameters fully recovered to normal values even in the clear presence of histological evidence of fibrosis.

To substantiate these observations, we measured transcript levels of established markers of fibrosis collagen-1a1 (*col1a1*), fibronectin (*fn1*), lysyl oxidase L2 (*loxl2*), and tenascin c (*tnc*) in lung homogenates over the entire time course. We observed a significant increase in all fibrosis markers during the peak of lung fibrosis (*day 14*) compared with controls (Fig. 4), albeit with different expression dynamics over the entire time course of lung fibrosis. In fact, *col1a1* was exclusively upregulated at *day 14* posttreatment, whereas *fn1* was significantly upregu-

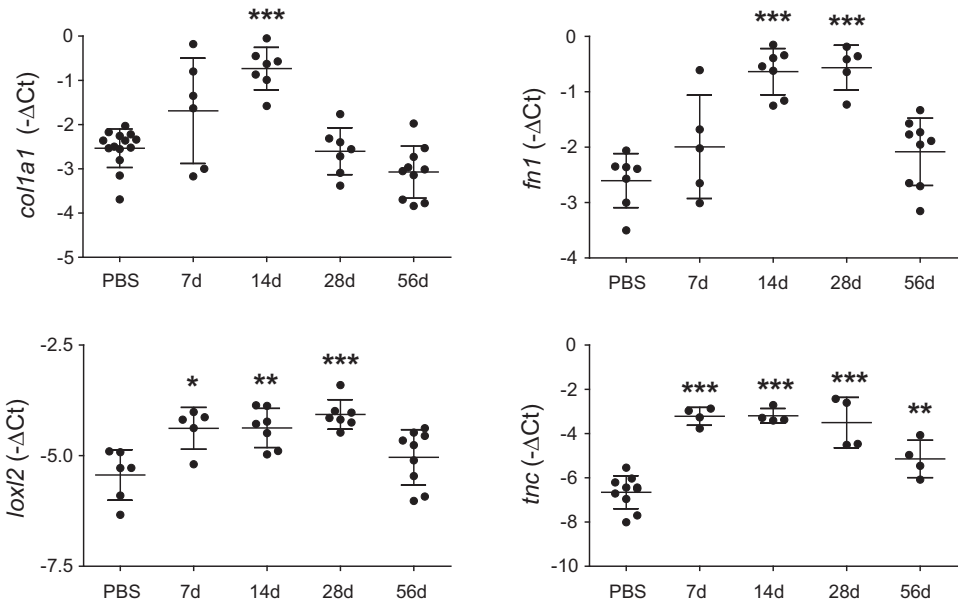

Fig. 4. The mRNA expression patterns of extracellular matrix markers in lung fibrosis. The quantitative RT-PCR analysis of expression levels of collagen-1a1 (*col1a1*), fibronectin (*fn1*), lysyl oxidase L2 (*loxl2*), and tenascin c (*tnc*) from PBS- and bleomycin-treated mice harvested 7, 14, 28, and 56 days after treatment. PBS represents a pool of PBS-treated mice for 7, 14, 28, and 56 days. Data are presented as means ± SD as 1-ΔCT relative expression to control (GAPDH). Statistical differences (*$P < 0.05$, **$P < 0.01$, and ***$P < 0.001$) were determined by one-way ANOVA.

lated from *day 14* until *day 28*. Expression of the ECM-modifying enzyme *loxl2* was increased from *day 7* to *day 28*, and decreased back to basal levels at *day 56*. Expression of *tnc* was highly increased at *day 7*, which was maintained up to *day 56*. These dynamics thus suggest different contributions of these ECM components to injury and scar formation in the lung.

Compartmentalized biomarker signatures during lung injury, fibrosis, and resolution. Next, we assessed protein expression using a five-analyte panel containing MMP-9, PAI-1, E-selectin, VCAM-1, and sICAM-1, according to previously reported biomarkers in IPF. In addition, MMP-7 was measured via ELISA (Fig. 5*A*). Two out of these six candidate proteins were significantly regulated during the onset and resolution of fibrosis when measured by Luminex in plasma: E-selectin was significantly increased at *day 7* and significantly decreased at *day 56* compared with controls, whereas sICAM-1 was significantly increased from *day 7* through *day 28*, after which levels normalized again. The increase in circulating sICAM-1 was validated by ELISA, which showed a significant increase in sICAM-1 levels at *day 14* after bleomycin treatment (Fig. 5*C*). Both assays showed similar regulation of sICAM-1, but ELISA values are well known to underestimate real concentrations compared with Luminex platforms (7). Interestingly, some of these candidate proteins were not detectable in BALF in the same individuals (Fig. 5*B*). From the six candidate proteins tested, four were detectable in BALF (MMP-7, MMP-9, sICAM-1, and PAI-1), out which two were significantly increased during fibrosis: PAI-1 was significantly increased exclusively at *day 7*, whereas MMP-7 was significantly increased at *day 7* and *day 14*, during the peak of fibrosis.

We correlated the selected protein levels with pulmonary compliance and analyzed the correlation coefficient of these two variables within all measured samples. No significant

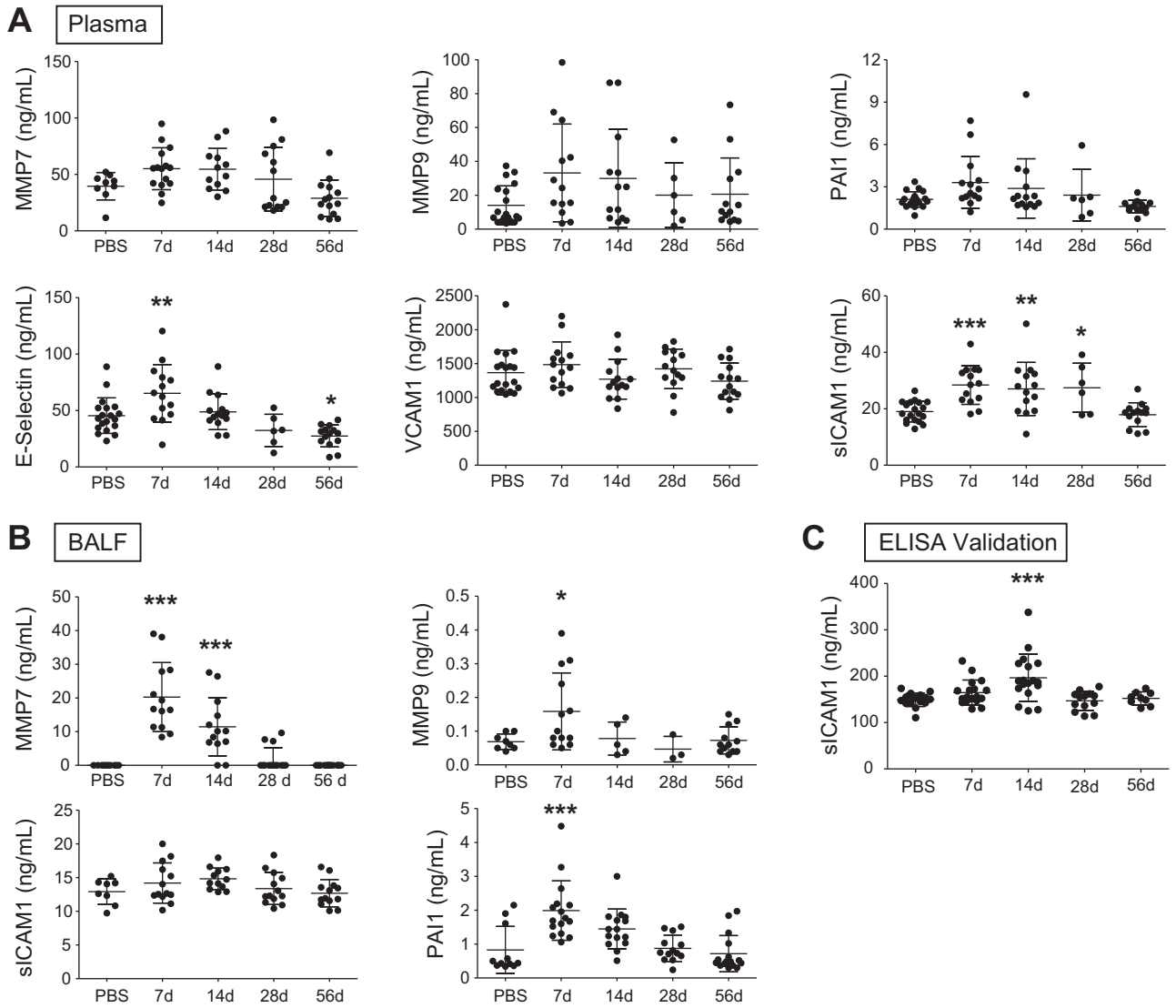

Fig. 5. Plasma and BALF biomarker profiling during lung injury and fibrosis. MMP-7 was measured by ELISA and MMP-9, PAI-1, E-selectin, VCAM-1, and sICAM-1 were measured by Luminex multiplex assay in plasma (*A*) and BALF (*B*) samples obtained from bleomycin- or PBS-treated mice over 7, 14, 28, and 56 days. In BALF measurement, VCAM-1 and E-selectin were nondetectable, and "n" vary according to detectability. *C*: sICAM-1 ELISA using plasma samples from PBS- and bleomycin-treated mice. PBS represents a pool of PBS-treated mice for 7, 14, 28, and 56 days. Data are presented as means ± SD. For statistical analysis, one-way ANOVA was used. For all experiments: $*P < 0.05$, $**P < 0.01$, and $***P < 0.001$.

correlation was observed for MMP-9, and VCAM-1. A weak but significant correlation was observed for MMP-7, and E-selectin; and a stronger and highly significant correlation ($P < 0.0001$) for PAI-1 and sICAM-1 with respect to protein plasma levels and lung function (Fig. 6).

Compartmentalized regulation of ICAM-1 during lung injury and fibrosis. To further determine whether sICAM-1 blood levels were regulated during the onset and progression of fibrosis in an intraindividual manner, we performed sequential bleedings from *day 0* to *day 15* and measured sICAM-1 levels every third day in control and bleomycin-treated mice. We observed that sICAM-1 levels were significantly increased as fibrosis developed (Fig. 7*A*). Importantly, Western blotting of whole lung homogenates revealed that ICAM-1 protein expression levels were significantly increased at *day 14* compared with PBS controls (Fig. 7*B*). Immunohistochemical staining demonstrated that ICAM-1 was strongly expressed in alveolar epithelial cells and endothelial cells in the healthy lung, and it was prominently expressed in hyperplastic alveolar epithelial cells and endothelial cells during fibrosis (Fig. 7*D*). To confirm this, we investigated whether sICAM-1 is shed from alveolar epithelial cells during fibrosis by analyzing supernatants of primary alveolar epithelial (pmATII) cells from PBS- and bleomycin-treated mice (*day 14*). We observed that supernatants from bleomycin-treated pmATII cells exhibited significantly increased levels of sICAM-1 compared with PBS-treated pmATII cells (Fig. 7*C*).

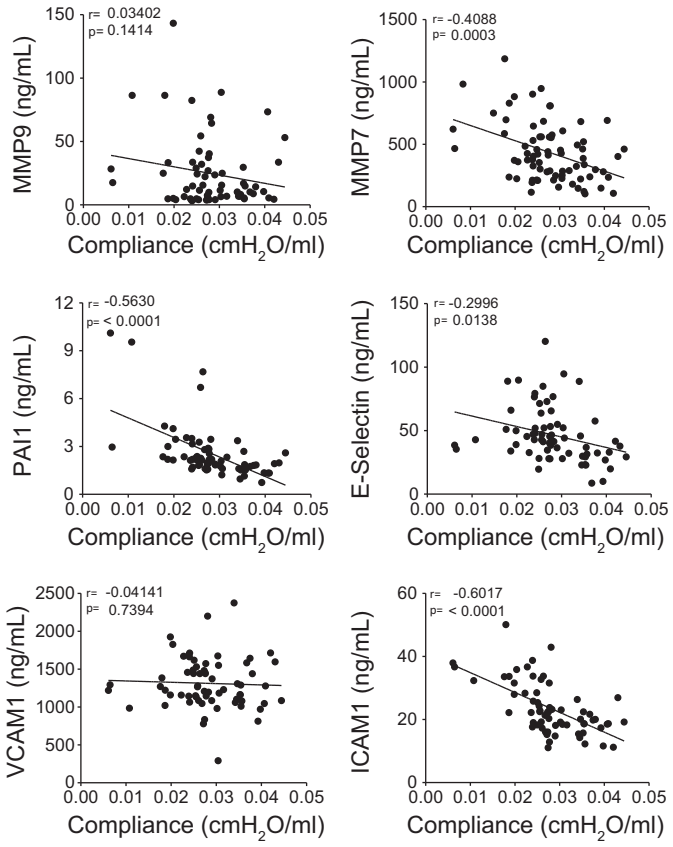

Fig. 6. Correlation of lung function and plasma biomarkers in lung injury and fibrosis. Correlation coefficients of lung compliance and plasma levels of selected candidates (MMP-9, MMP-7, PAI-1, E-selectin, VCAM-1, or sICAM-1) were analyzed for subjects treated with bleomycin after *days 7*, *14*, *28*, and *56*, and respective PBS controls. Correlations between lung compliance and plasma signatures were determined using Pearson's correlation coefficient. Significance of the correlation analysis was set at $P < 0.05$.

DISCUSSION

We have witnessed an unprecedented gain in our understanding of the pathomechanisms driving lung fibrosis in the past years, including the assessment of mRNA and miRNA expression patterns in the fibrotic lung, both in murine and human studies. Two therapies for IPF have recently been approved in Europe, the United States, and a variety of other countries (18, 29), both of which decelerate the lung function decline in patients with IPF. Despite these major achievements, we are still unable to stop progression, or, better, reverse the loss of functional lung tissue in IPF (10). The development of better diagnostic tools and continued efforts for drug development in IPF, using better refined and defined animal models and complex phenotypic assays, therefore continue to be a major challenge to the scientific community (42). To this end, we sought to comprehensively assess recently described biomarkers in IPF in the bleomycin-induced model of lung fibrosis, in a compartmentalized manner, to increase the accuracy of interventions and outcome measures during drug testing.

Although the comparison between the bleomycin-induced model of pulmonary fibrosis and IPF has been highly controversial (2), recent studies show strong commonalities on distinct levels, encouraging the continuous use of the model for preclini (4, 26). In humans, IPF lesions are continuous and progressive, contributing to permanent and irreversible lung scarring. In mice, the bleomycin-induced fibrotic lesions are heterogeneous, time-limited, and self-resolving, bringing the advantage of analyzing the dynamics of injury-fibrosis-resolution and assess heterogeneity in an intraindividual manner. At first, the inflammatory phase takes place within the first 7 days, followed by increased ECM deposition with a maximum at *day 14*, and resolution from *days 21–28* onward. Largely, lung function returns to basal levels at 56 days after bleomycin treatment, as we have previously reported (31).

Importantly, the spatio-temporal heterogeneity of lung fibrosis increases the complexity in achieving these goals. Well-established systematic measurements, such as pulmonary function tests (e.g., FVC, FEV_1), are in daily clinical use to assess restrictive lung disease, but they remain unspecific and with limited sensitivity, possibly preventing early detection of patients with lung fibrosis (32). In addition, only 14% of patients with early interstitial lung disease exhibit changes in high-resolution computed tomography (14, 40), whereas 32% of these patients exhibit changes in transbronchial biopsy (8). These data strongly suggest that a number of fibrotic lesions, in particular early lesions, are not detected using a combination of up-to-date imaging and lung function measurements in the clinical setting. This notion is supported by the data reported in our study. We show that in mice, the maximum lung function decline was observed at *day 14* after treatment. Lung function returned to baseline levels, whereas histological analysis still demonstrated a significant amount of fibrosis in these individuals, demonstrating the need for specific biomarkers detecting the presence of tissue fibrosis.

To avoid reader-dependent and region-of-interest selection bias, we developed a whole-lung, semiautomatized quantifica-

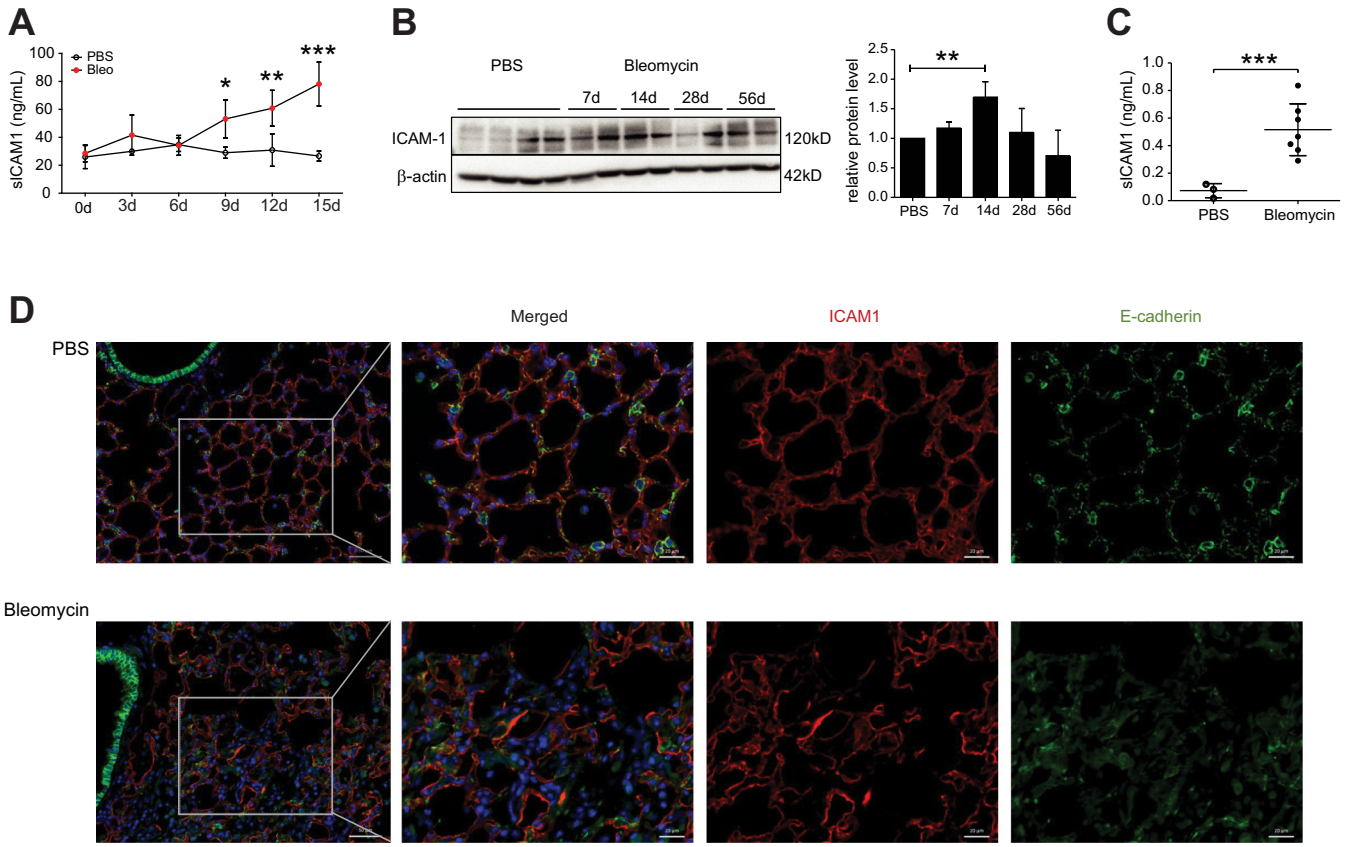

Fig. 7. Compartmentalization of ICAM-1 levels during lung injury and fibrosis. *A*: repetitive blood sampling every 3 days from *day 0* to *day 15* were obtained for PBS- (empty circle) and bleomycin-treated (red circle) mice, and plasma sICAM-1 levels were analyzed. Statistical differences were determined by one-way ANOVA. *B*: whole lung homogenate protein levels of ICAM-1 were assessed by Western blotting ($n = 3$ blots were quantified by image densitometry). Relative protein levels are presented as ratio target protein to β-actin and normalized to PBS as 1. Statistical differences were determined by one-way ANOVA. *C*: primary murine ATII cells were isolated from PBS- or bleomycin-treated mice (14 days) and cultured for 5 days. Supernatants were collected, and sICAM-1 was measured by ELISA. Statistical differences were determined by *t*-test. *D*: immunofluorescence staining for ICAM-1 (red), E-cadherin (green), and DAPI (blue) of PBS- (*top*) and bleomycin-treated (14 days) mice (*bottom*). Gray squares show lower magnification of zoomed areas (right), the scale bar represents 50 μm in nonzoom pictures (*left*), and 20 μm in zoomed pictures (*right*). For all experiments significance was set as follows: $*P < 0.05$, $**P < 0.01$, and $***P < 0.001$.

tion system. With this method, we were able to provide a robust, broader assessment of the affected lung by quantifying the alveolar space loss during fibrosis. In some severe cases, alveolar loss went up to 30%, and was maintained over time, although lung function improved. This might reflect a different molecular/cellular composition of the lung parenchyma during the scar formation process. It is important to clarify that both parameters, lung function and histology, are equally required to understand a given disease process, because each of them may reflect different aspects of the disease. In the lung fibrosis model of adenovirus-mediated overexpression of active TGF-β (6), good correlations between histomorphological, radiological, and functional changes were observed (1). Notably, this model is a progressive and persistent model of fibrosis, supporting that during the peak of fibrosis, but not necessarily during the initiation or resolution thereof, these parameters comprehensively assess the disease status of the individual.

Interestingly, we found that single ECM components vary significantly during the evolution of fibrosis in the lung. For instance, *col1a1* and *fn1* were predominantly increased at the peak of fibrosis (when the lung exhibits maximum stiffness), whereas other ECM components maintained high expression levels at all time points, supporting that some ECM members might be causally responsible for lung function decline, and therefore critically determine the increased parenchymal stiffness of the lung.

Because physiological measures and histopathology are at times poor predictors of short- and long-term outcome, we profiled peripheral blood components as reflectors of the fibrotic process. Richards and colleagues (28) recently demonstrated that patients with IPF display a unique plasma signature that reflects disease severity (by integrating MMP-7, VCAM-1, S100A-12, ICAM-1, and IL-8) (28). Thus we selected candidate markers with the aim of detecting a characteristic signature of lung injury, fibrosis, and resolution in the bleomycin model. We found that sICAM-1 was significantly increased at *day 7* and remained increased as the injury was maintained. This expression was compartmentally regulated and detected in the blood, but not BALF. Compartmental regulation of ICAM-1 is detected in patients with IPF in who levels of ICAM-1 are higher in the peripheral blood than in BALF (36).

The sICAM-1 has been previously reported as a marker for epithelial injury in kidney disorders (39) because it is a target of proteinases that shed it from the cell membrane (11). Recently, in a cohort of patients that have received lung transplant with primary graft dysfunction (34), sICAM-1 was

used as a predictor of mortality, which improved when sICAM-1 was analyzed in combination with other markers (e.g., sICAM-1–PAI-1 or sICAM-1–sRAGE). Importantly, increased levels of sICAM-1 in progressive injury have been reported in other models of lung injury (21). In fact, BALF levels of sICAM-1 were associated with epithelial dynamics and transdifferentiation. Although our data do not show a significant increase in sICAM in the BALF of bleomycin-treated mice, we show that primary murine ATII cells from fibrotic mice secrete and/or shed higher levels of sICAM into the supernatant, demonstrating that lung ATII cells are an important source of sICAM during injury, fibrosis, and resolution thereof.

Interestingly, ICAM-1 plays a critical role during lung injury and fibrosis in leukocyte kinetics. In arteries, ICAM-1 does not increase during the initial injury and fibrotic phase of bleomycin-treated mice. Instead, in venules and capillaries, there is an increase in its expression, accompanied by an increase in leukocyte rolling, a phenomenon inhibited by treatment with anti-ICAM-1 monoclonal antibody (30). Furthermore, blockage of ICAM-1 via monoclonal antibodies inhibits leukocyte recruitment, but does not decrease hydroxyproline content or histopathological fibrosis, and therefore does not attenuate fibrosis (20). On the other hand, fibrotic ICAM1$^{-/-}$ mice exhibit decreased collagen content when compared with littermate controls. Moreover, mice with double knockout for ICAM-1 and L-selectin show a dramatic reduction in collagen deposition and fibrosis in response to bleomycin compared with littermate controls or single-knockout mice (16). Taken together, these data suggest that ICAM-1 determines the severity in lung fibrosis. Here, we show that not only endothelial cells, but also alveolar epithelial cells, express abundant amounts of ICAM-1 during disease, which is actively secreted to their environment. As such, epithelial ICAM-1, likely with the help of other adhesion molecules, is a critical contributor to fibrosis via increased secretion/shedding of ICAM-1 to the extracellular compartment.

Our data also show that sICAM-1 varies among individuals during the peak of fibrosis (*day 14*), yet this variation exhibited a strong correlation with compliance, reflecting that sICAM-1 can monitor disease severity in mice. In humans, sICAM-1 levels correlate with survival, even better when combined with other biomarkers. Shijubo and colleagues (35) recently performed repetitive measures of ICAM-1 in four patients with IPF and one patient with sarcoidosis. They found that in rapidly declining patients with IPF (albeit $n = 3$), serum levels of ICAM-1 gradually increased in repetitive visits, when disease worsened until death within a period of 3–12 mo (35). Furthermore, Okuda and others (25) recently reported that in the early phase of acute exacerbations of IPF, ICAM-1 is increased in patients with IPF and might serve as a predictive indicator for prognosis. Taken together, these data demonstrate that, similar to fibrotic mice, ICAM-1 levels might predict disease severity, exacerbations, and mortality in patients with IPF.

We initially measured sICAM-1 in a multianalyte, bead-based assay with the Luminex platform. To corroborate our findings, we validated the upregulation of sICAM-1 by ELISA, in which we observed a significant increase in sICAM-1 at *day 14*. The differences in the concentrations of sICAM-1 using the Luminex and ELISA assays likely results from multiple factors attributable to interassay variation, epitope specificity from manufacturer to manufacturer, dynamic range differences between fluorescence-based detection and absorbance-based assay quantification, all of which are currently debated parameters limiting the area of biomarker research (7).

In summary, our studies demonstrate that ICAM-1 is expressed in the healthy lung epithelium. During injury and fibrosis, ICAM-1 is shed and its plasma levels increase, which correlate well with lung function decline in experimental lung fibrosis. Plasma levels of sICAM-1 measured at *day* 9 after the induction of fibrosis may predict worsening of lung function, and at the same time, higher levels of sICAM-1 were associated with increased mortality. These studies indicate that sICAM-1 could be considered as an indicator of ongoing lung injury and fibrosis and might help to monitor disease progression and therapeutic responses in preclinical models of fibrosis.

ACKNOWLEDGMENTS

We thank Daniela Dietel, Constanze Heise, and Katharina Lippl for providing excellent technical assistance, and the Helmholtz Association for supporting this work.

GRANTS

The study was supported by the Helmholtz Association and the German Center for Lung Research (DZL).

DISCLOSURES

No conflicts of interest, financial or otherwise are declared by the authors.

AUTHOR CONTRIBUTIONS

I.E.F., M.K., A.x.Y., and O.E. conception and design of research; I.E.F., O.V.A., and K.M. performed experiments; I.E.F., O.V.A., and O.E. analyzed data; I.E.F., O.V.A., M.K., A.x.Y., and O.E. interpreted results of experiments; I.E.F. prepared figures; I.E.F. drafted manuscript; I.E.F., O.V.A., K.M., M.K., A.x.Y., and O.E. edited and revised manuscript; I.E.F., O.V.A., K.M., M.K., A.x.Y., and O.E. approved final version of manuscript.

REFERENCES

1. **Ask K, Labiris R, Farkas L, Moeller A, Froese A, Farncombe T, McClelland GB, Inman M, Gauldie J, Kolb MR.** Comparison between conventional and "clinical" assessment of experimental lung fibrosis. *J Transl Med* 6: 16, 2008.
2. **B Moore B, Lawson WE, Oury TD, Sisson TH, Raghavendran K, Hogaboam CM.** Animal models of fibrotic lung disease. *Am J Respir Cell Mol Biol* 49: 167–179, 2013.
3. **Barkauskas CE, Noble PW.** Cellular mechanisms of tissue fibrosis. 7. New insights into the cellular mechanisms of pulmonary fibrosis. *Am J Physiol Cell Physiol* 306: C987–C996, 2014.
4. **Bauer Y, Tedrow J, de Bernard S, Birker-Robaczewska M, Gibson KF, Guardela BJ, Hess P, Klenk A, Lindell KO, Poirey S, Renault B, Rey M, Weber E, Nayler O, Kaminski N.** A novel genomic signature with translational significance for human idiopathic pulmonary fibrosis. *Am J Respir Cell Mol Biol* 52: 217–231, 2015.
5. **Behr J.** Evidence-based treatment strategies in idiopathic pulmonary fibrosis. *Eur Respir Rev* 22: 163–168, 2013.
6. **Bonniaud P, Margetts PJ, Kolb M, Haberberger T, Kelly M, Robertson J, Gauldie J.** Adenoviral gene transfer of connective tissue growth factor in the lung induces transient fibrosis. *Am J Respir Crit Care Med* 168: 770–778, 2003.
7. **Breen EC, Reynolds SM, Cox C, Jacobson LP, Magpantay L, Mulder CB, Dibben O, Margolick JB, Bream JH, Sambrano E, Martinez-Maza O, Sinclair E, Borrow P, Landay AL, Rinaldo CR, Norris PJ.** Multisite comparison of high-sensitivity multiplex cytokine assays. *Clin Vaccine Immunol* 18: 1229–1242, 2011.
8. **Casoni GL, Tomassetti S, Cavazza A, Colby TV, Dubini A, Ryu JH, Carretta E, Tantalocco P, Piciucchi S, Ravaglia C, Gurioli C, Romagnoli M, Gurioli C, Chilosi M, Poletti V.** Transbronchial lung cryobi-

opsy in the diagnosis of fibrotic interstitial lung diseases. *PLoS One* 9: e86716, 2014.
9. **Dancey C, Reidy J.** *Statistics Without Maths for Psychology: Using SPSS for Windows*. London: Prentice Hall, 2004.
10. **du Bois RM.** Strategies for treating idiopathic pulmonary fibrosis. *Nat Rev Drug Discov* 9: 129–140, 2010.
11. **Essick E, Sithu S, Dean W, D'Souza S.** Pervanadate-induced shedding of the intercellular adhesion molecule (ICAM)-1 ectodomain is mediated by membrane type-1 matrix metalloproteinase (MT1-MMP). *Mol Cell Biochem* 314: 151–159, 2008.
12. **Fernandez IE, Eickelberg O.** The impact of TGF-beta on lung fibrosis: from targeting to biomarkers. *Proc Am Thorac Soc* 9: 111–116, 2012.
13. **Fernandez IE, Eickelberg O.** New cellular and molecular mechanisms of lung injury and fibrosis in idiopathic pulmonary fibrosis. *Lancet* 380: 680–688, 2012.
14. **Flaherty KR, Khanna D.** Idiopathic or connective tissue disease-associated interstitial lung disease: a case of HRCT mimicry. *Thorax* 69: 205–206, 2014.
15. **Hadi AM, Mouchaers KT, Schalij I, Grunberg K, Meijer GA, Vonk-Noordegraaf A, van der Laarse WJ, Belien JA.** Rapid quantification of myocardial fibrosis: a new macro-based automated analysis. *Cell Oncol (Dordr)* 34: 343–354, 2011.
16. **Hamaguchi Y, Nishizawa Y, Yasui M, Hasegawa M, Kaburagi Y, Komura K, Nagaoka T, Saito E, Shimada Y, Takehara K, Kadono T, Steeber DA, Tedder TF, Sato S.** Intercellular adhesion molecule-1 and L-selectin regulate bleomycin-induced lung fibrosis. *Am J Pathol* 161: 1607–1618, 2002.
17. **John G, Kohse K, Orasche J, Reda A, Schnelle-Kreis J, Zimmermann R, Schmid O, Eickelberg O, Yildirim AO.** The composition of cigarette smoke determines inflammatory cell recruitment to the lung in COPD mouse models. *Clin Sci (Lond)* 126: 207–221, 2014.
18. **King TE Jr, Bradford WZ, Castro-Bernardini S, Fagan EA, Glaspole I, Glassberg MK, Gorina E, Hopkins PM, Kardatzke D, Lancaster L, Lederer DJ, Nathan SD, Pereira CA, Sahn SA, Sussman R, Swigris JJ, Noble PW; ASCEND Study Group.** A phase 3 trial of pirfenidone in patients with idiopathic pulmonary fibrosis. *N Engl J Med* 370: 2083–2092, 2014.
19. **Ley B, Bradford WZ, Vittinghoff E, Weycker D, du Bois RM, Collard HR.** Predictors of mortality poorly predict common measures of disease progression in idiopathic pulmonary fibrosis. *Am J Respir Crit Care Med*. First published March 3, 2016.
20. **Matsuse T, Teramoto S, Katayama H, Sudo E, Ekimoto H, Mitsuhashi H, Uejima Y, Fukuchi Y, Ouchi Y.** ICAM-1 mediates lung leukocyte recruitment but not pulmonary fibrosis in a murine model of bleomycin-induced lung injury. *Eur Respir J* 13: 71–77, 1999.
21. **Mendez MP, Morris SB, Wilcoxen S, Greeson E, Moore B, Paine R 3rd.** Shedding of soluble ICAM-1 into the alveolar space in murine models of acute lung injury. *Am J Physiol Lung Cell Mol Physiol* 290: L962–L970, 2006.
22. **Mercer PF, Abbott-Banner K, Adcock IM, Knowles RG.** Translational models of lung disease. *Clin Sci (Lond)* 128: 235–256, 2015.
23. **Mouratis MA, Aidinis V.** Modeling pulmonary fibrosis with bleomycin. *Curr Opin Pulm Med* 17: 355–361, 2011.
24. **Mutze K, Vierkotten S, Milosevic J, Eickelberg O, Konigshoff M.** Enolase 1 (ENO1) and protein disulfide-isomerase associated 3 (PDIA3) regulate Wnt/beta-catenin-driven trans-differentiation of murine alveolar epithelial cells. *Dis Model Mech* 8: 877–890, 2015.
25. **Okuda R, Matsushima H, Aoshiba K, Oba T, Kawabe R, Honda K, Amano M.** Soluble intercellular adhesion molecule-1 for stable and acute phases of idiopathic pulmonary fibrosis. *Springerplus* 4: 657, 2015.
26. **Peng R, Sridhar S, Tyagi G, Phillips JE, Garrido R, Harris P, Burns L, Renteria L, Woods J, Chen L, Allard J, Ravindran P, Bitter H, Liang Z, Hogaboam CM, Kitson C, Budd DC, Fine JS, Bauer CM, Stevenson CS.** Bleomycin induces molecular changes directly relevant to idiopathic pulmonary fibrosis: a model for "active" disease. *PLoS One* 8: e59348, 2013.
27. **Raghu G, Collard HR, Egan JJ, Martinez FJ, Behr J, Brown KK, Colby TV, Cordier JF, Flaherty KR, Lasky JA, Lynch DA, Ryu JH, Swigris JJ, Wells AU, Ancochea J, Bouros D, Carvalho C, Costabel U, Ebina M, Hansell DM, Johkoh T, Kim DS, King TE Jr, Kondoh Y, Myers J, Muller NL, Nicholson AG, Richeldi L, Selman M, Dudden RF, Griss BS, Protzko SL, Schünemann HJ; ATS/ERS/JRS/ALAT Committee on Idiopathic Pulmonary Fibrosis.** An official ATS/ERS/JRS/ALAT statement: idiopathic pulmonary fibrosis: evidence-based guidelines for diagnosis and management. *Am J Respir Crit Care Med* 183: 788–824, 2011.
28. **Richards TJ, Kaminski N, Baribaud F, Flavin S, Brodmerkel C, Horowitz D, Li K, Choi J, Vuga LJ, Lindell KO, Klesen M, Zhang Y, Gibson KF.** Peripheral blood proteins predict mortality in idiopathic pulmonary fibrosis. *Am J Respir Crit Care Med* 185: 67–76, 2012.
29. **Richeldi L, du Bois RM, Raghu G, Azuma A, Brown KK, Costabel U, Cottin V, Flaherty KR, Hansell DM, Inoue Y, Kim DS, Kolb M, Nicholson AG, Noble PW, Selman M, Taniguchi H, Brun M, Le Maulf F, Girard M, Stowasser S, Schlenker-Herceg R, Disse B, Collard HR; INPULSIS Trial Investigators.** Efficacy and safety of nintedanib in idiopathic pulmonary fibrosis. *N Engl J Med* 370: 2071–2082, 2014.
30. **Sato N, Suzuki Y, Nishio K, Suzuki K, Naoki K, Takeshita K, Kudo H, Miyao N, Tsumura H, Serizawa H, Suematsu M, Yamaguchi K.** Roles of ICAM-1 for abnormal leukocyte recruitment in the microcirculation of bleomycin-induced fibrotic lung injury. *Am J Respir Crit Care Med* 161: 1681–1688, 2000.
31. **Schiller HB, Fernandez IE, Burgstaller G, Schaab C, Scheltema RA, Schwarzmayr T, Strom TM, Eickelberg O, Mann M.** Time- and compartment-resolved proteome profiling of the extracellular niche in lung injury and repair. *Mol Syst Biol* 11: 819, 2015.
32. **Schmidt SL, Tayob N, Han MK, Zappala C, Kervitsky D, Murray S, Wells AU, Brown KK, Martinez FJ, Flaherty KR.** Predicting pulmonary fibrosis disease course from past trends in pulmonary function. *Chest* 145: 579–585, 2014.
33. **Scotton CJ, Hayes B, Alexander R, Datta A, Forty EJ, Mercer PF, Blanchard A, Chambers RC.** Ex vivo micro-computed tomography analysis of bleomycin-induced lung fibrosis for preclinical drug evaluation. *Eur Respir J* 42: 1633–1645, 2013.
34. **Shah RJ, Bellamy SL, Localio AR, Wickersham N, Diamond JM, Weinacker A, Lama VN, Bhorade S, Belperio JA, Crespo M, Demissie E, Kawut SM, Wille KM, Lederer DJ, Lee JC, Palmer SM, Orens J, Reynolds J, Shah A, Wilkes DS, Ware LB, Christie JD.** A panel of lung injury biomarkers enhances the definition of primary graft dysfunction (PGD) after lung transplantation. *J Heart Lung Transplant* 31: 942–949, 2012.
35. **Shijubo N, Imai K, Aoki S, Hirasawa M, Sugawara H, Koba H, Tsujisaki M, Sugiyama T, Hinoda Y, Yachi A, Asakawa M, Suzuki A.** Circulating intercellular adhesion molecule-1 (ICAM-1) antigen in sera of patients with idiopathic pulmonary fibrosis. *Clin Exp Immunol* 89: 58–62, 1992.
36. **Shijubo N, Imai K, Shigehara K, Honda Y, Koba H, Tsujisaki M, Hinoda Y, Yachi A, Ohmichi M, Hiraga Y, Abe S.** Soluble intercellular adhesion molecule-1 (ICAM-1) in sera and bronchoalveolar lavage fluid of patients with idiopathic pulmonary fibrosis and pulmonary sarcoidosis. *Clin Exp Immunol* 95: 156–161, 1994.
37. **Staab-Weijnitz CA, Fernandez IE, Knuppel L, Maul J, Heinzelmann K, Juan-Guardela BM, Hennen E, Preissler G, Winter H, Neurohr C, Hatz R, Lindner M, Behr J, Kaminski N, Eickelberg O.** FK506-binding protein 10, a potential novel drug target for idiopathic pulmonary fibrosis. *Am J Respir Crit Care Med* 192: 455–467, 2015.
38. **Strand MJ, Sprunger D, Cosgrove GP, Fernandez-Perez ER, Frankel SK, Huie TJ, Olson AL, Solomon J, Brown KK, Swigris JJ.** Pulmonary function and survival in idiopathic vs secondary usual interstitial pneumonia. *Chest* 146: 775–785, 2014.
39. **Therrien FJ, Agharazii M, Lebel M, Lariviere R.** Neutralization of tumor necrosis factor-alpha reduces renal fibrosis and hypertension in rats with renal failure. *Am J Nephrol* 36: 151–161, 2012.
40. **Walsh SL, Sverzellati N, Devaraj A, Keir GJ, Wells AU, Hansell DM.** Connective tissue disease related fibrotic lung disease: high resolution computed tomographic and pulmonary function indices as prognostic determinants. *Thorax* 69: 216–222, 2014.
41. **Wells AU, Desai SR, Rubens MB, Goh NS, Cramer D, Nicholson AG, Colby TV, du Bois RM, Hansell DM.** Idiopathic pulmonary fibrosis: a composite physiologic index derived from disease extent observed by computed tomography. *Am J Respir Crit Care Med* 167: 962–969, 2003.
42. **Wynn TA, Ramalingam TR.** Mechanisms of fibrosis: therapeutic translation for fibrotic disease. *Nat Med* 18: 1028–1040, 2012.

2.1.1. Author Contributions

Isis E. Fernandez	*in vivo* experiments and full mice handling of bleomycin-induced lung fibrosis and PBS controls, (Figure 1, 2, 3, 4, 5, 7); broncho-alveolar lavage and plasma harvesting for cell counts, Luminex and ELISAs (Fig. 1, 4, 5, 6, 7A, 7C); lung function measurement (Fig. 1, 3, 6); immunohistochemistry of H&E (Fig. 2), Masson Trichrome (Fig. 2), and Immunofluorescence (Fig. 7A); design and performance of semi-automatized histological evaluation with image J (Fig. 2B, C); qPCR of lung tissue homogenates (Fig. 4); Luminex and ELISAs (Fig. 4, 5, 6, 7A, 7C); study design, preparation of figures, writing and editing the manuscript
Oana V. Amarie	Support with *in vivo* experiments and teaching of bleomycin-induced lung fibrosis model, and mice handling.
Kathrin Mutze	Alveolar epithelial type 2 isolation from bleomycin mice and control, supernatant harvesting from cultured cells (Fig. 7C)
Melanie Königshoff	Supervision of Kathrin Mutze
Ali Ö. Yildirim	Supervision of Oana V. Amarie
Oliver Eickelberg	Design of the study, supervision of I. E. Fernandez, editing the manuscript

2.2. Pharmacokinetic and pharmacometabolomic study of pirfenidone in normal mouse tissues using high mass resolution MALDI-FTICR-mass spectrometry imaging

Na Sun, **Isis E. Fernandez**, Mian Wei, Ying Wu, Michaela Aichler, Oliver Eickelberg and Axel Walch

published first in

Histochemistry and Cell Biology. 2016 Feb;145(2):201-211. DOI 10.1007/s00418-015-1382-7

Histochem Cell Biol (2016) 145:201–211
DOI 10.1007/s00418-015-1382-7

ORIGINAL PAPER

Pharmacokinetic and pharmacometabolomic study of pirfenidone in normal mouse tissues using high mass resolution MALDI-FTICR-mass spectrometry imaging

Na Sun[1] · Isis E. Fernandez[2] · Mian Wei[1] · Yin Wu[1] · Michaela Aichler[1] · Oliver Eickelberg[2] · Axel Walch[1]

Accepted: 26 October 2015 / Published online: 8 December 2015

Abstract Given the importance of pirfenidone as the first worldwide-approved drug for idiopathic pulmonary fibrosis treatment, its pharmacodynamic properties and the metabolic response to pirfenidone treatment have not been fully elucidated. The aim of the present study was to get molecular insights of pirfenidone-related pharmacometabolomic response using MALDI-FTICR-MSI. Quantitative MALDI-FTICR-MSI was carried out for determining the pharmacokinetic properties of pirfenidone and its related metabolites 5-hydroxymethyl pirfenidone and 5-carboxy pirfenidone in lung, liver and kidney. To monitor the effect of pirfenidone administration on endogenous cell metabolism, additional in situ endogenous metabolite imaging was performed in lung tissue sections. While pirfenidone is highly abundant and delocalized across the whole micro-regions of lung, kidney and liver, 5-hydroxymethyl pirfenidone and 5-carboxy pirfenidone demonstrate heterogeneous distribution patterns in lung and kidney. In situ endogenous metabolite imaging study of lung tissue indicates no significant effects of pirfenidone on metabolic pathways. Remarkably, we found 129 discriminative *m/z* values which represent clear differences between control and treated lungs, the majority of which are currently unknown. PCA analysis and heatmap view can accurately distinguish control and treated groups. This is the first pharmacokinetic study to investigate the tissue distribution of orally administered pirfenidone and its related metabolites simultaneously in organs without labeling. The combination of pharmametabolome with histological features provides detailed mapping of drug effects on metabolism as response of heathy lung tissue to pirfenidone treatment.

Keywords Pirfenidone · Idiopathic pulmonary fibrosis · 5-Hydroxymethyl pirfenidone · 5-Carboxy pirfenidone · Pharmacokinetics · Pharmacometabolomics · Mass spectrometry imaging

Abbreviations

$AUC_{0-\infty}$	Area under the curve from 0 to infinity
C_{max}	Maximum concentration
CASI	Continuous accumulation of selected ions
CID	Collision-induced dissociation
CMC	Carboxymethyl cellulose
FTICR	Fourier transform ion cyclotron resonance
$T_{1/2}$	Half-life
IPF	Idiopathic pulmonary fibrosis
ITO	Indium tin oxide
LC–MS/MS	Liquid chromatography–tandem mass spectrometry
MALDI-MSI	Matrix-assisted laser desorption/ionization-mass spectrometry imaging
Pirfenidone-d5	5-Methyl-*N*-phenyl-2-1H-pyridone-d5
t_{max}	Time to maximum concentration
9-AA	9-Aminoacridine

Oliver Eickelberg and Axel Walch have contributed equally to this work.

Electronic supplementary material The online version of this article (doi:10.1007/s00418-015-1382-7) contains supplementary material, which is available to authorized users.

✉ Oliver Eickelberg
oliver.eickelberg@helmholtz-muenchen.de

✉ Axel Walch
axel.walch@helmholtz-muenchen.de

[1] Research Unit Analytical Pathology, German Research Center for Environmental Health (GmbH), Helmholtz Zentrum München, Neuherberg, Germany

[2] Comprehensive Pneumology Center, German Center for Lung Research (DZL), Ludwig Maximilian University München, Helmholtz Zentrum München, Neuherberg, Germany

Introduction

Idiopathic pulmonary fibrosis (IPF) is a chronic, progressive parenchymal lung disease characterized by exaggerated extracellular matrix deposition within the lungs in the absence of known stimuli (Fernandez and Eickelberg 2012; Nalysnyk et al. 2012; Raghu et al. 2011). IPF exhibits the worst prognosis of all diffuse parenchymal lung diseases with a medium survival after diagnosis of 3–5 years (King et al. 2011). Pirfenidone was the first drug approved for IPF treatment, initially in the EU and recently in the USA, after it was demonstrated that pirfenidone slowed IPF progression by decreasing FEV1 (forced expiratory volume in 1 s) decline in multiple studies (King et al. 2014; Noble et al. 2011). Although pirfenidone treatment is now routinely and often used in clinical practice as a therapeutic strategy for IPF, its detailed mechanisms of action have not been fully elucidated.

Traditionally, pharmacokinetic studies employ liquid chromatography–tandem mass spectrometry (LC–MS/MS), owing to its high detection and quantification accuracy and its capacity to analyze a broad range of sample concentrations (Lee and Kerns 1999). However, LC–MS/MS measurements require extraction of the compounds of interest prior to measurement. This introduces a loss of spatial information, which is an important factor to consider as compounds may have inhomogeneous distribution in tissues (Mouton et al. 2008). In contrast, matrix-assisted laser desorption/ionization-mass spectrometry imaging (MALDI-MSI) mass spectra are acquired by measuring spots, referred to as pixels, in a predefined raster across sample tissue sections, resulting in a two-dimensional distribution map for each measured *m/z* value. This allows the acquisition of spatial expression profiles, while preserving cellular and molecular integrity, combining the molecule's spatial organization with specific histological features (Balluff et al. 2011; Norris and Caprioli 2013; Walch et al. 2008). Mass spectrometers with high resolving power and sub-ppm mass accuracy, such as Fourier transform ion cyclotron resonance (FTICR) and orbitrap, allow resolution of compound peaks from endogenous species with similar nominal masses (Castellino et al. 2011; Cornett et al. 2008; Römpp et al. 2011). These advances broaden MSI's potential for pharmacokinetic and pharmacometabolomic studies, which is capable of performing simultaneous compound and endogenous metabolite imaging in the full MS scan mode, often without requiring MS/MS experiments (Cornett et al. 2008; Römpp et al. 2011).

Here we show for the first time that MALDI-FTICR-MSI is a novel platform for determining the pharmacokinetic properties of pirfenidone and its related metabolites, 5-hydroxymethyl pirfenidone and 5-carboxy pirfenidone. Additionally, to gain molecular insight as response of pirfenidone treatment in lung tissue, we performed endogenous metabolite imaging analysis to elucidate the drug's effects on metabolism and pathways. The correlation of pharmacological and metabolomic data provides comprehensive information that indicates response to drug treatment.

Materials and methods

Animals

Eight- to ten-week-old female C57BL/6N mice were obtained from Charles River Laboratories. The experiments were performed under strict governmental and international guidelines and were approved by the local government for the administrative region of Upper Bavaria. The protocol was approved by the ethics committee of the regional governmental commission for animal protection.

Drug administration and tissue collection

Pirfenidone (Selleckchem, Houston, USA) was dissolved in carboxymethyl cellulose (CMC) and administered by oral gavage at a dose of 500 mg/kg body weight. Control mice received CMC alone. Control and treated animals were killed at 10, 30, 45, 60, 90 and 240 min following drug administration. Three independent biological replicates were performed for each time point. The liver, kidneys and lungs were immediately dissected, snap-frozen in liquid nitrogen and stored at −80 °C until sectioned.

Tissue sectioning

Frozen tissues were cut into 12-µm-thick sections at −20 °C in a cryo-microtome (Leica CM1950, Leica Microsystems, Germany). The left lung lobes (non-inflated) were sectioned vertically along the long, flat, frontal plane to maximize the anatomical features. The left kidneys were sectioned midline. The left liver lobes were sliced in such a way to get maximum tissue areas.

The sections were thaw-mounted onto indium tin oxide (ITO)-coated MALDI target slides (Bruker Daltonics, Germany) and stored in −80 °C freezer until use. After the tissue sectioning, the MALDI-MSI measurements were performed as soon as possible. The maximum storage time of the tissue sections in −80 °C is 2 days.

Quantitative MALDI-FTICR-MSI of pirfenidone and related metabolites on lung, kidney and liver sections at different time intervals

For quantitative MALDI-MSI analysis of pirfenidone and related metabolites, we used a MSI quantification

approach, which was adapted from previous publications (Kallback et al. 2012; Pirman et al. 2013). 5-methyl-*N*-phenyl-2-1H-pyridone-d5 (pirfenidone-d5, Santa Cruz Biotechnology, Germany) was used as internal standard to compensate for ion suppression effects due to the biochemical microenvironment and varying histological structures. Briefly, tissue sections were spray-coated with pirfenidone-d5 internal standard solution (0.1 mmol/L pirfenidone-d5 in 50 % methanol) using a SunCollect™ automatic sprayer (Sunchrom, Friedrichsdorf, Germany). Four layers were applied with a flow rate of 5, 15, 30 and 40 µL/min, respectively. Following internal standard application, a 30 mg/mL super-DHB matrix (Sigma-Aldrich, Germany) in a mixture of 50:50:0.2 methanol:H_2O:trifluoroacetic acid (v/v) was applied using an automated spray coating machine (ImagePrep, Bruker Daltonics, Germany) to simultaneously extract and crystallize the analytes and internal standard.

To create an absolute quantification calibration curve, a 1 mmol/L synthetic pirfenidone stock solution in 50 % (v/v) methanol was prepared. The stock solution was serially diluted with H_2O to the following standard concentrations: 1, 0.4, 0.1, 0.06, 0.04, 0.01 and 0.005 mmol/L. Diluted pirfenidone standard solutions and an H_2O blank (0.3 µL) were spotted onto control kidney, liver or lung tissue sections. The internal pirfenidone-d5 standard and super-DHB matrix were homogenously deposited as described above.

MALDI-FTICR-MSI (Solarix 7T, Bruker Daltonics, Germany) was performed in continuous accumulation of selected ions (CASI) mode, which enhanced the low abundance species intensities, allowing for their detection. MSI measurements were performed with a 70 µm spatial resolution. Mass spectra were acquired in positive mode using 100 laser shots at a frequency of 1 kHz. The mass-selective quadrupole was set to 186.1 *m/z* with a window of 130 *m/z*. MALDI-FTICR-MS resolution of the drug peaks (pirfenidone *m/z* 186.0913, 5-hydroxymethyl pirfenidone *m/z* 202.0863 and 5-carboxy pirfenidone *m/z* 216.0655) was between 140,000 and 180,000 analyzed by Bruker Compass Data Analysis 4.2 (Bruker Daltonics, Germany). For the identification of pirfenidone, the ions of m/z 186.0913 were accumulated by MALDI-FTICR-MS using CASI mode and fragmented using collision-induced dissociation (CID).

MALDI-FTICR-MSI and pharmacokinetic data analysis

The acquired spectra were processed using flexImaging software v. 4.0 (Bruker Daltonics, Germany). The analyte signal was normalized to the pirfenidone-d5 internal standard signal (MH^+ *m/z* 191.1227) to compensate for ion suppression effects. A calibration curve was established for each tissue type. Average spotted standard intensity was determined and correlated to the standard concentration over the area of the spot (pmol/mm^2). The data were displayed as the drug signal intensity plotted against the amount of drug per mm^2. Subsequently, the appropriate tissue section drug concentrations were calculated based on the signal intensity with respect to the calibration curve concentration.

For pharmacokinetic analysis, the maximum concentration (C_{max}), time to maximum concentration (t_{max}), half-life ($T_{1/2}$) and area under the curve from 0 to infinity ($AUC_{0-\infty}$) were estimated by non-compartmental analysis using Phoenix® WinNonlin® software v. 6.3 (Pharsight Corp., Cary, NC). The elimination rate constant was calculated by linear regression from the terminal linear concentrations (last four time points). Three biological replicates were performed.

H&E staining and histology

Following the MALDI imaging experiments, the matrix was removed with 70 % ethanol. The tissue sections were stained with hematoxylin and eosin. Slides were scanned with a MIRAX DESK digital slide-scanning system (Carl Zeiss MicroImaging, Göttingen, Germany).

MADLI-MSI for endogenous metabolite imaging

Endogenous metabolite imaging was performed on lung tissue following 45-min pirfenidone treatment. Control mice received CMC alone. Three independent biological replicates were performed. The matrix solution was prepared by dissolving 9-aminoacridine (9-AA) hydrochloride monohydrate matrix (Sigma-Aldrich, Germany) at 10 mg/mL in 70 % methanol and sprayed by a SunCollect™ automatic sprayer (Sunchrom, Friedrichsdorf, Germany). The flow rate was performed at 10, 20, 30 and 40 µL/min, respectively, for the first 4 layers. The following 4 layers were performed at 40 µL/min. The MALDI-MSI experiments were performed on MALDI-FTICR-MS using 50 laser shots at a frequency of 500 Hz. Mass imaging data were acquired in negative ionization mode with 70 µm spatial resolution. Signals from mass range of *m/z* 50–1000 were collected. For identification of metabolites, on tissue MS/MS analysis was performed by MALDI-FTICR-MS using CASI mode. Metabolites were either identified by comparing the observed MS/MS spectra with standard compounds or by matching accurate mass with databases (mass accuracy ≤3 ppm, METLIN, http://metlin.scripps.edu/; Human Metabolome Database, http://www.hmdb.ca/; MassTRIX, http://masstrix3.helmholtz-muenchen.de/masstrix3/) (Buck et al. 2015; Sun et al. 2014).

Statistical analysis of endogenous metabolite imaging data

The acquired MSI data underwent spectra processing in flexImaging. The raw data were normalized against the root-mean-square of all data points. The average spectra of defined regions of interest were exported as.csv files and subsequently processed by MATLAB® R2013a (Mathworks, USA). A self-implemented MATLAB analysis pipeline was generated based on the work of McDonnell et al. 2010 (McDonnell et al. 2010). Baseline correction was completed by interpolating between given equally spaced intervals (spacing 0.02 Da). Resampling was performed using a 0.005 Da step width, and the smoothing operation was carried out using a Kaiser window of size 3. Using an adapted version of the LIMPIC algorithm (Mantini et al. 2007), peaks were picked using a minimal peak width of 0.0005, a noise-threshold of 4 and an intensity threshold percentage of 0.01. Isotopes were excluded. To identify statistically significant differences in *m/z* values, the peak lists were analyzed with the Student's *t* test. As a result, a list of significantly different metabolites could be achieved with the corresponding $p \leq 0.05$ and intensity fold change ≥ 2.

Results

Pirfenidone and related metabolite distribution as imaged by MALDI-FTICR-MSI

According to published antifibrotic and pharmacokinetic studies of pirfenidone in animal models (Schaefer et al. 2011), we chose a single oral dose of 500 mg/kg body weight pirfenidone in C57BL/6N mice, which enables the detection of the low abundant metabolite products of pirfenidone. The chemical structures of pirfenidone and the two related metabolites, 5-hydroxymethyl pirfenidone and 5-carboxy pirfenidone, are shown in Fig. 1. MALDI-FTICR-MSI was used to perform pharmacokinetic studies of pirfenidone, 5-hydroxymethyl pirfenidone and 5-carboxy pirfenidone in lung, liver and kidney. Acquired mass spectra showed that pirfenidone, 5-hydroxymethyl pirfenidone and 5-carboxy pirfenidone were successfully detected in positive ion mode with the $[M+H]^+$ ions located at *m/z* 186.0913, 202.0863 and 216.0655, respectively (Fig. 2). On tissue MS/MS spectrum of the peak 186.0913 confirmed the identity of pirfenidone in the dosed lung sections (Fig. 3). Figure 4 shows the MSI of pirfenidone, 5-hydroxymethyl pirfenidone and 5-carboxy pirfenidone with corresponding histologically stained tissue sections. Pirfenidone is abundant across all tissue compartments in lung, liver and kidney. In contrast, the two metabolic products demonstrate different distribution patterns in both the lung and kidney. For example, 5-hydroxymethyl pirfenidone is mainly localized along the major bronchi. In kidney, the highest abundance of the two metabolites was predominantly observed in the medulla.

Quantification of pirfenidone and related metabolites in different tissue sections

MALDI-MSI quantification was performed to track the drug transport into specific organs and tissue compartments. The quantification is based on MSI analysis of the treated tissue sections compared with pirfenidone calibration standards deposited on control tissue sections. All calculations were conducted following normalization to the pirfenidone-d5 internal standard signal in order to minimize potential artefacts (Kallback et al. 2012). The pirfenidone concentration was divided by the corresponding area of the pixel (pmol/mm^2) and plotted against the peak intensity to establish a calibration curve. As an example, Fig. 5 shows the calibration curve generated for quantification study in lung tissue (3 replicates). The data showed

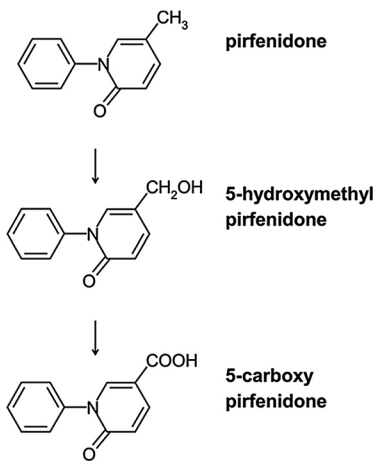

Fig. 1 Chemical structures of pirfenidone, 5-hydroxymethyl pirfenidone and 5-carboxy pirfenidone

	Neutral monoisotopic mass	$(M+H)^+$ monoisotopic mass	Molecular formula
pirfenidone	185.0841	186.0913	$C_{12}H_{11}NO$
5-hydroxymethyl pirfenidone	201.0790	202.0863	$C_{12}H_{11}NO_2$
5-carboxy pirfenidone	215.0582	216.0655	$C_{12}H_9NO_3$

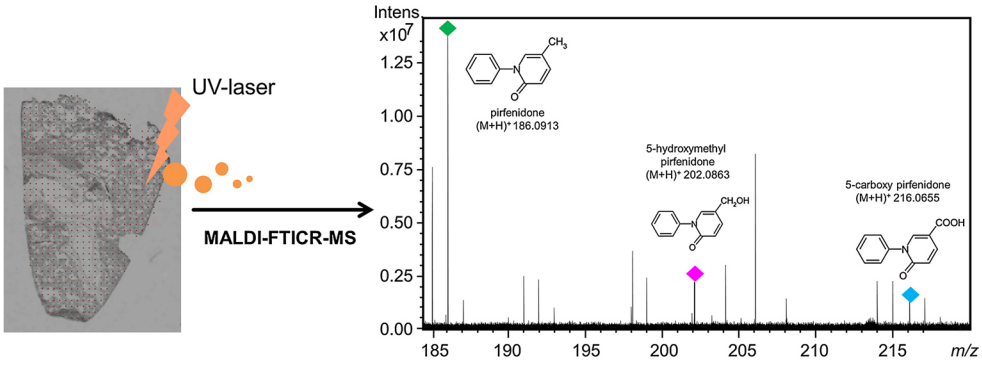

Fig. 2 A typical MALDI-FTICR-MSI mass spectra acquired from the lung tissue. Pirfenidone, 5-hydroxymethyl pirfenidone and 5-carboxy pirfenidone were detected in positive mode as $[M+H]^+$ ions at *m/z* 186.0913, 202.0863 and 216.0655, respectively

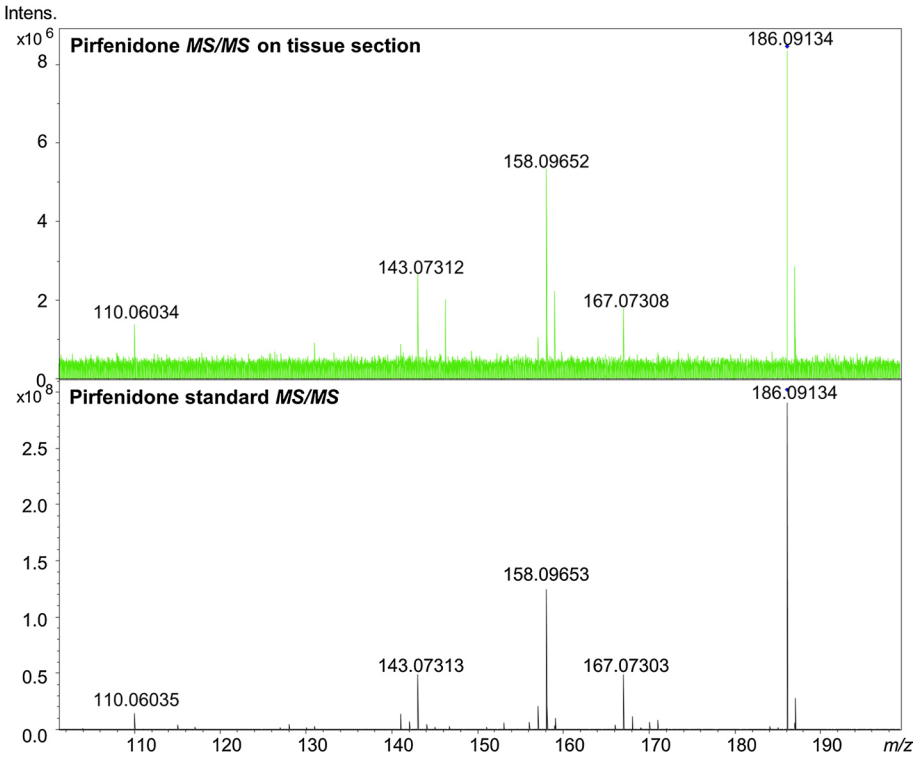

Fig. 3 Identification of pirfenidone in dosed lung sections. The on tissue MS/MS spectrum of pirfenidone (*m/z* 186.0913) shows a clear patten which matches the reference pirfenidone

sufficient linearity and reproducibility for downstream analysis. The concentration of pirfenidone in treated tissue was calculated by correlating its intensity value to the control tissue-specific calibration curve. Because of the structural similarity of 5-hydroxymethyl pirfenidone and 5-carboxy pirfenidone to the parent drug, the same calibration curve was also used to calculate their concentrations. These quantified data were employed for further pharmacokinetic analysis.

Pharmacokinetic analysis

The time courses and MSI images of pirfenidone and related metabolites, 5-hydroxymethyl pirfenidone and 5-carboxy pirfenidone, from lung tissue at 10, 30, 45, 60, 90 and 240 after oral drug administration are shown in Fig. 6. The highest concentration was observed for pirfenidone, followed by 5-hydroxymethyl pirfenidone and then 5-carboxy pirfenidone. The pharmacokinetic parameters were calculated using non-compartmental analysis in Phoenix® WinNonlin® v. 6.3. The estimated pharmacokinetic parameters of pirfenidone in lung, liver and kidney are listed in Table 1. The liver reached its maximum drug level at 30 min, followed by kidney and lung at 45 min. In addition, the liver showed the highest maximum concentration (C_{max}) and the largest area under the curve (AUC), which might be a result of the first-pass effect of the drug and explain the major gastrointestinal side effects (Kashikar et al. 2014). The degree of drug tissue perfusion was ranked as liver, kidney and lung, in descending order. This

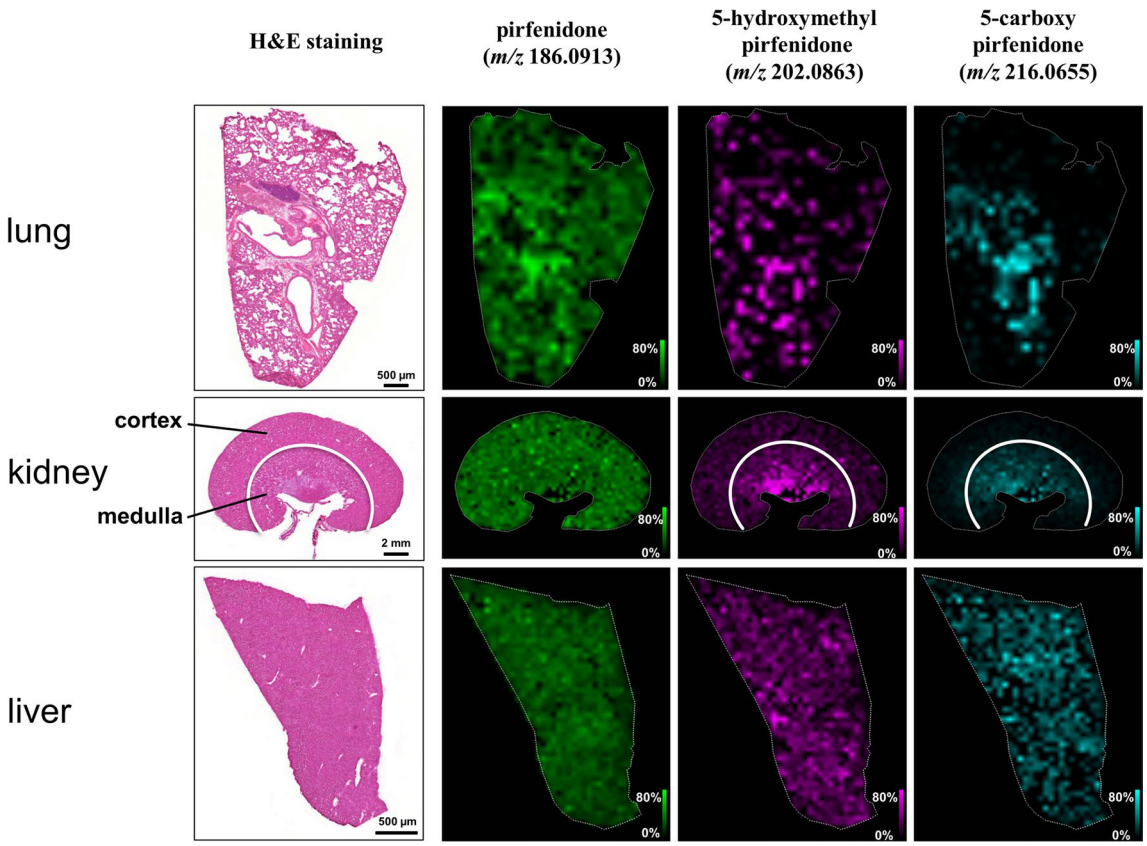

Fig. 4 The distribution of pirfenidone and related metabolites in lung, kidney and liver tissue sections from a mouse, 45 min following oral administration. MSI data were acquired with a 70 µm spatial resolution

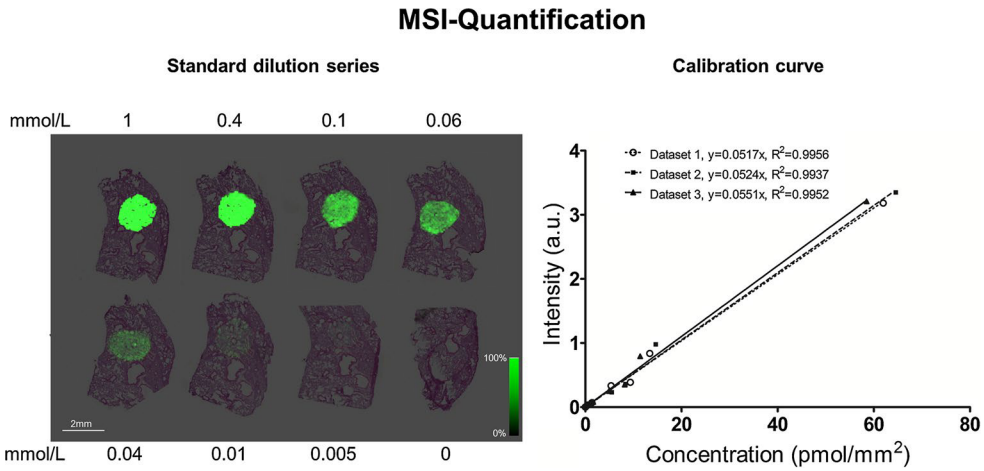

Fig. 5 Calibration curve of pirfenidone for MALDI-MSI quantification. As an example, a representative image of the calibration standard solutions of pirfenidone at different concentrations spotted onto control lung tissue is shown here. The calibration curve was created based on the intensity of the calibration standard peak as a function of the concentration per area (pmol/mm^2). Three replicates were carried out

is consistent with degree of blood perfusion associated with these organs (Giri et al. 2002). The time of maximum concentration (t_{max}) is 30 min in liver, 45 min in lung and kidney. The $T_{1/2}$ is 46 min in liver, 67 min in lung and 49 min in kidney. These data are comparable with previous plasma-based pharmacokinetic studies of humans and animal model studies by oral administration of pirfenidone (t_{max}: 16–60 min, $T_{1/2}$: 16–150 min) (Bruss et al. 2004; Shi et al. 2007; Wang et al. 2006).

Endogenous metabolite imaging

The administration of drugs can influence cell metabolism (Clayton et al. 2006; Ellero-Simatos et al. 2014; Wikoff

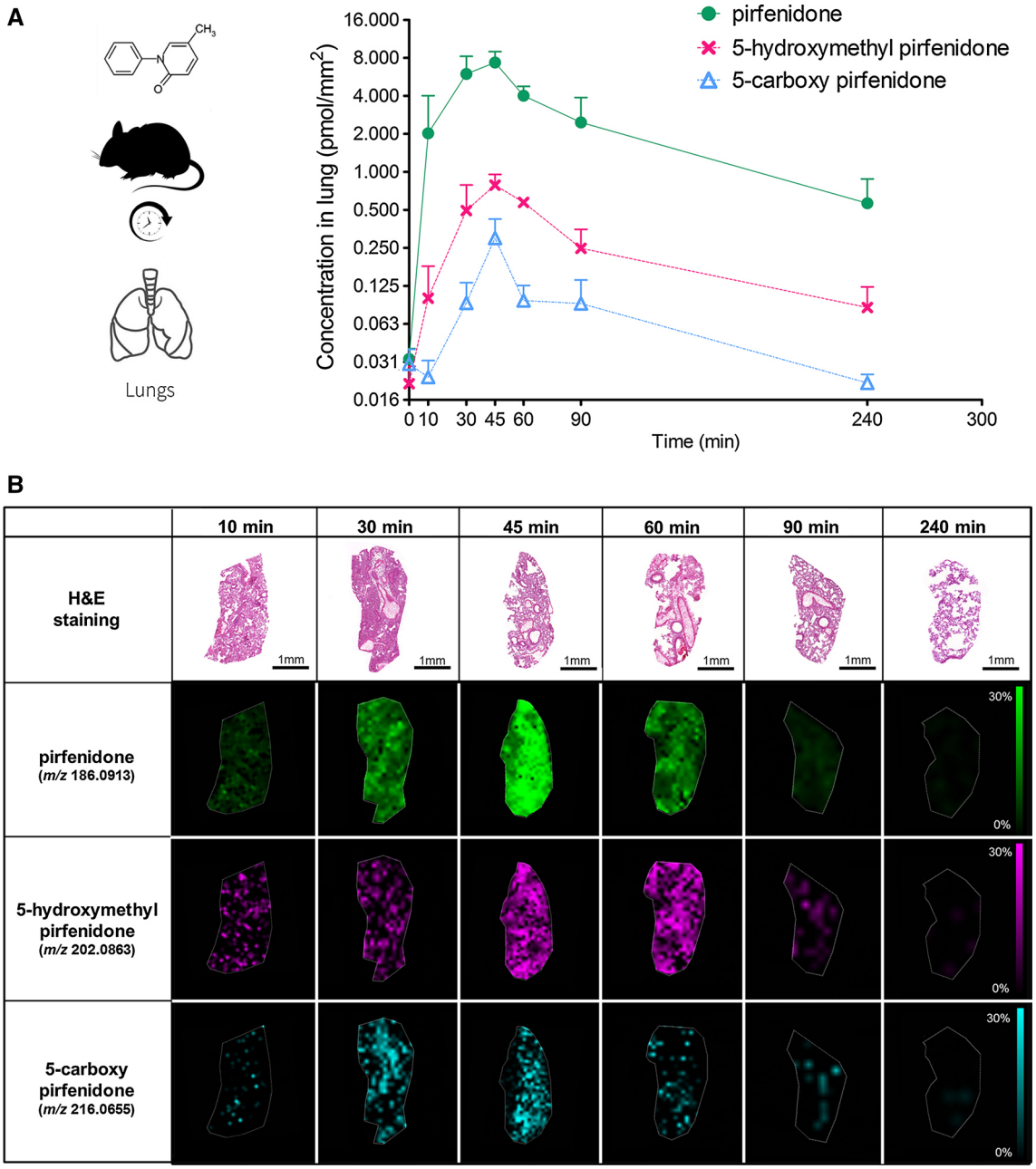

Fig. 6 **a** Time course of pirfenidone and related metabolites, 5-hydroxymethyl pirfenidone and 5-carboxy pirfenidone, in lung tissue by MALDI-FTICR-MSI. Data were acquired from three biological replicates. Log2 scale is used for y-axis. *Error bars* indicate standard error (3 biological replicates). **b** MALDI-MSI images of lung tissue of pirfenidone (186.0913 ± 0.002 Da) and the two metabolites, 5-hydroxymethyl pirfenidone (202.0863 ± 0.002 Da) and 5-carboxy pirfenidone (216.0655 ± 0.002 Da), at time points 10, 30, 45, 60, 90 and 240 min following drug administration

et al. 2013). To investigate the metabolic response to the administration of pirfenidone, in situ endogenous metabolite imaging was performed on lung tissue after 45-min (t_{max}) pirfenidone treatment. 9-AA was proven as a matrix that exhibits very few matrix-derived interferences in the low mass range, achieved high sensitivity and high linearity in negative ion mode for a wide range of low molecular weight metabolites (Edwards and Kennedy 2005; Miura et al. 2010a, b; Shroff et al. 2007). Therefore, in this study, we chose 9-AA for the endogenous metabolite imaging study, aiming for the simultaneous detection of a variety of cellular metabolites, i.e., nucleotide derivatives, central

Table 1 Pharmacokinetic parameters following a single oral pirfenidone dose (500 mg/kg) in mice (3 biological replicates)

Organ	C_{max} (pmol/mm^2)	t_{max} (min)	$T_{1/2}$ (min)	$AUC_{0-\infty}$ (min^2 pmol/mm^2)
Lung	7.36	45	67	658
Liver	19.3	30	46	2563
Kidney	8.29	45	49	959

C_{max} and t_{max} were taken directly from the observed data. $T_{1/2}$ and $AUC_{0-\infty}$ indicate terminal elimination of half-life and area under the concentration–time curve from time 0 to infinity, respectively

metabolic pathway metabolites, redox-related metabolites and amino acids. We found 129 discriminative *m/z* values that demonstrate clear differences between treated and control lungs, the majority of which are currently unknown (Supplementary data 1). PCA analysis and heatmap view can accurately distinguish between control and treated groups (Fig. 7). No significant effects on known metabolic pathways could be identified. As examples, nucleotide derivatives, glycolysis/gluconeogenesis, citrate cycle and redox-related metabolites remain unchanged after administration of pirfenidone (Fig. 8).

Discussion

Pharmacometabolomics is an emerging field that aims to monitor the effects of compounds on metabolic levels (Clayton et al. 2006; Ellero-Simatos et al. 2014; Wikoff et al. 2013). In this study, we used a state-of-the-art high mass resolution MALDI-FTICR-MSI quantification approach to investigate the pharmacokinetic and pharmacometabolomic properties of pirfenidone. This is the first study to visualize metabolic response to pirfenidone treatment and quantify orally administered pirfenidone and its related metabolites simultaneously in the lung and different organs without labeling. The data represented no obvious effects of pirfenidone on known metabolic pathways under physiological conditions. However, we observed alterations in 129 masses, indicating a clear response to pirfenidone treatment. Although the majority of them are unknown and the related mechanisms of actions remain elusive, these findings open new aspect for elucidating the metabolic signature of pirfenidone treatment. Further identification and/or experimental validation of these masses could provide insight into the mechanism of variation in drug response and predict treatment outcomes.

The pharmacokinetic parameters demonstrated rapidly absorption, metabolism and excretion of pirfenidone. These

Fig. 7 **a** MALDI-FTICR-MSI images of 8 unknown masses, which represent clear response after pirfenidone treatment. **b** PCA accurately distinguishes pirfenidone-treated lung samples from control groups. **c** Heatmap of the 129 discriminative masses which indicates clear separation between the control and pirfenidone-treated groups

results are consistent with plasma-based pharmacokinetic studies in humans and non-clinical species (Bruss et al. 2004, 2008; Giri et al. 2002; Shi et al. 2007; Wang et al. 2006). In contrast to previously published studies using intravenous pirfenidone administration (Bruss et al. 2008; Giri et al. 2002), the use of orally administered pirfenidone produces a more appropriate pharmacokinetic result, as it most closely resembles the clinical drug administration protocol. Moreover, compared with plasma pharmacokinetics studies, determining pirfenidone concentrations in organs could provide valuable information about drug efficacy and bioavailability.

High-resolution MALDI-FTICR-MSI enabled accurate localization of parent drug and its metabolites in various tissue types and their associated micro-regions. The two metabolic products of pirfenidone demonstrate heterogeneous distribution patterns in lung and kidney, whereas the parent drug is highly abundant and delocalized across the whole micro-regions of lung, kidney and liver. According to previous publications, pirfenidone is primarily metabolized by cytochrome P450 (CYPIA2), resulting in a stepwise formation of 5-hydroxymethyl pirfenidone and 5-carboxy pirfenidone (Giri et al. 2002; Schaefer et al. 2011). Studies on pirfenidone in experimental animal models reported anti-fibrotic activities in tissues, such as lung (Iyer et al. 1999), liver (Zhao et al. 2009) and kidney (Miric et al. 2001). Recently, the anti-fibrotic effects of two pirfenidone metabolites, 5-hydroxymethyl pirfenidone and 5-carboxy pirfenidone, were demonstrated with WI-38 cells in an in vitro lung fibroblast model (Togami et al. 2013). The comprehensive spatial distribution map correlates the differential biological function of the parent drug and metabolites with histological features, allowing for the elucidation of both the drug's biotransformation route and its mechanism of action.

In conclusion, our results demonstrate that MALDI-MSI can be employed to examine drug pharmacokinetic metabolism and elimination in multiple organs at a histological level. The quantitative analysis of pirfenidone in principal organs provides valuable information on both the general pharmacokinetic parameters and the micro-regional distribution. In the future, this technology would allow correlation of anti-fibrotic drugs to areas of fibrosis in the lung and will potentially unravel anti-remodeling processes in lung tissue via drug–metabolite–metabolome correlations.

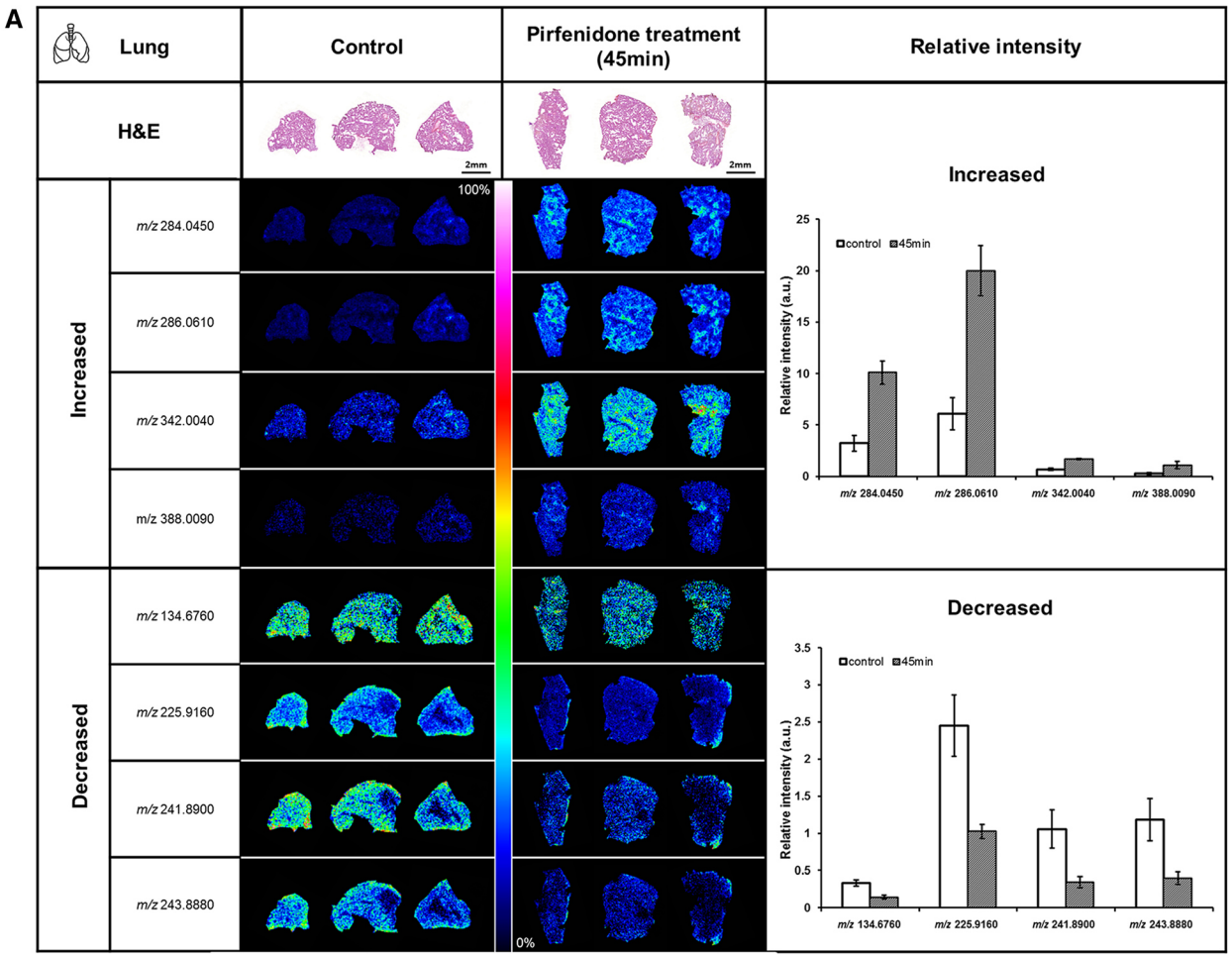
A
Lung
Control
Pirfenidone treatment (45min)
Relative intensity
H&E
2mm
2mm
Increased
m/z 284.0450
m/z 286.0610
m/z 342.0040
m/z 388.0090
Decreased
m/z 134.6760
m/z 225.9160
m/z 241.8900
m/z 243.8880
100%
0%
Increased
control 45min
Relative intensity (a.u.)
m/z 284.0450
m/z 286.0610
m/z 342.0040
m/z 388.0090
Decreased
control 45min
Relative intensity (a.u.)
m/z 134.6760
m/z 225.9160
m/z 241.8900
m/z 243.8880

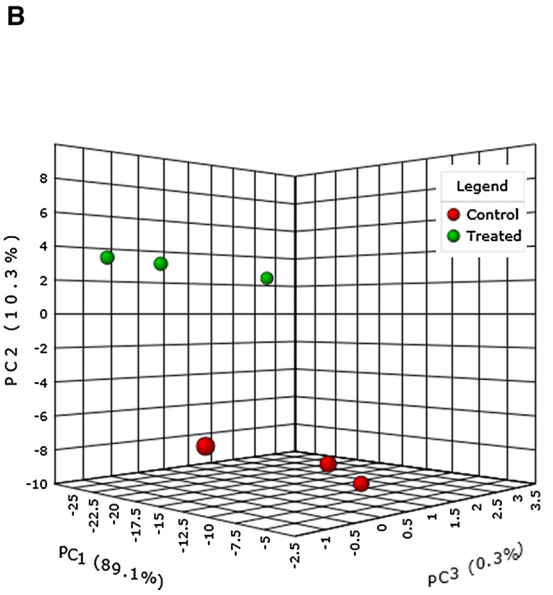
B
Legend
Control
Treated
PC2 (10.3%)
PC1 (89.1%)
PC3 (0.3%)

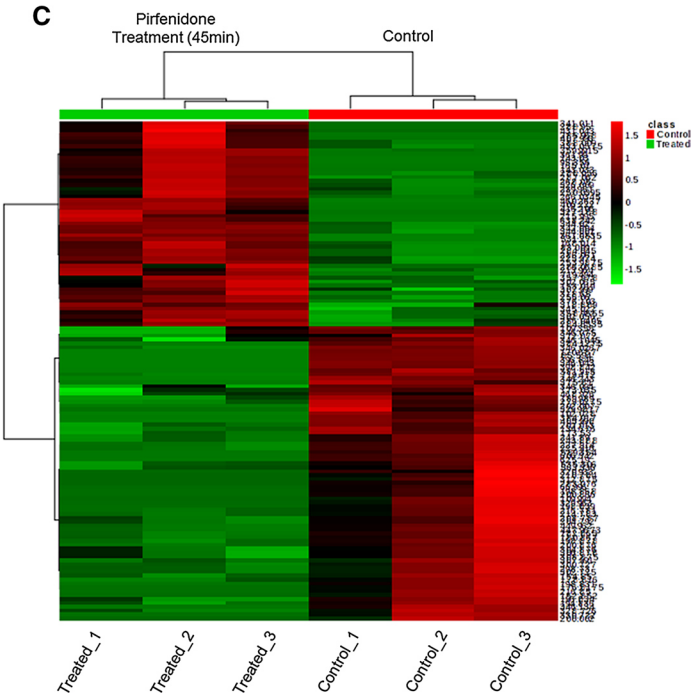
C
Pirfenidone Treatment (45min)
Control
class
Control
Treated
Treated_1
Treated_2
Treated_3
Control_1
Control_2
Control_3

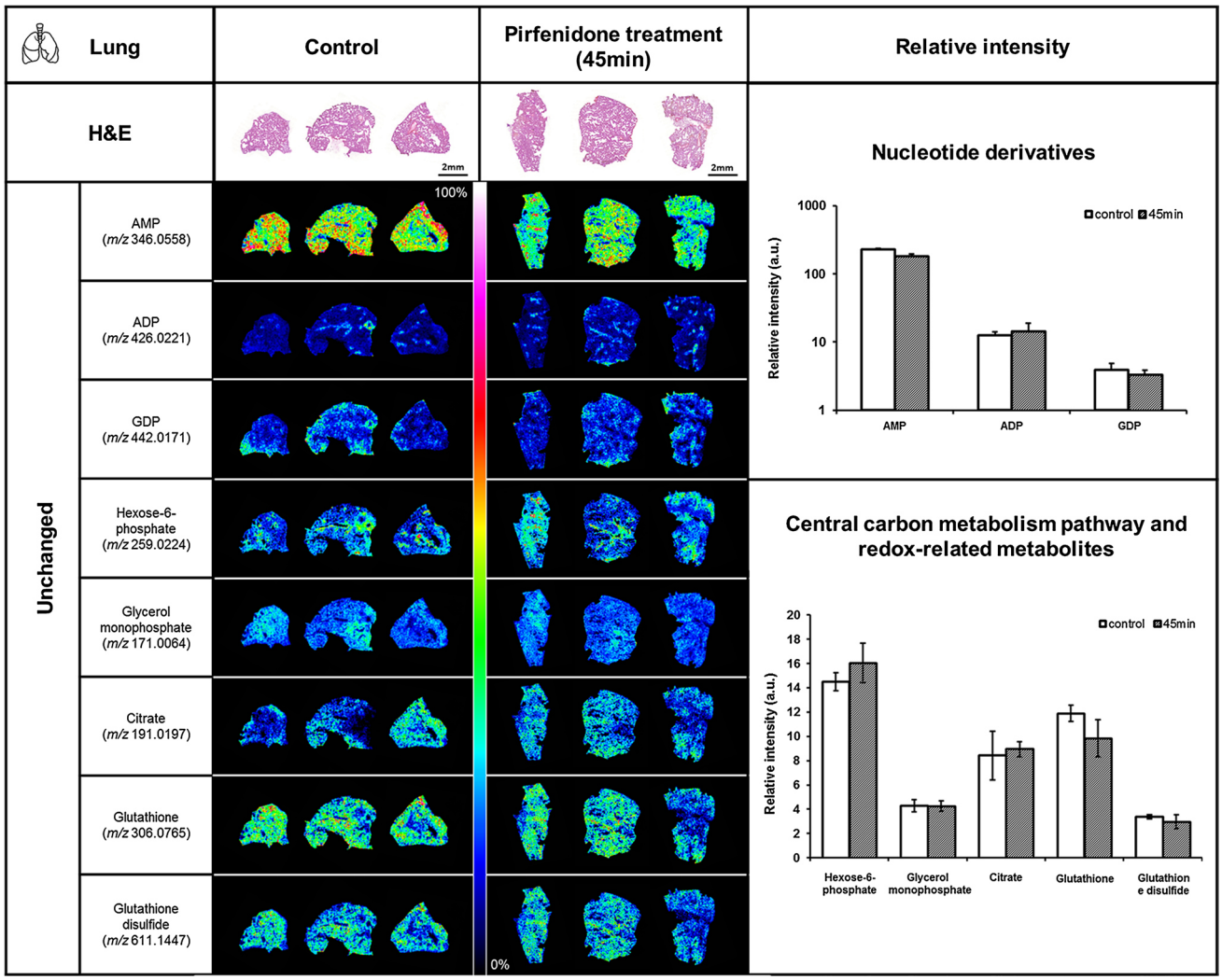

Fig. 8 In-situ endogenous metabolic imaging studies of lung tissue indicate no significant effects on known metabolic pathways. As examples, nucleotide derivatives, central carbon metabolism pathway and redox-related metabolites remain unchanged after administration of pirfenidone. The identification of ADP, AMP, GDP, citrate, glutathione and glutathione disulfide was carried out by *on tissue* MS/MS using MALDI-FTICR. The identification of hexose-6-phosphate and glycerol monophosphate was performed by accurate MS match with the databases (accuracy, 3 ppm)

Acknowledgments The authors would like to thank Claudia-Marieke Pflüger, Ulrike Buchholz, Gabriele Mettenleiter and Andreas Voss from the Research Unit Analytical Pathology, Constanze Heise and Daniela Dietel from the Comprehensive Pneumology Center, and Xiaomeng Wan from the University of North Carolina at Chapel Hill for providing technical assistance. We thank Alice Ly from the Research Unit Analytical Pathology for proofreading our manuscript.

Funding sources The study was supported by Helmholtz Zentrum München (TKP-Project), the German Center for Lung Research (DZL), the Ministry of Education and Research of the Federal Republic of Germany (BMBF) (01ZX1310B and 01IB10004E) and the Deutsche Forschungsgemeinschaft (SFB 824 TP Z02 and H01258/3-1).

Compliance with ethical standards

Conflict of interest The authors have declared no conflict of interest.

References

Balluff B, Schone C, Hofler H, Walch A (2011) MALDI imaging mass spectrometry for direct tissue analysis: technological advancements and recent applications. Histochem Cell Biol 136:227–244. doi:10.1007/s00418-011-0843-x

Bruss ML, Margolin SB, Giri SN (2004) Pharmacokinetics of orally administered pirfenidone in male and female beagles. J Vet Pharmacol Ther 27:361–367. doi:10.1111/j.1365-2885.2004.00612.x

Bruss ML, Stanley SD, Margolin SB, Giri SN (2008) Pharmacokinetics and metabolism of intravenous pirfenidone in sheep. Biopharm Drug Dispos 29:119–126. doi:10.1002/bdd.595

Buck A et al (2015) High-resolution MALDI-FT-ICR MS imaging for the analysis of metabolites from formalin-fixed paraffin-embedded clinical tissue samples. J Pathol. doi:10.1002/path.4560

Castellino S, Groseclose MR, Wagner D (2011) MALDI imaging mass spectrometry: bridging biology and chemistry in drug development. Bioanalysis 3:2427–2441. doi:10.4155/bio.11.232

Clayton TA et al (2006) Pharmaco-metabonomic phenotyping and personalized drug treatment. Nature 440:1073–1077. doi:10.1038/nature04648

Cornett DS, Frappier SL, Caprioli RM (2008) MALDI-FTICR imaging mass spectrometry of drugs and metabolites in tissue. Anal Chem 80:5648–5653. doi:10.1021/ac800617s

Edwards JL, Kennedy RT (2005) Metabolomic analysis of eukaryotic tissue and prokaryotes using negative mode MALDI time-of-flight mass spectrometry. Anal Chem 77:2201–2209. doi:10.1021/ac048323r

Ellero-Simatos S et al (2014) Pharmacometabolomics reveals that serotonin is implicated in aspirin response variability. CPT Pharmacom Syst Pharmacol 3:e125. doi:10.1038/psp.2014.22

Fernandez IE, Eickelberg O (2012) New cellular and molecular mechanisms of lung injury and fibrosis in idiopathic pulmonary fibrosis. Lancet 380:680–688. doi:10.1016/S0140-6736(12)61144-1

Giri SN, Wang Q, Xie Y, Lango J, Morin D, Margolin SB, Buckpitt AR (2002) Pharmacokinetics and metabolism of a novel antifibrotic drug pirfenidone, in mice following intravenous administration. Biopharm Drug Dispos 23:203–211. doi:10.1002/bdd.311

Iyer SN, Gurujeyalakshmi G, Giri SN (1999) Effects of pirfenidone on transforming growth factor-beta gene expression at the transcriptional level in bleomycin hamster model of lung fibrosis. J Pharmacol Exp Ther 291:367–373

Kallback P, Shariatgorji M, Nilsson A, Andren PE (2012) Novel mass spectrometry imaging software assisting labeled normalization and quantitation of drugs and neuropeptides directly in tissue sections. J Proteomics 75:4941–4951. doi:10.1016/j.jprot.2012.07.034

Kashikar V, Dhole S, Kandekar U, Khose P (2014) Study of mucoadhesive microsphere of pirfenidone for nasal drug delivery. Asian J Pharm 8:43–50

King TE Jr, Pardo A, Selman M (2011) Idiopathic pulmonary fibrosis. Lancet 378:1949–1961. doi:10.1016/S0140-6736(11)60052-4

King TE Jr et al (2014) A phase 3 trial of pirfenidone in patients with idiopathic pulmonary fibrosis. N Engl J Med 370:2083–2092. doi:10.1056/NEJMoa1402582

Lee MS, Kerns EH (1999) LC/MS applications in drug development. Mass Spectrom Rev 18:187–279. doi:10.1002/(SICI)1098-2787(1999)18:3/4<187:AID-MAS2>3.0.CO;2-K

Mantini D et al (2007) LIMPIC: a computational method for the separation of protein MALDI-TOF-MS signals from noise. BMC Bioinform 8:101. doi:10.1186/1471-2105-8-101

McDonnell LA, van Remoortere A, de Velde N, van Zeijl RJ, Deelder AM (2010) Imaging mass spectrometry data reduction: automated feature identification and extraction. J Am Soc Mass Spectrom 21:1969–1978. doi:10.1016/j.jasms.2010.08.008

Miric G, Dallemagne C, Endre Z, Margolin S, Taylor SM, Brown L (2001) Reversal of cardiac and renal fibrosis by pirfenidone and spironolactone in streptozotocin-diabetic rats. Br J Pharmacol 133:687–694. doi:10.1038/sj.bjp.0704131

Miura D, Fujimura Y, Tachibana H, Wariishi H (2010a) Highly sensitive matrix-assisted laser desorption ionization-mass spectrometry for high-throughput metabolic profiling. Anal Chem 82:498–504. doi:10.1021/ac901083a

Miura D, Fujimura Y, Yamato M, Hyodo F, Utsumi H, Tachibana H, Wariishi H (2010b) Ultrahighly sensitive in situ metabolomic imaging for visualizing spatiotemporal metabolic behaviors. Anal Chem 82:9789–9796. doi:10.1021/ac101998z

Mouton JW, Theuretzbacher U, Craig WA, Tulkens PM, Derendorf H, Cars O (2008) Tissue concentrations: do we ever learn? J Antimicrob Chemother 61:235–237. doi:10.1093/jac/dkm476

Nalysnyk L, Cid-Ruzafa J, Rotella P, Esser D (2012) Incidence and prevalence of idiopathic pulmonary fibrosis: review of the literature. Eur Respir Rev 21:355–361. doi:10.1183/09059180.00002512

Noble PW et al (2011) Pirfenidone in patients with idiopathic pulmonary fibrosis (CAPACITY): two randomised trials. Lancet 377:1760–1769. doi:10.1016/S0140-6736(11)60405-4

Norris JL, Caprioli RM (2013) Analysis of tissue specimens by matrix-assisted laser desorption/ionization imaging mass spectrometry in biological and clinical research. Chem Rev 113:2309–2342. doi:10.1021/cr3004295

Pirman DA, Kiss A, Heeren RM, Yost RA (2013) Identifying tissue-specific signal variation in MALDI mass spectrometric imaging by use of an internal standard. Anal Chem 85:1090–1096. doi:10.1021/ac3029618

Raghu G et al (2011) An official ATS/ERS/JRS/ALAT statement: idiopathic pulmonary fibrosis: evidence-based guidelines for diagnosis and management. Am J Respir Crit Care Med 183:788–824. doi:10.1164/rccm.2009-040GL

Römpp A, Guenther S, Takats Z, Spengler B (2011) Mass spectrometry imaging with high resolution in mass and space (HR(2) MSI) for reliable investigation of drug compound distributions on the cellular level. Anal Bioanal Chem 401:65–73. doi:10.1007/s00216-011-4990-7

Schaefer CJ, Ruhrmund DW, Pan L, Seiwert SD, Kossen K (2011) Antifibrotic activities of pirfenidone in animal models. Eur Respir Rev 20:85–97. doi:10.1183/09059180.00001111

Shi S, Wu J, Chen H, Chen H, Wu J, Zeng F (2007) Single- and multiple-dose pharmacokinetics of pirfenidone, an antifibrotic agent, in healthy Chinese volunteers. J Clin Pharmacol 47:1268–1276. doi:10.1177/0091270007304104

Shroff R, Muck A, Svatos A (2007) Analysis of low molecular weight acids by negative mode matrix-assisted laser desorption/ionization time-of-flight mass spectrometry. Rapid Commun Mass Spectrom 21:3295–3300. doi:10.1002/rcm.3216

Sun N et al (2014) High-resolution metabolite imaging of light and dark treated retina using MALDI-FTICR mass spectrometry. Proteomics 14:913–923. doi:10.1002/pmic.201300407

Togami K, Kanehira Y, Tada H (2013) Possible involvement of pirfenidone metabolites in the antifibrotic action of a therapy for idiopathic pulmonary fibrosis. Biol Pharm Bull 36:1525–1527

Walch A, Rauser S, Deininger SO, Hofler H (2008) MALDI imaging mass spectrometry for direct tissue analysis: a new frontier for molecular histology. Histochem Cell Biol 130:421–434. doi:10.1007/s00418-008-0469-9

Wang Y, Zhao X, Zhong J, Chen Y, Liu X, Wang G (2006) Simple determination of pirfenidone in rat plasma via high-performance liquid chromatography. Biomed Chromatogr 20:1375–1379. doi:10.1002/bmc.708

Wikoff WR et al (2013) Pharmacometabolomics reveals racial differences in response to atenolol treatment. PLoS ONE 8:e57639. doi:10.1371/journal.pone.0057639

Zhao XY, Zeng X, Li XM, Wang TL, Wang BE (2009) Pirfenidone inhibits carbon tetrachloride- and albumin complex-induced liver fibrosis in rodents by preventing activation of hepatic stellate cells. Clin Exp Pharmacol Physiol 36:963–968. doi:10.1111/j.1440-1681.2009.05194.x

2.2.1. Author Contributions

Na Sun	Performed MALDI-FTICR measurements, analyze the data (Fig. 1-8), study design, preparation figure, writing and editing of manuscript.
Isis E. Fernandez	Performed animal experiments, treated mice with Pirfenidone, harvested tissues (Fig. 2, 3, 4, 5, 6, 7A, 8). Study design, preparation and editing of manuscript.
Mian Wei	Performed MALDI-FTICR measurements.
Ying Wu	Performed MALDI-FTICR measurements.
Michaela Aichler	Data interpretation and analysis, editing of manuscript
Oliver Eickelberg	Supervision of I. E. Fernandez, study design, editing of manuscript
Axel Walch	Supervision of N. Sun, study design, preparation and editing of manuscript

2.2.2. Supplemental Information

Pharmacokinetic and pharmacometabolomic study of pirfenidone in normal mouse tissues using high mass resolution MALDI-FTICR-mass spectrometry imaging

Na Sun, **Isis E. Fernandez**, Mian Wei, Ying Wu, Michaela Aichler, Oliver Eickelberg and Axel Walch

Supplementary data 1: List of the 129 discriminative masses which represent clear differences between control and treated lungs.

Decreased after pirfenidone treatment

m/z	Pirfenidone treatment (45min)_1	Pirfenidone treatment (45min)_2	Pirfenidone treatment (45min)_3	Control_1	Control_2	Control_3	p value	Ratio (treated /control)
66.9960	0	0	0	0.0673	0.1164	0.0551	0.0132	0
85.5940	0	0	0	0.0593	0.0627	0.0589	0	0
102.0280	0	0	0	0.0529	0.0641	0.0637	0.0001	0
109.3560	0	0	0.0759	0.0934	0.1125	0.1048	0.0391	0.24
109.9940	0	0	0	0.1186	0.1692	0.0573	0.0237	0
120.6870	0	0	0	0.1174	0.1269	0.114	0	0
134.6760	0.1151	0.151	0.1602	0.2853	0.3413	0.3642	0.0023	0.43
152.8520	0	0	0	0.17	0.2001	0.0747	0.0172	0
154.8500	0.0679	0	0.0615	0.2559	0.291	0.1154	0.0373	0.20
173.0350	0	0.2259	0.1962	0.336	0.4433	0.3777	0.0341	0.36
173.5300	0.0906	0.1285	0.1142	0.2117	0.2416	0.2542	0.0017	0.47
176.8175	0	0	0	0.1171	0.1434	0.0629	0.0104	0
178.8160	0	0	0.055	0.2041	0.2514	0.107	0.0217	0.10
180.8670	0.1411	0.0941	0.1118	0.3757	0.5249	0.2783	0.0191	0.29
182.8650	0.1449	0.0985	0.1126	0.3908	0.5446	0.3031	0.015	0.29
189.9890	0	0	0.1047	0.2311	0.288	0.3222	0.005	0.12
194.8360	0.0806	0	0.0563	0.2219	0.2445	0.1405	0.0167	0.23

196.8340	0.0825	0	0	0.1957	0.2236	0.1302	0.0163	0.15
198.8310	0	0	0	0.1045	0.1248	0.0656	0.0048	0
198.8390	0	0	0	0.0823	0.1155	0.0517	0.0107	0
198.8680	0	0	0	0.1032	0.1803	0.0773	0.0177	0
198.8780	0.0535	0	0.0542	0.2293	0.2965	0.1527	0.0136	0.16
200.0020	0	0	0	0.1642	0.1471	0.0528	0.0248	0
200.8660	0	0	0	0.1173	0.2091	0.0906	0.0179	0
200.8760	0.0616	0.0537	0.0681	0.2333	0.3265	0.1643	0.0188	0.25
202.0070	0	0	0	0.0581	0.0656	0.0826	0.0007	0
202.0130	0.079	0.109	0.0989	0.1732	0.218	0.1982	0.003	0.49
204.7920	1.0953	0.8674	0.784	1.7203	2.4632	1.4237	0.0418	0.49
208.7870	0.7221	0.5425	0.4845	1.1409	1.6494	0.9311	0.0431	0.47
210.7840	0	0	0	0.0753	0.1323	0.0532	0.021	0
214.7830	0.09	0.0715	0.0942	0.3147	0.463	0.1924	0.0387	0.26
216.7810	0.0837	0.0722	0.0942	0.3153	0.4681	0.1971	0.0365	0.26
216.8500	0	0	0	0.1181	0.1344	0.0628	0.0083	0
225.9160	1.0976	1.0561	0.9206	2.3399	2.9061	2.1052	0.0043	0.42
227.9140	1.0143	0.994	0.8584	2.2499	2.7844	1.9875	0.0044	0.41
241.8900	0.2702	0.4238	0.3342	1.0411	1.3198	0.8037	0.0102	0.32
243.8880	0.3155	0.483	0.3843	1.1696	1.4753	0.9024	0.0103	0.33
279.0275	0.0557	0.0593	0.0819	0.1467	0.178	0.2128	0.0055	0.37
283.0760	0	0	0	0.0565	0.1041	0.0514	0.0136	0
298.7300	0.3216	0.316	0.2031	0.9748	1.2344	0.4981	0.0468	0.31

300.7270	0.6235	0.636	0.3987	1.8206	2.2637	0.9986	0.0393	0.33
302.7250	0.341	0.3515	0.223	1.0378	1.3159	0.537	0.0467	0.32
304.8760	0.826	0.4295	0.1913	1.4943	1.938	0.963	0.0435	0.33
306.8780	1.0962	0.6019	0.2703	1.9194	2.4828	1.2658	0.0443	0.35
307.9910	0	0.0547	0	0.2535	0.2947	0.0899	0.0405	0.09
308.8750	1.1134	0.6134	0.2734	1.9163	2.4917	1.2697	0.0461	0.35
312.8750	0	0	0	0.0869	0.1395	0.0506	0.0232	0.00
320.9330	0	0	0	0.0591	0.1288	0.0704	0.0163	0.00
328.7260	0.054	0	0	0.1857	0.1658	0.0826	0.0252	0.12
329.9630	0	0	0	0.26	0.3797	0.1152	0.0302	0
329.9817	0	0	0	0.0696	0.0898	0.1302	0.0056	0
330.7220	0	0	0	0.1588	0.155	0.0711	0.011	0
346.0267	0.1742	0	0	1.0655	1.2344	1.1414	0.0001	0.05
346.0430	0	0	0	6.0208	6.6161	6.3938	0	0
346.0750	0	0	1.3397	1.6982	1.8987	1.731	0.042	0.25
346.0940	0	0.219	0	0.3546	0.4097	0.3418	0.0176	0.20
346.1045	0.0926	0	0.1256	0.1844	0.217	0.1669	0.0444	0.38
346.1340	0	0	0	0.0841	0.0801	0.0538	0.0016	0
346.2430	0	0	0	0.0563	0.0568	0.0614	0	0
372.0720	0.1859	0.2662	0.8604	1.5521	1.3997	0.8963	0.0438	0.34
375.8100	0	0	0	0.0625	0.0527	0.0698	0.0002	0
381.9150	0	0	0	0.0685	0.0581	0.0572	0.0001	0
384.0170	0	0	0	0.0622	0.082	0.0731	0.0002	0

384.1275	0	0	0	0.6506	0.7275	0.5459	0.0003	0
396.8460	0	0	0	0.0542	0.0565	0.0541	0	0
398.8420	0	0	0	0.0542	0.059	0.0562	0	0
405.9980	0	0	0	0.61	0.7845	0.6998	0.0002	0
447.9673	0.2204	0.1655	0.1556	0.705	0.9606	0.475	0.0197	0.25
449.9620	0.1715	0.1052	0.0983	0.6347	0.9222	0.4196	0.0224	0.19
468.9260	0.136	0.3221	0.3526	0.4288	0.6392	0.5624	0.0404	0.50
535.3060	0.1749	0.2507	0.2585	0.4648	0.6439	0.3814	0.0305	0.46
563.3360	0.0873	0.1253	0.1277	0.2129	0.3088	0.1725	0.05	0.49
589.3540	0	0	0	0.0656	0.0851	0.0548	0.0015	0
606.3420	0	0	0	0.0614	0.0867	0.0575	0.0017	0
625.1900	0	0	0	0.0768	0.1065	0.0698	0.0017	0
719.4720	0.1591	0	0	2.3521	2.1574	2.0033	0	0.02

Increased after pirfenidone treatment

m/z	Pirfenidone treatment (45min)_1	Pirfenidone treatment (45min)_2	Pirfenidone treatment (45min)_3	Control_1	Control_2	Control_3	p value	Ratio (treated /control)
83.0090	0.156	0.2267	0.171	0	0	0.0679	0.0066	8.16
95.3560	0.1952	0.3301	0.2811	0	0	0	0.0024	Inf
143.0300	0.1474	0.237	0.1971	0	0	0	0.0017	Inf
143.0330	0.1153	0.2164	0.1812	0	0	0	0.0045	Inf
153.0190	0.056	0.0927	0.1123	0	0	0	0.0062	Inf

165.0100	0.0559	0.0849	0.0719	0	0	0	0.0011	Inf
168.0140	0.1863	0.2657	0.2065	0.054	0.0529	0.0867	0.0041	3.40
213.9640	0.9285	0.4855	0.924	0.1728	0.0499	0	0.0106	10.50
215.9950	0.0866	0.0632	0.0618	0	0	0	0.0009	Inf
225.9740	0.5178	0.5892	0.5409	0.1622	0.1655	0.3051	0.0028	2.60
239.9510	0.2519	0.5329	0.469	0.1218	0.1393	0.2226	0.0471	2.59
250.0395	0.6486	1.2738	1.0511	0.3369	0.4144	0.4729	0.0357	2.43
253.9875	0.1332	0.1905	0.1769	0	0	0.0733	0.0089	6.83
256.0600	0.2976	0.3243	0.3511	0.114	0.1437	0.1596	0.0008	2.33
266.0345	0.5061	0.9102	0.7921	0.2604	0.2819	0.3058	0.0198	2.60
268.0500	1.5477	2.7412	2.2887	0.534	0.6189	0.8857	0.0141	3.23
284.0450	8.9457	11.1789	10.2076	2.6939	2.8528	4.1111	0.0009	3.14
284.0535	0.1851	0.2674	0.2772	0	0.0988	0	0.0088	7.38
285.9680	0.0748	0.117	0.0753	0	0	0	0.0031	Inf
286.0405	0.262	0.3795	0.3412	0.1537	0.2112	0.1263	0.0185	2.00
286.0610	17.6674	22.5029	19.8583	5.1833	5.2234	7.8811	0.0011	3.28
286.0685	0.7295	0.2248	0.874	0	0	0	0.0363	Inf
287.0620	1.2352	1.6508	1.4474	0.6291	0.6973	0.5433	0.003	2.32
288.0560	0.6251	0.8822	0.798	0.3088	0.3954	0.3517	0.0064	2.18
288.9500	0.0817	0.1767	0.1065	0	0	0	0.0129	Inf
302.0560	0.1704	0.2325	0.2444	0.0689	0.0772	0	0.0076	4.43
302.0650	0.1067	0.1831	0.2302	0.0534	0.0613	0	0.0296	4.53
307.9990	0.0855	0.0951	0.1136	0	0.0507	0.0601	0.0402	2.65

318.6500	0.0637	0.0641	0.0922	0	0	0	0.0015	Inf
318.8890	0.0965	0.0827	0.09	0	0.07	0	0.0486	3.84
326.0090	0.0938	0.1629	0.1364	0	0	0.0509	0.0123	7.73
327.1880	0.0913	0.079	0.0525	0	0	0	0.0029	Inf
341.0110	0.0595	0.1168	0.0854	0	0	0	0.0062	Inf
342.0040	1.6425	1.698	1.7473	0.5912	0.6268	0.81	0.0002	2.51
344.0010	0.2715	0.3079	0.2895	0	0.0504	0.0834	0.0008	6.49
344.0200	4.3667	4.2929	4.086	1.0601	1.0421	1.7145	0.0002	3.34
345.0220	0.1355	0.1422	0.1391	0.0593	0.0696	0	0.0116	3.23
357.9780	0.1504	0.3077	0.3212	0.0797	0	0.0878	0.0296	4.65
358.9555	0.3625	0.4911	0.5065	0.2213	0.2174	0.1621	0.0069	2.26
359.9915	0.3679	0.6069	0.5594	0.2022	0.1904	0.1878	0.0122	2.64
361.0835	0.0899	0.0813	0.0786	0	0	0	0	Inf
361.9900	0.0948	0.1717	0.1583	0	0	0	0.004	Inf
376.1030	0.1069	0.1348	0.1537	0	0	0	0.0006	Inf
388.0090	0.8284	1.5169	0.9608	0.2366	0.2493	0.3964	0.0204	3.75
406.2220	0.1753	0.1928	0.1342	0	0	0	0.0007	Inf
407.9960	0.1143	0.2015	0.124	0	0	0	0.006	Inf
416.2060	0.105	0.1097	0.076	0	0	0	0.0008	Inf
431.0430	0.0673	0.1458	0.0766	0	0	0	0.0175	Inf
433.0575	0.4448	0.7667	0.4745	0	0.0534	0.1416	0.0109	8.65
460.2637	0.0869	0.0877	0.0724	0	0	0	0.0001	Inf
531.2710	0.0553	0.0597	0.0564	0	0	0	0	Inf

638.2420	0.2224	0.1776	0.1435	0	0	0	0.0014	Inf
719.4940	3.2603	1.8352	2.9413	0	0	0	0.0034	Inf

Supplementary data 2: *On tissue MS/MS* data of ADP, AMP, GDP, citrate, glutathione and glutathione disulfide.

- The identification of ADP, AMP, GDP, citrate, glutathione and glutathione disulfide were carried out by *on tissue MS/MS* using MALDI-FTICR.
- The metabolite standards were purchased from Sigma-Aldrich (Sigma-Aldrich, Munich, Germany)
- The *on tissue MS/MS* spectra matched well with the standard metabolites. These data indicate the identity of the target metabolites.

ADP

On tissue MS/MS

Standard *MS/MS*

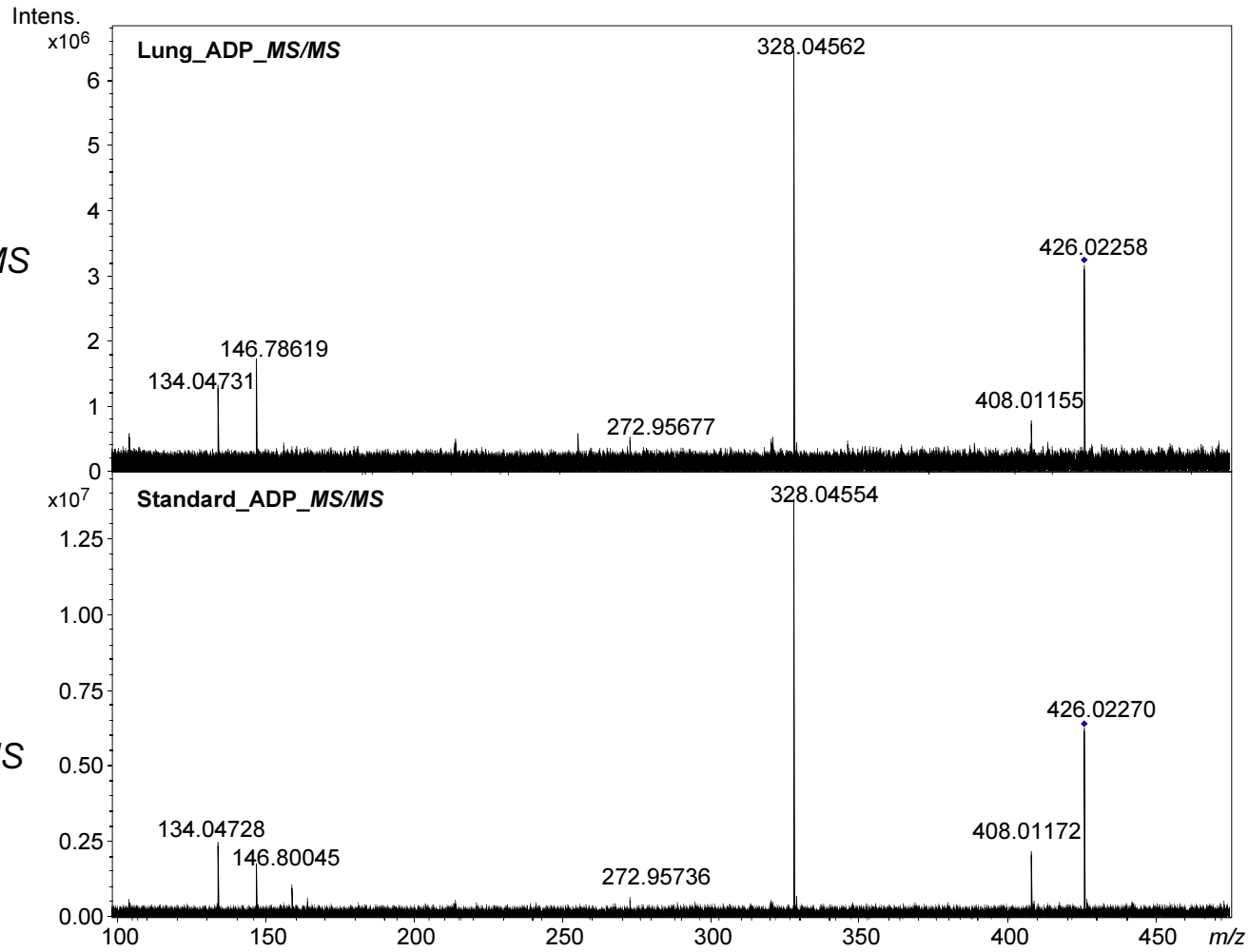

AMP

On tissue MS/MS

Standard *MS/MS*

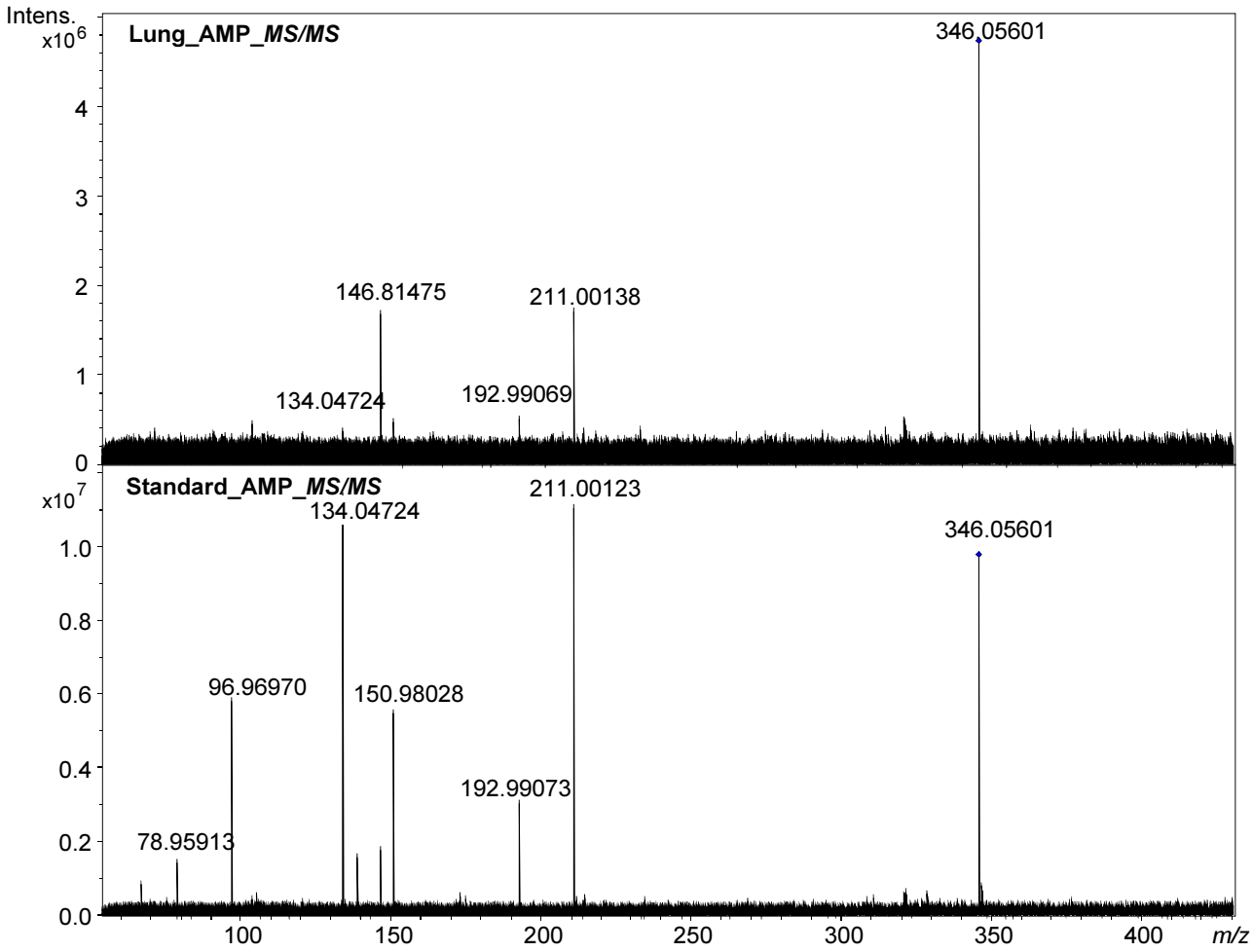

GDP

On tissue MS/MS

Standard *MS/MS*

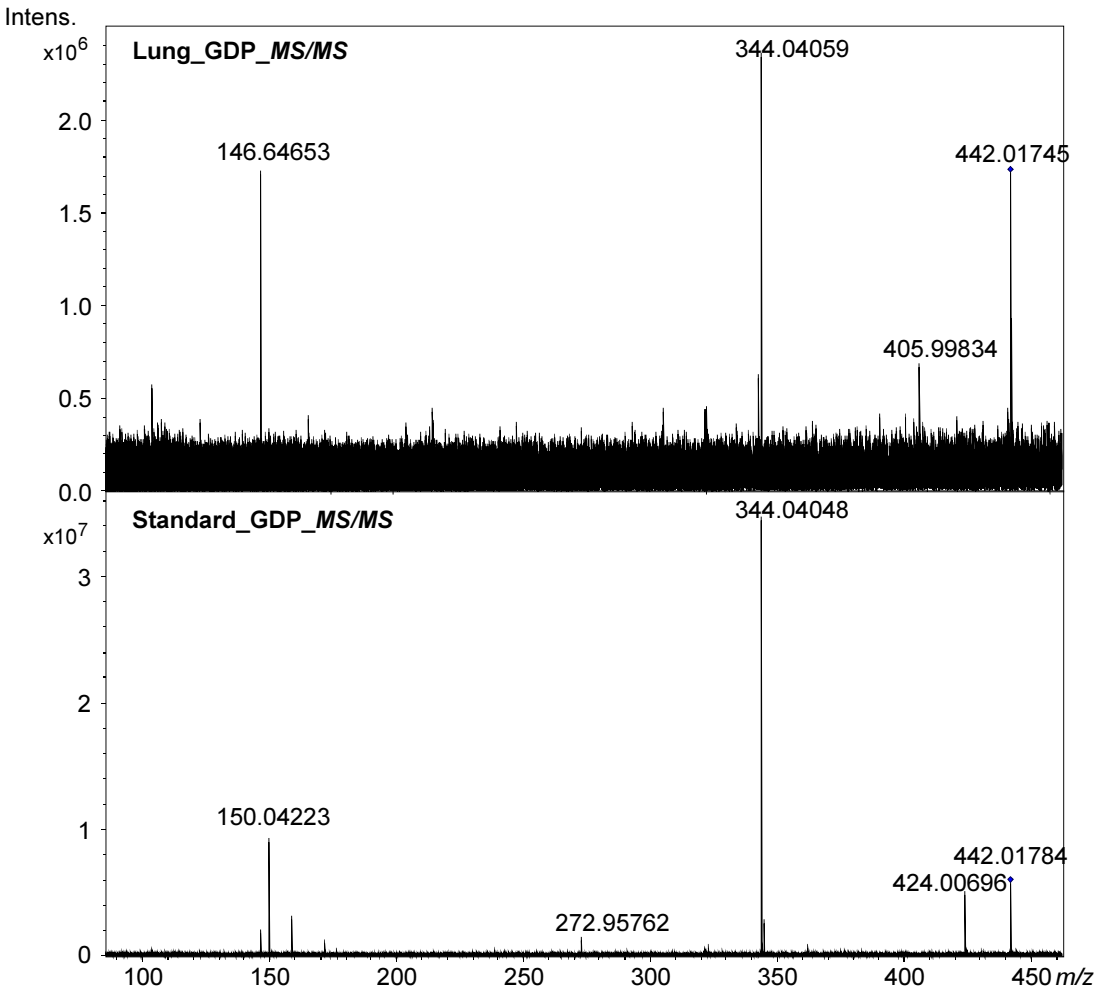

Citrate

On tissue MS/MS

Standard *MS/MS*

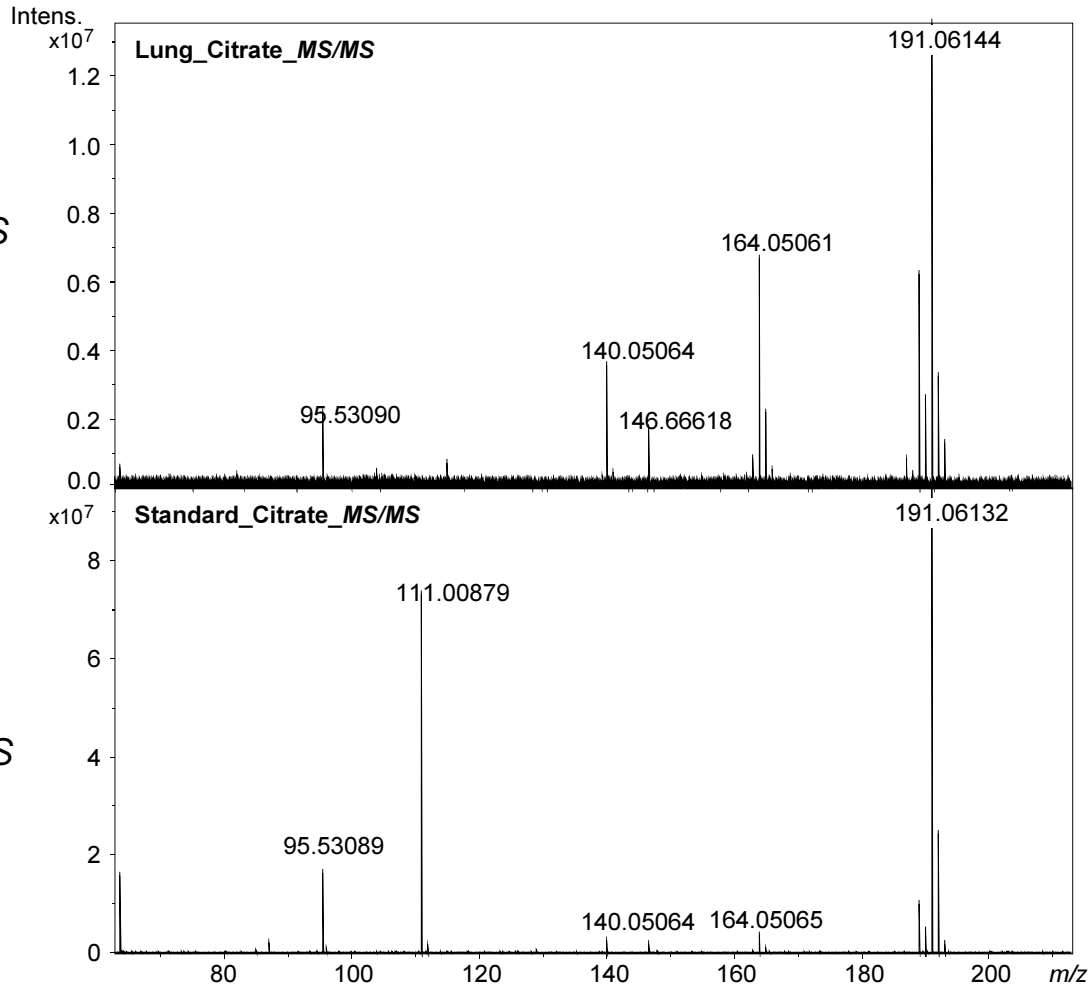

Glutathione

On tissue MS/MS

Standard *MS/MS*

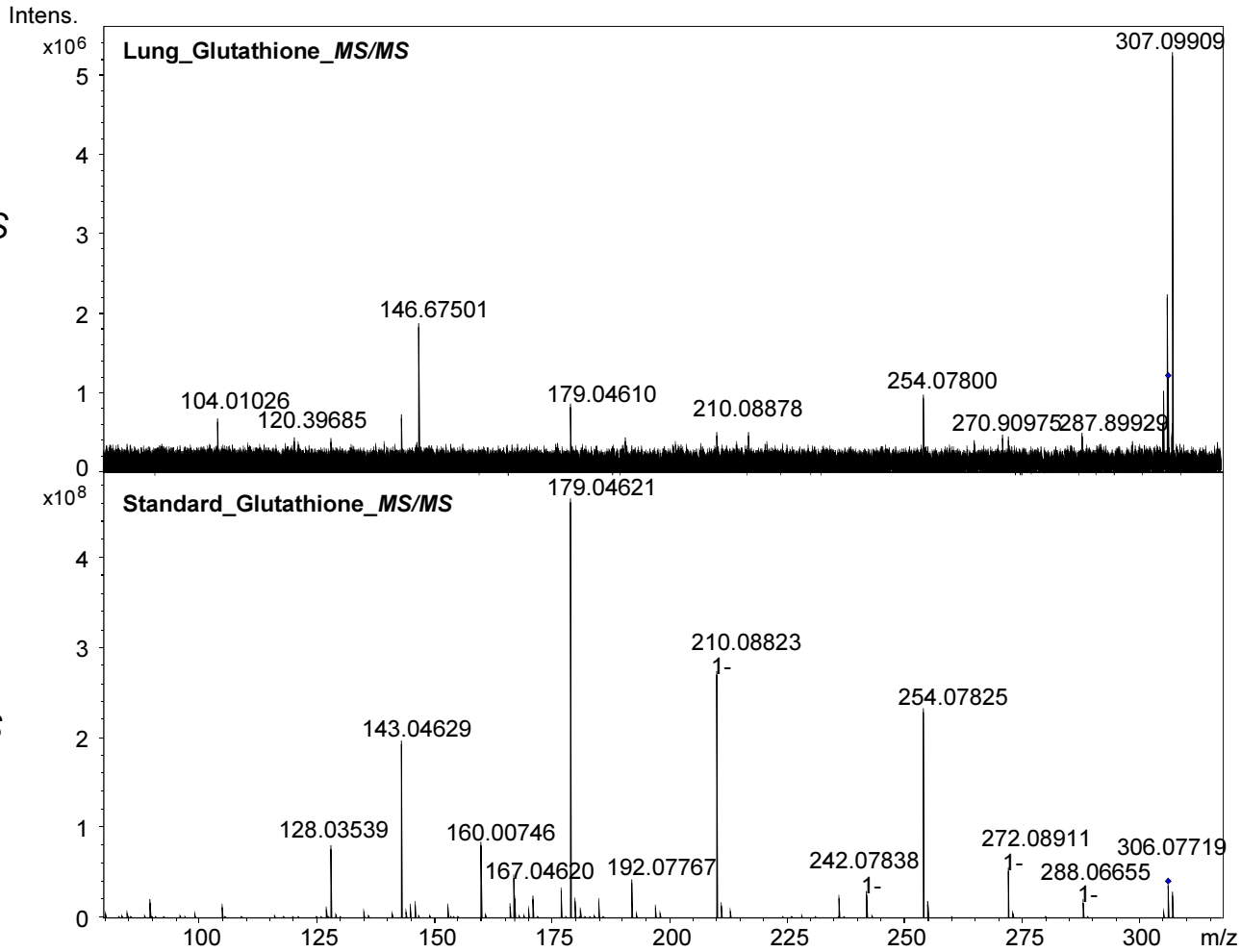

Glutathione disulfide

On tissue MS/MS

Standard *MS/MS*

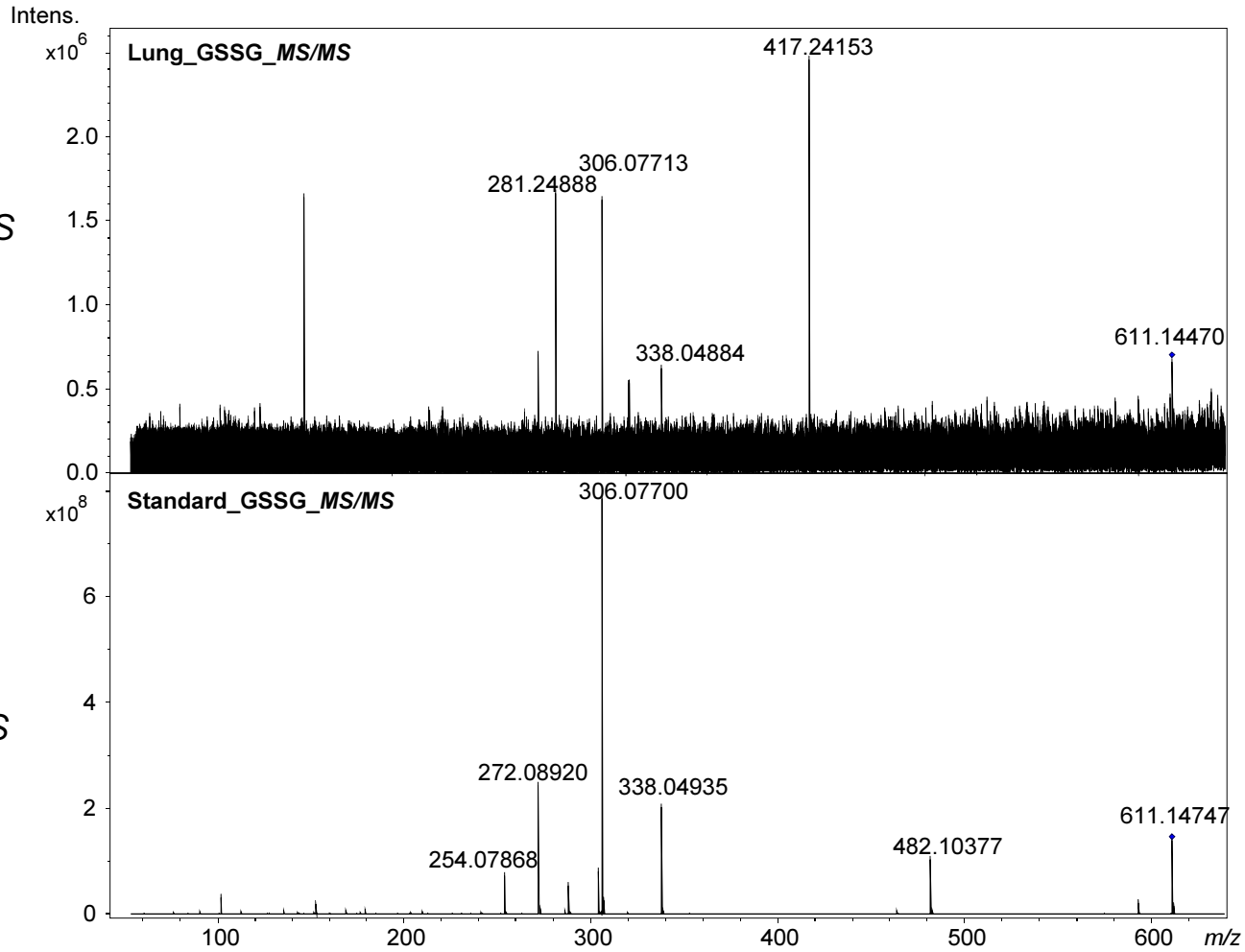

3. Discussion[1]

IPF is a lethal disease with a median survival lower that many cancer types. In the past decade, we have witnessed an unprecedented increase of understanding the mechanisms driving lung fibrosis. The gain of knowledge in IPF pathogenesis has moved the field from an untreatable condition with high mortality rates, to steady growing potential therapeutic routes.

Through the implementation of these studies we could: first, determine the importance of imaging for subclinical disease detection in mice and detected that plasma levels of ICAM1 strongly correlate with disease severity. Second, we describe for the first time the matrisome dynamics during initiation, peak and resolution of fibrosis. Third, we applied MALDI-FTICR-MSI imaging as detection tool for pharmacokinetic and pharmacometabolomic detection of pirfenidone in fibrotic and normal mouse lungs. Thus, we develop novel tools and applied technologies to better understand IPF and the bleomycin-induced pulmonary fibrosis model, in forward and reverse translational approaches

3.1. Compartmentalized assessment of biomarkers in injury and repair

. In translational medical research, mice models are essential for studying biological processes in mammalians (Vandamme, 2014). To date, animal experiments remain crucial to understand the fundamental mechanisms

[1] Parts are based on the discussion in [(Fernandez et al., 2016a; Schiller et al., 2015; Sun et al., 2015; Sun et al., 2018)]

underlying the onset of disease and to discover methods to prevent, diagnose and treat them (Barre-Sinoussi & Montagutelli, 2015). The comparison between mice models and human diseases remains controversial, and possibly will continue to be so. Particulary, the bleomycin-induced pulmonary model fibrosis and IPF has also been highly debated, it is self-resolving and does not fully recapitulate IPF (Tashiro et al., 2017). However, it is currently the best-characterized and most commonly applied (Jenkins et al., 2017). Many studies show strong commonalities on distinct levels, encouraging its continuous use for preclinical testing (Bauer et al., 2015; Peng et al., 2013).

Currently, diagnosis and disease course prediction in idiopathic pulmonary fibrosis primarily relies on lung function measures (Erbes et al., 1997). Peripheral circulating biomarkers are constantly proposed for diagnosis and outcome, yet their correlation with lung function and histology remains unclear (Drakopanagiotakis et al., 2018). Here, we comprehensively assessed human-relevant circulating biomarkers in fibrotic mice and correlated their abundance with lung function and histology during the onset, progression, and resolution of lung fibrosis.

We observed that lung function decline is not a prerequisite for histologically evident fibrosis, especially in onset and resolution of injury (Fernandez et al., 2016a). This supports that early micro- and macroscopic changes in the lung might precede lung function decline. This seems to be a feature shared between mice and humans, where imaging has shown to be the only available tool for early disease detection (Washko et al., 2011), in subclinical scenarios before a dramatic loss-of-organ function happens (Sack et al., 2017), and can also be associated with genetic predisposition (Hunninghake et al., 2013). Furthermore, we detected that plasma levels of ICAM1 could determine the severity of lung fibrosis in mice. Being sICAM1 the human-relevant marker that provided the tighter correlation with lung function decline during the peak of fibrosis in mice. We detected that ICAM1 was shed from injured epithelial cells and probably

released to the circulation. In IPF, ICAM1 has being shown as marker of disease severity (Richards et al., 2012) and acute exacerbations (Okuda et al., 2015), reflecting its value in ongoing epithelial injury. Taking together, this data demonstrate that in similarity to mice, ICAM1 levels might predict disease severity, exacerbations, and mortality in IPF patients.

Next, we monitored mice from the onset of inflammation and fibrosis to its full recovery by a combined analysis of proteome, secretome and transcriptome of total lung tissue and broncho alveolar lavage (BAL) (Schiller et al., 2015). Taking advantage of the self-regenerative properties of the bleomycin induced-fibrosis model, we were first in comprehensively characterizing the lung ECM dynamics upon injury and repair. We perform measurements at day 3 (early inflammation), day 7 (late inflammation), day 14 (fibrosis), day 28 (remodeling) and day 56 (resolution) (Fernandez et al., 2016a). In the lung tissue, we quantified 8,019 protein groups, a total of 3,032 of these proteins (154 matrisome components), changed significantly in at least one of the time points. To grant clinical relevance to the significantly regulated targets in our data, we correlated protein abundance with lung compliance for each mouse of the study. For instance, Tenascin C abundance showed a negative correlation, meaning the more Tenascin C the lower the compliance, therefore the stiffer the tissue. In contrast, for Collagen-IVa5, a collagen subunit required for basal membrane stability, we observed a positive correlation, reflecting the loss and destruction of basal membrane components during fibrosis (Barkauskas & Noble, 2014). Furthermore, we revealed novel ECM components that have not being described before in the fibrosis-resolution context, as Emilin-2 and collagen-XXVIII, which are now relevant targets under study. In conclusion, with these studies we provide an extensive, state-of-the-art resource of methods and novel molecules for the field of lung injury, repair and regeneration.

3.2. MALDI imaging: a tool for drug detection and monitoring

Matrix-Assisted Laser Desorption/Ionization-Mass Spectrometry Imaging (MALDI-MSI), with Fourier-Transform Ion Cyclotron Resonance (FTICR) and Orbitrap, is the use of matrix-assisted laser desorption ionization as a mass spectrometry imaging technique in which the sample, for example a thin tissue section, is moved in two dimensions while the mass spectrum is recorded (Chaurand et al., 2006). MALDI imaging is a versatile technique that gained special interest as a tool to discover and visualize the spatial distribution of molecules. Since small molecules ionize easier by MALDI, a high mass accuracy and resolution mass spectrometer can be employed such as Fourier-transform ion cyclotron resonance (FT-ICR), allowing to make hypotheses on chemical formulas directly from the exact masses of the detected peaks. It enables the simultaneous mapping of the spatial distribution of a wide range variety of analytes such as metabolites, lipids, peptides and proteins (Aichler et al., 2017) (Ly et al., 2015). The ability of MALDI imaging to simultaneously record the distributions of hundreds of molecules in tissue makes it a powerful discovery method for molecular pathology (Balluff et al., 2011). MALDI-MSI combines the chemical specificity of modern mass spectrometry with the imaging capabilities of microscopy; it allows a highly multiplexed and untargeted analysis of biomolecular ions and enables their localization within the tissue section.

3.3. Tools for drug detection and monitoring: Pirfenidone as a metabolic regulator in fibrosis

Pirfenidone is one of the two drugs approved for the treatment of idiopathic pulmonary fibrosis (Behr, 2013). Yet, the precise mechanism of action, distribution in the lung parenchyma and metabolic effect is largely unknown. Here, we used a state-of-the-art technology for *in-situ* drug detection and

imaging, to better understand the dynamic behavior of pirfenidone in the normal and fibrotic lung of mice and humans. Initially, we performed high-resolution quantitative MALDI-FTICR MSI to visualize and quantify orally administered pirfenidone and putative metabolites in the lung, together with visualizing the *in-situ* pharmacometabolic response (Sun et al., 2015). As a proof-of-concept, and to primarily understand the effect in the healthy lung, we orally administer pirfenidone in unchallenged mice, in different time points, to assess *in-situ* detection. Although in the -healthy lung, we did not observe an obvious effect on known metabolic pathways, we detected significant alterations in 129 unknown masses, demonstrating an *in-situ* effect of pirfenidone. Pharmacokinetic detection in the blood and multiple organs (e.g. liver, lung and kidney) were concordant with studies in plasma of human and other species (Bruss et al., 2004; Bruss et al., 2008; Giri et al., 2002; Shi et al., 2007; Wang et al., 2006).

In order to understand the significance and impact of pirfenidone treatment in mice and human with lung fibrosis, we performed high-resolution MALDI-FTICR-MSI imaging in bleomycin-induced fibrosis mice and controls, and in donor and IPF patients, both treated with pirfenidone and treatment naïve (Sun et al., 2018). Our study demonstrates, for the first time, in situ metabolic alterations during fibrosis and analyses the pharmacometabolic effect of pirfenidone in fibrotic tissue of mice and humans. In detail, we demonstrated an increase of pirfenidone and related metabolites in fibrotic tissue. We further detected the mass spectra of fibrotic areas, to unequivocally assess metabolite detection in specific areas of interest (Figure 8).

Having a closer look into the distribution of pirfenidone and its putative metabolites, we observed that 5-hydroxymethyl pirfenidone (m/z 202.0863) and 5-carboxy pirfenidone (m/z 216.0655) are more abundant in fibrotic areas with higher collagen-1 deposition than in non-fibrotic areas (Figure 7F). Suggesting that the distribution, and possibly the metabolism, of pirfenidone are enhanced

in fibrosis and accumulation in affected areas might be required for its anti-fibrotic effects. For instance, in lung fibroblasts, 5-hydroxymethyl pirfenidone and 5-carboxy pirfenidone inhibit TGF-β-induced collagen synthesis, demonstrating that pirfenidone metabolites also have anti-fibrotic activities (Togami et al., 2013).

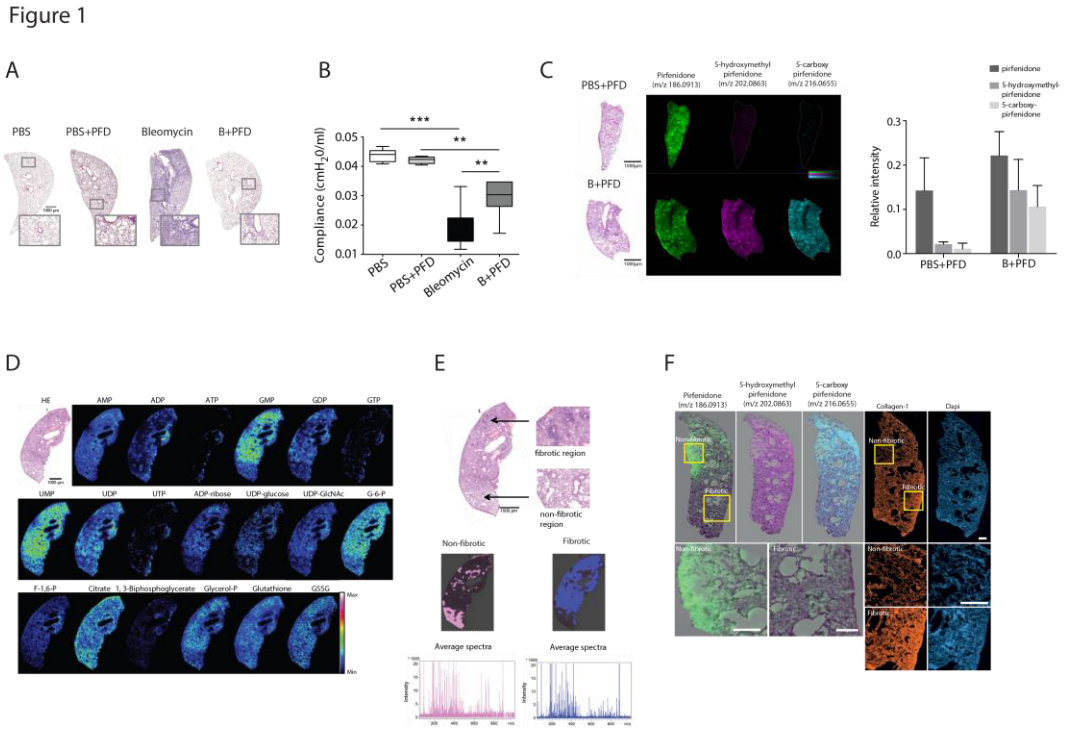

Figure7. Pirfenidone detection in bleomycin-induced pulmonary fibrosis mice lungs. a) Haematoxylin and Eosin (H&E) staining of sectioned lungs from mice treated with phosphate-buffered saline (PBS), PBS+pirfenidone (PBS+PFD), bleomycin to induce fibrosis, and bleomycin+pirfenidone (B+PFD). b) Lung compliance measurements of mice from each treatment group. Data are shown as mean ± standard deviation (SD), and asterisks (*, **, ***) indicate significant differences ($p \leq 0.05$, 0.01, 0.001, respectively). c) Left panel: mass spectrometry imaging (MSI) distribution of pirfenidone and its related metabolites, 5-hydroxymethyl pirfenidone and 5-carboxy pirfenidone, in lungs from PBS+PFD and B+PFD-treated mice. Right panel: relative quantification of pirfenidone and related metabolites in lungs from PBS+PFD and B+PFD-treated mice. d) Heterogeneous distribution pattern of central pathway-related endogenous metabolites in lung tissue from B+PFD-treated mice: UDP-GlcNAc (UDP-N-acetylglucosamine), G-6-P (glucose-6-phosphate), F-1,6-P (fructose-1,6-bisphosphate), glycerol-P (glycerol monophosphate), GSSG (glutathione disulphide). e) H&E images with zoomed regions of non-fibrotic and fibrotic tissue are illustrated. Spatial segmentation of histological components through unsupervised hierarchical clustering reflects the histological components of fibrotic (blue) and non-fibrotic area (pink). f) Immunofluorescence staining for collagen type 1 in sectioned

lungs from the B+PFD-treated group. (Taken from Sun N*, Fernandez IE*, et al., ERJ *accepted* Jul 2018)

Using this technology, we are able to completely dissect metabolic pathways and determine their spatial distribution, as well as quantifying the intensity of detection. Last, we identified overlapping and exclusive metabolic fingerprints that characterize the fibrotic response in human and mice, together with the pharmacometabolic response to pirfenidone in fibrosis. For instance, we observed an overlapping increase in the ascorbate and aldarate metabolism in mice and human during fibrosis. This confirms the enhancement in collagen metabolism and production observed in organ fibrosis. In mice, ascorbate and aldarate metabolism decreases after pirfenidone treatment. Ascorbate is a crucial co-substrate for the enzymes responsible for post-translational hydroxylation of prolyl and lysyl residues necessary for rendering the collagen triple helix thermostable, as well as, for the extracellular cross-linking of collagen fibres (Hata & Senoo, 1989; Murad et al., 1983), which makes it critical for collagen synthesis and processing. The enhancement of ascorbate and aldarate metabolism during fibrosis, and the decrease upon pirfenidone administration, demonstrates the anti-fibrotic effect of pirfenidone. This further confirms its effect in collagen processing, supporting its effect in inhibiting collagen fibril formation in IPF fibroblast (Knuppel et al., 2017).

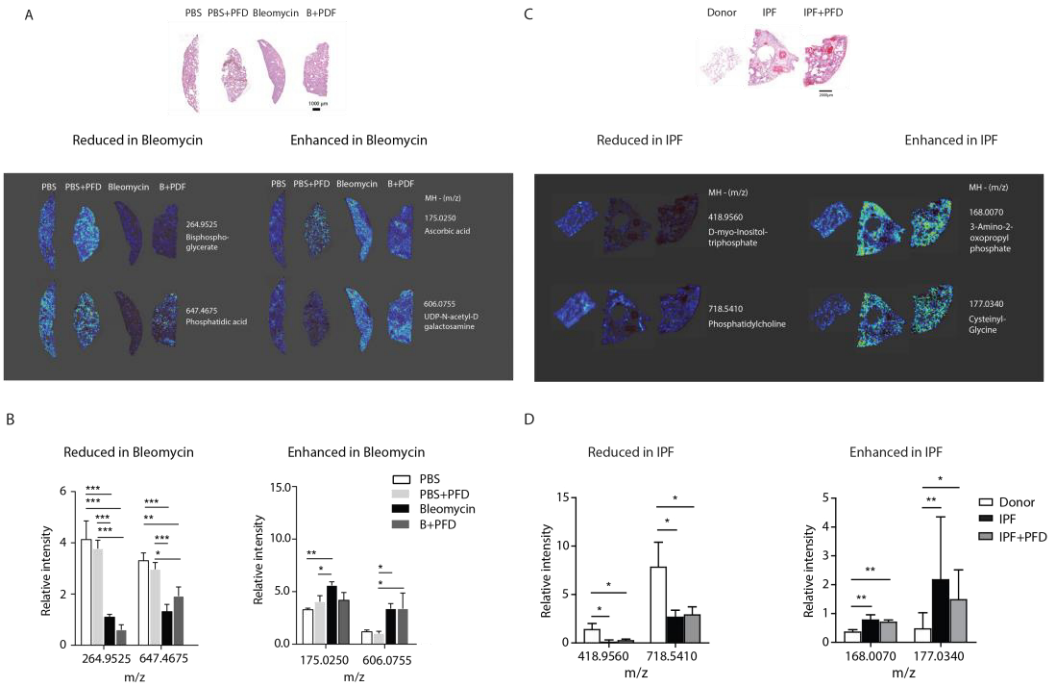

Figure 8. Pathway analysis of discriminative metabolic alterations in bleomycin-induced fibrosis and IPF patients with and without pirfenidone treatment and controls. A) On the right, representative images of metabolites reduced in fibrosis: bisphosphoglycerate (m/z 264.9525), phosphatidic acid (m/z 647.4675). On the left, from top to bottom, representative images of metabolites enhanced in fibrosis: ascorbic acid (m/z 175.0250), UDP-N-acetyl-D-galactosamine (606.0755). B) Relative quantification of metabolites in mice treated with PBS, PBS+PFD, bleomycin, and B+PFD. C) On the right, representative images of metabolites reduced in IPF: D-myo-Inositoltriphosphate (m/z 418.9565), phosphatidylcholine (m/z 718.5410). On the left, from top to bottom, representative images of metabolites enhanced in IPF: 3-Amino-2-oxopropylphosphate (m/z 168.0070), cyteinyl-glycine (m/z 177.0340). D) Relative quantification of the depicted metabolites in donor, IPF, and pirfenidone-treated IPF (IPF+PFD). One-way ANOVA was used for statistical analysis, with the Bonferroni *post-hoc* test. Asterisks (*, **, ***) indicate significant differences ($p \leq 0.05$, 0.01, 0.001, respectively) between control and treated group. (Taken and modified from Sun N*, Fernandez IE*, et al., ERJ *accepted* Aug 2018).

In order to identify the similarities and differences in regulation of pirfenidone in mice and human fibrosis, we performed pathway enrichment analysis. We could confirm overlapping and distinctive features in mice and human fibrosis (Table 1). As mentioned earlier (chapter 1), it is topic of discussion that bleomycin-induced pulmonary fibrosis is a self-resolving, easily manipulated model, that does not fully recapitulate IPF (Jenkins et al., 2017). While other studies show shared features on mice and humans fibrosis on different levels, supporting its use (Jenkins et al., 2017). The vast knowledge gained in years of

studying the bleomycin-induced pulmonary fibrosis model allows us to study metabolic effects that occur during early stage pirfenidone treatments. For instance, in the lung pirfenidone and its metabolites are detectable maximum 45 minutes after administration (Sun et al., 2015). We successfully detected an increase in pirfenidone and its related drug metabolites in mice fibrotic lungs, but not in humans. This effect might be due to the timely controlled administration of the drug in mice, a difficult setting to control clinically in pre-transplanted patients right before their surgical procedure. Second, pirfenidone treatment in mice occurred from disease initiation to peak of fibrosis (d 7-14), whereas our IPF cohort was at end-stage disease. Thus, our data may also reflect important differences in treatment responses at different disease stages. Despite the factors mentioned above, with the introduction of transbronchial cryobiopsies for earlier diagnosis of diffuse parenchymal lung diseases (38), differences can be minimized, and the applicability of MALDI imaging for metabolite profiling or pharmacometabolic drug responses should be considered.

	Discriminative pathways	Bleomycine induced-pulmonary fibrosis	IPF
Reduced in fibrosis	Glycolysis or Gluconeogenesis	yes	no
	Linoleic acid metabolism	no	yes
	Inositol phosphate metabolism	no	yes
	Starch and sucrose metabolism	no	yes
Enahnced in fibrosis	Pentose and glucuronate interconversions	yes	yes
	Ascorbate and aldarate metabolism	yes	yes
	Amino sugar and nucleotide sugar metabolism	yes	no
	Pentose phosphate pathway	yes	no
	Fructose and mannose metabolism	yes	yes
	Vitamin B6 metabolism	no	yes
	Glutathione metabolism	no	yes
Reduced upon Pirfenidone	Ascorbate and aldarate metabolism	yes	no
Enahnced upon Pirfenidone	Glycolysis or Gluconeogenesis	no	yes

Table 1. Overlapping and distinctive features of Pirfenidone treatment in human and mice. (Taken from Sun N*, Fernandez IE*, et al., ERJ *accepted* Aug 2018)

Among the differentially regulated central metabolic pathways we observed that intermediates in glycolysis, nucleotide metabolism, and the pentose phosphate pathway are altered in fibrotic regions compared with healthy lungs (Table 1). IPF related alterations in glycolysis have been reported previously, acting as positive control (Zhao et al., 2017). Dysregulated glycolysis promotes elevated lactate levels, thus facilitating disease progression in IPF (Kottmann et al., 2012). This metabolic switch towards oxidative pentose phosphate pathway in fibrosis might indicate the elevated energy demand and higher energy consumption present in fibrosis. Consistent with this, we found lower levels of ATP in IPF patients. Similarly, extracellular ATP is decreased in bronchoalveolar lavage fluid from IPF samples (Riteau et al., 2010), and others have shown decreased intracellular ATP in IPF tissue (Kang et al., 2016), which may result from accumulation of dysfunctional mitochondria that promote fibrosis (Bueno et al., 2015). Collectively, these findings suggest an altered energy household in IPF.

Taken together, these identified alterations in metabolites support the idea that metabolic profiles are transformed in regions affected by pulmonary fibrosis. The combination of pharmaco- and metabolomics in this study will ultimately lead to an improved understanding of disease mechanisms of pulmonary fibrosis and mechanism of action of pirfenidone. Moreover, understanding of pirfenidone metabolism and the cellular mechanism of action of this drug may facilitate the prediction of individual responses to antifibrotic drugs. The label-free MALDI-MSI technique achieved simultaneous detection, visualization, and quantification of both exogenous (drugs and their related metabolites) and endogenous metabolites, highlighting compelling competitive advantages over traditional analytical techniques. This approach shed light on the spatiotemporal behaviours of drugs and endogenous metabolites, and these findings are broadly applicable to drug efficacy studies and metabolism of bioactive small molecules involved in fibrosis and other pathological conditions

4. Conclusions and future directions

Advances in IPF knowledge show an exciting time ahead, where analysis of the genetic makeup and biomarkers will dictate therapeutic approaches, subphenotype provide pathway-driven tailored therapies. Hence, implementing clinically routine genotyping and biomarker testing is essential for future patient stratification and personalized treatment. To address the unmet need for effective IPF therapy, a number of new drugs are now being evaluated in clinical trials. Interestingly, these drug candidates are targeting three pivotal hypothesis of IPF pathophysiology: fibroblasts, ECM, and the immune system.

Other novel target candidates have been recently revealed, showing once more that affecting collagen metabolism might serve as a mechanism to prevent continuous ECM remodeling. That is the case of FK506-binding protein 10 (FKBP10), a collagen chaperone, increased in IPF, and critical for collagen-1 secretion (Staab-Weijnitz et al., 2015), a potential novel target in IPF that deserve further evaluation. Recently, treatment with human recombinant Pentraxin 2, a monocyte regulator, showed in a phase 2, randomized, double blind, placebo-controlled trial a slower decline in lung function over 28 weeks, - uncovering a novel therapy for IPF patients (Raghu et al., 2018; van den Blink et al., 2016).

Remarkable efforts form basic, translational and clinical scientists are coming to light in an era of growing biomarkers and treatments for IPF. In which, biomarker-driven personalized medicine, and combination therapies might be required to stop progression, or in best case to reverse disease.

5. References

Allen, R. J., Porte, J., Braybrooke, R., Flores, C., Fingerlin, T. E., Oldham, J. M., Guillen-Guio, B., Ma, S. F., Okamoto, T., John, A. E., et al. (2017). Genetic variants associated with susceptibility to idiopathic pulmonary fibrosis in people of European ancestry: a genome-wide association study. *Lancet Respir Med*, 5 (11): 869-880. doi: 10.1016/S2213-2600(17)30387-9.

Arase, Y., Suzuki, F., Suzuki, Y., Akuta, N., Kobayashi, M., Kawamura, Y., Yatsuji, H., Sezaki, H., Hosaka, T., Hirakawa, M., et al. (2008). Hepatitis C virus enhances incidence of idiopathic pulmonary fibrosis. *World J Gastroenterol*, 14 (38): 5880-6.

Araya, J., Kojima, J., Takasaka, N., Ito, S., Fujii, S., Hara, H., Yanagisawa, H., Kobayashi, K., Tsurushige, C., Kawaishi, M., et al. (2013). Insufficient autophagy in idiopathic pulmonary fibrosis. *Am J Physiol Lung Cell Mol Physiol*, 304 (1): L56-69. doi: 10.1152/ajplung.00213.2012.

Barkauskas, C. E. & Noble, P. W. (2014). Cellular mechanisms of tissue fibrosis. 7. New insights into the cellular mechanisms of pulmonary fibrosis. *Am J Physiol Cell Physiol*, 306 (11): C987-96. doi: 10.1152/ajpcell.00321.2013.

Barre-Sinoussi, F. & Montagutelli, X. (2015). Animal models are essential to biological research: issues and perspectives. *Future Sci OA*, 1 (4): FSO63. doi: 10.4155/fso.15.63.

Bauer, Y., Tedrow, J., de Bernard, S., Birker-Robaczewska, M., Gibson, K. F., Guardela, B. J., Hess, P., Klenk, A., Lindell, K. O., Poirey, S., et al. (2015). A novel genomic signature with translational significance for human idiopathic pulmonary fibrosis. *Am J Respir Cell Mol Biol*, 52 (2): 217-31. doi: 10.1165/rcmb.2013-0310OC.

Bauer, Y., White, E. S., de Bernard, S., Cornelisse, P., Leconte, I., Morganti, A., Roux, S. & Nayler, O. (2017). MMP-7 is a predictive biomarker of disease progression in patients with idiopathic pulmonary fibrosis. *ERJ Open Res*, 3 (1). doi: 10.1183/23120541.00074-2016.

Baumgartner, K. B., Samet, J. M., Stidley, C. A., Colby, T. V. & Waldron, J. A. (1997). Cigarette smoking: a risk factor for idiopathic pulmonary fibrosis. *Am J Respir Crit Care Med*, 155 (1): 242-8. doi: 10.1164/ajrccm.155.1.9001319.

Baumgartner, K. B., Samet, J. M., Coultas, D. B., Stidley, C. A., Hunt, W. C., Colby, T. V. & Waldron, J. A. (2000). Occupational and environmental risk factors for idiopathic pulmonary fibrosis: a multicenter case-control study. Collaborating Centers. *Am J Epidemiol*, 152 (4): 307-15.

Behr, J. (2013). Evidence-based treatment strategies in idiopathic pulmonary fibrosis. *Eur Respir Rev*, 22 (128): 163-8. doi: 10.1183/09059180.00001013.

Bolanos, A. L., Milla, C. M., Lira, J. C., Ramirez, R., Checa, M., Barrera, L., Garcia-Alvarez, J., Carbajal, V., Becerril, C., Gaxiola, M., et al. (2012). Role of Sonic Hedgehog in idiopathic pulmonary fibrosis. *Am J Physiol Lung Cell Mol Physiol*, 303 (11): L978-90. doi: 10.1152/ajplung.00184.2012.

Bruss, M. L., Margolin, S. B. & Giri, S. N. (2004). Pharmacokinetics of orally administered pirfenidone in male and female beagles. *J Vet Pharmacol Ther*, 27 (5): 361-7. doi: 10.1111/j.1365-2885.2004.00612.x.

Bruss, M. L., Stanley, S. D., Margolin, S. B. & Giri, S. N. (2008). Pharmacokinetics and metabolism of intravenous pirfenidone in sheep. *Biopharm Drug Dispos*, 29 (2): 119-26. doi: 10.1002/bdd.595.

Bueno, M., Lai, Y. C., Romero, Y., Brands, J., St Croix, C. M., Kamga, C., Corey, C., Herazo-Maya, J. D., Sembrat, J., Lee, J. S., et al. (2015). PINK1 deficiency impairs mitochondrial homeostasis and promotes lung fibrosis. *J Clin Invest*, 125 (2): 521-38. doi: 10.1172/JCI74942.

Camelo, A., Dunmore, R., Sleeman, M. A. & Clarke, D. L. (2014). The epithelium in idiopathic pulmonary fibrosis: breaking the barrier. *Front Pharmacol*, 4: 173. doi: 10.3389/fphar.2013.00173.

Carrington, R., Jordan, S., Pitchford, S. C. & Page, C. P. (2018). Use of animal models in IPF research. *Pulm Pharmacol Ther*, 51: 73-78. doi: 10.1016/j.pupt.2018.07.002.

Catane, R., Schwade, J. G., Turrisi, A. T., 3rd, Webber, B. L. & Muggia, F. M. (1979). Pulmonary toxicity after radiation and bleomycin: a review. *Int J Radiat Oncol Biol Phys*, 5 (9): 1513-8.

Cavazza, A., Rossi, G., Carbonelli, C., Spaggiari, L., Paci, M. & Roggeri, A. (2010). The role of histology in idiopathic pulmonary fibrosis: an update. *Respir Med*, 104 Suppl 1: S11-22. doi: 10.1016/j.rmed.2010.03.013.

Christensen, P. J., Goodman, R. E., Pastoriza, L., Moore, B. & Toews, G. B. (1999). Induction of lung fibrosis in the mouse by intratracheal instillation of fluorescein isothiocyanate is not T-cell-dependent. *Am J Pathol*, 155 (5): 1773-9. doi: 10.1016/S0002-9440(10)65493-4.

Claussen, C. A. & Long, E. C. (1999). Nucleic Acid recognition by metal complexes of bleomycin. *Chem Rev*, 99 (9): 2797-816.

Collard, H. R., Calfee, C. S., Wolters, P. J., Song, J. W., Hong, S. B., Brady, S., Ishizaka, A., Jones, K. D., King, T. E., Jr., Matthay, M. A., et al. (2010). Plasma biomarker profiles in acute exacerbation of idiopathic pulmonary fibrosis. *Am J Physiol Lung Cell Mol Physiol*, 299 (1): L3-7. doi: 10.1152/ajplung.90637.2008.

Cool, C. D., Groshong, S. D., Rai, P. R., Henson, P. M., Stewart, J. S. & Brown, K. K. (2006). Fibroblast foci are not discrete sites of lung injury or repair: the fibroblast reticulum. *Am J Respir Crit Care Med*, 174 (6): 654-8. doi: 10.1164/rccm.200602-205OC.

Cottin, V. & Cordier, J. F. (2012). Velcro crackles: the key for early diagnosis of idiopathic pulmonary fibrosis? *Eur Respir J*, 40 (3): 519-21. doi: 10.1183/09031936.00001612.

Davis, G. S., Leslie, K. O. & Hemenway, D. R. (1998). Silicosis in mice: effects of dose, time, and genetic strain. *J Environ Pathol Toxicol Oncol*, 17 (2): 81-97.

Degryse, A. L., Tanjore, H., Xu, X. C., Polosukhin, V. V., Jones, B. R., McMahon, F. B., Gleaves, L. A., Blackwell, T. S. & Lawson, W. E. (2010). Repetitive intratracheal bleomycin models several features of idiopathic pulmonary fibrosis. *Am J Physiol Lung Cell Mol Physiol*, 299 (4): L442-52. doi: 10.1152/ajplung.00026.2010.

Desai, O., Winkler, J., Minasyan, M. & Herzog, E. L. (2018). The Role of Immune and Inflammatory Cells in Idiopathic Pulmonary Fibrosis. *Front Med (Lausanne)*, 5: 43. doi: 10.3389/fmed.2018.00043.

Drakopanagiotakis, F., Wujak, L., Wygrecka, M. & Markart, P. (2018). Biomarkers in idiopathic pulmonary fibrosis. *Matrix Biol*, 68-69: 404-421. doi: 10.1016/j.matbio.2018.01.023.

Epaud, R., Delestrain, C., Louha, M., Simon, S., Fanen, P. & Tazi, A. (2014). Combined pulmonary fibrosis and emphysema syndrome associated with ABCA3 mutations. *Eur Respir J*, 43 (2): 638-41. doi: 10.1183/09031936.00145213.

Erbes, R., Schaberg, T. & Loddenkemper, R. (1997). Lung function tests in patients with idiopathic pulmonary fibrosis. Are they helpful for predicting outcome? *Chest*, 111 (1): 51-7.

Evans, W. E., Yee, G. C., Crom, W. R., Pratt, C. B. & Green, A. A. (1982). Clinical pharmacology of bleomycin and cisplatin. *Drug Intell Clin Pharm*, 16 (6): 448-58.

Fernandez, I. E. & Eickelberg, O. (2012). The impact of TGF-beta on lung fibrosis: from targeting to biomarkers. *Proc Am Thorac Soc*, 9 (3): 111-6. doi: 10.1513/pats.201203-023AW.

Fernandez, I. E., Amarie, O. V., Mutze, K., Konigshoff, M., Yildirim, A. O. & Eickelberg, O. (2016a). Systematic phenotyping and correlation of biomarkers with lung function and histology in lung fibrosis. *Am J Physiol Lung Cell Mol Physiol*, 310 (10): L919-27. doi: 10.1152/ajplung.00183.2015.

Fernandez, I. E., Greiffo, F. R., Frankenberger, M., Bandres, J., Heinzelmann, K., Neurohr, C., Hatz, R., Hartl, D., Behr, J. & Eickelberg, O. (2016b). Peripheral blood myeloid-derived suppressor cells reflect disease status in idiopathic pulmonary fibrosis. *Eur Respir J*, 48 (4): 1171-1183. doi: 10.1183/13993003.01826-2015.

Fingerlin, T. E., Murphy, E., Zhang, W., Peljto, A. L., Brown, K. K., Steele, M. P., Loyd, J. E., Cosgrove, G. P., Lynch, D., Groshong, S., et al. (2013). Genome-wide association study identifies multiple susceptibility loci for pulmonary fibrosis. *Nat Genet*, 45 (6): 613-20. doi: 10.1038/ng.2609.

Flaherty, K. R., Fell, C. D., Huggins, J. T., Nunes, H., Sussman, R., Valenzuela, C., Petzinger, U., Stauffer, J. L., Gilberg, F., Bengus, M., et al. (2018). Safety of nintedanib added to pirfenidone treatment for idiopathic pulmonary fibrosis. *Eur Respir J*, 52 (2). doi: 10.1183/13993003.00230-2018.

Giri, S. N., Wang, Q., Xie, Y., Lango, J., Morin, D., Margolin, S. B. & Buckpitt, A. R. (2002). Pharmacokinetics and metabolism of a novel antifibrotic drug pirfenidone, in mice following intravenous administration. *Biopharm Drug Dispos*, 23 (5): 203-11. doi: 10.1002/bdd.311.

Greene, K. E., King, T. E., Jr., Kuroki, Y., Bucher-Bartelson, B., Hunninghake, G. W., Newman, L. S., Nagae, H. & Mason, R. J. (2002). Serum surfactant proteins-A and -D as biomarkers in idiopathic pulmonary fibrosis. *Eur Respir J*, 19 (3): 439-46.

Haston, C. K. & Travis, E. L. (1997). Murine susceptibility to radiation-induced pulmonary fibrosis is influenced by a genetic factor implicated in susceptibility to bleomycin-induced pulmonary fibrosis. *Cancer Res*, 57 (23): 5286-91.

Hata, R. & Senoo, H. (1989). L-ascorbic acid 2-phosphate stimulates collagen accumulation, cell proliferation, and formation of a three-dimensional tissuelike substance by skin fibroblasts. *J Cell Physiol*, 138 (1): 8-16. doi: 10.1002/jcp.1041380103.

Hu, B., Wu, Z., Bai, D., Liu, T., Ullenbruch, M. R. & Phan, S. H. (2015). Mesenchymal deficiency of Notch1 attenuates bleomycin-induced pulmonary fibrosis. *Am J Pathol*, 185 (11): 3066-75. doi: 10.1016/j.ajpath.2015.07.014.

Hunninghake, G. M., Hatabu, H., Okajima, Y., Gao, W., Dupuis, J., Latourelle, J. C., Nishino, M., Araki, T., Zazueta, O. E., Kurugol, S., et al. (2013). MUC5B promoter polymorphism and interstitial lung abnormalities. *N Engl J Med*, 368 (23): 2192-200. doi: 10.1056/NEJMoa1216076.

Hutchinson, J., Fogarty, A., Hubbard, R. & McKeever, T. (2015). Global incidence and mortality of idiopathic pulmonary fibrosis: a systematic review. *Eur Respir J*, 46 (3): 795-806. doi: 10.1183/09031936.00185114.

Idiopathic Pulmonary Fibrosis Clinical Research, N., Raghu, G., Anstrom, K. J., King, T. E., Jr., Lasky, J. A. & Martinez, F. J. (2012). Prednisone, azathioprine, and N-acetylcysteine for pulmonary fibrosis. *N Engl J Med*, 366 (21): 1968-77. doi: 10.1056/NEJMoa1113354.

Jenkins, R. G., Simpson, J. K., Saini, G., Bentley, J. H., Russell, A. M., Braybrooke, R., Molyneaux, P. L., McKeever, T. M., Wells, A. U., Flynn, A., et al. (2015). Longitudinal change in collagen degradation biomarkers in idiopathic pulmonary fibrosis: an analysis from the prospective, multicentre PROFILE study. *Lancet Respir Med*, 3 (6): 462-72. doi: 10.1016/S2213-2600(15)00048-X.

Jenkins, R. G., Moore, B. B., Chambers, R. C., Eickelberg, O., Konigshoff, M., Kolb, M., Laurent, G. J., Nanthakumar, C. B., Olman, M. A., Pardo, A., et al. (2017). An Official American Thoracic Society Workshop Report: Use of Animal Models for the Preclinical Assessment of Potential Therapies for Pulmonary Fibrosis. *Am J Respir Cell Mol Biol*, 56 (5): 667-679. doi: 10.1165/rcmb.2017-0096ST.

Jules-Elysee, K. & White, D. A. (1990). Bleomycin-induced pulmonary toxicity. *Clin Chest Med*, 11 (1): 1-20.

Kanematsu, T., Kitaichi, M., Nishimura, K., Nagai, S. & Izumi, T. (1994). Clubbing of the fingers and smooth-muscle proliferation in fibrotic changes in the lung in patients with idiopathic pulmonary fibrosis. *Chest*, 105 (2): 339-42.

Kang, Y. P., Lee, S. B., Lee, J. M., Kim, H. M., Hong, J. Y., Lee, W. J., Choi, C. W., Shin, H. K., Kim, D. J., Koh, E. S., et al. (2016). Metabolic Profiling Regarding Pathogenesis of Idiopathic Pulmonary Fibrosis. *J Proteome Res*, 15 (5): 1717-24. doi: 10.1021/acs.jproteome.6b00156.

Karimi-Shah, B. A. & Chowdhury, B. A. (2015). Forced vital capacity in idiopathic pulmonary fibrosis--FDA review of pirfenidone and nintedanib. *N Engl J Med*, 372 (13): 1189-91. doi: 10.1056/NEJMp1500526.

Kendall, R. T. & Feghali-Bostwick, C. A. (2014). Fibroblasts in fibrosis: novel roles and mediators. *Front Pharmacol*, 5: 123. doi: 10.3389/fphar.2014.00123.

King, T. E., Jr., Pardo, A. & Selman, M. (2011). Idiopathic pulmonary fibrosis. *Lancet*, 378 (9807): 1949-61. doi: 10.1016/S0140-6736(11)60052-4.

King, T. E., Jr., Bradford, W. Z., Castro-Bernardini, S., Fagan, E. A., Glaspole, I., Glassberg, M. K., Gorina, E., Hopkins, P. M., Kardatzke, D., Lancaster, L., et al. (2014). A phase 3 trial of pirfenidone in patients with idiopathic pulmonary fibrosis. *N Engl J Med*, 370 (22): 2083-92. doi: 10.1056/NEJMoa1402582.

Knuppel, L., Ishikawa, Y., Aichler, M., Heinzelmann, K., Hatz, R., Behr, J., Walch, A., Bachinger, H. P., Eickelberg, O. & Staab-Weijnitz, C. A. (2017). A Novel Antifibrotic Mechanism of Nintedanib and Pirfenidone. Inhibition of Collagen Fibril Assembly. *Am J Respir Cell Mol Biol*, 57 (1): 77-90. doi: 10.1165/rcmb.2016-0217OC.

Kolb, M., Margetts, P. J., Anthony, D. C., Pitossi, F. & Gauldie, J. (2001). Transient expression of IL-1beta induces acute lung injury and chronic repair leading to pulmonary fibrosis. *J Clin Invest*, 107 (12): 1529-36. doi: 10.1172/JCI12568.

Konigshoff, M., Kramer, M., Balsara, N., Wilhelm, J., Amarie, O. V., Jahn, A., Rose, F., Fink, L., Seeger, W., Schaefer, L., et al. (2009). WNT1-inducible signaling protein-1 mediates pulmonary fibrosis in mice and is upregulated in humans with idiopathic pulmonary fibrosis. *J Clin Invest*, 119 (4): 772-87. doi: 10.1172/JCI33950.

Korfei, M., Ruppert, C., Mahavadi, P., Henneke, I., Markart, P., Koch, M., Lang, G., Fink, L., Bohle, R. M., Seeger, W., et al. (2008). Epithelial endoplasmic reticulum stress and apoptosis in sporadic idiopathic pulmonary fibrosis. *Am J Respir Crit Care Med*, 178 (8): 838-46. doi: 10.1164/rccm.200802-313OC.

Kotsianidis, I., Nakou, E., Bouchliou, I., Tzouvelekis, A., Spanoudakis, E., Steiropoulos, P., Sotiriou, I., Aidinis, V., Margaritis, D., Tsatalas, C., et al. (2009). Global impairment of CD4+CD25+FOXP3+ regulatory T cells in idiopathic pulmonary fibrosis. *Am J Respir Crit Care Med*, 179 (12): 1121-30. doi: 10.1164/rccm.200812-1936OC.

Kottmann, R. M., Kulkarni, A. A., Smolnycki, K. A., Lyda, E., Dahanayake, T., Salibi, R., Honnons, S., Jones, C., Isern, N. G., Hu, J. Z., et al. (2012). Lactic acid is elevated in idiopathic pulmonary fibrosis and induces myofibroblast differentiation via pH-dependent activation of transforming growth factor-beta. *Am J Respir Crit Care Med*, 186 (8): 740-51. doi: 10.1164/rccm.201201-0084OC.

Kropski, J. A., Pritchett, J. M., Zoz, D. F., Crossno, P. F., Markin, C., Garnett, E. T., Degryse, A. L., Mitchell, D. B., Polosukhin, V. V., Rickman, O. B., et al. (2015). Extensive phenotyping of individuals at risk for familial interstitial pneumonia reveals clues to the pathogenesis of interstitial lung disease. *Am J Respir Crit Care Med*, 191 (4): 417-26. doi: 10.1164/rccm.201406-1162OC.

Kropski, J. A., Young, L. R., Cogan, J. D., Mitchell, D. B., Lancaster, L. H., Worrell, J. A., Markin, C., Liu, N., Mason, W. R., Fingerlin, T. E., et al. (2017). Genetic Evaluation and Testing of Patients and Families with Idiopathic Pulmonary Fibrosis. *Am J Respir Crit Care Med*, 195 (11): 1423-1428. doi: 10.1164/rccm.201609-1820PP.

Lai, D. M., Shu, Q. & Fan, J. (2016). The origin and role of innate lymphoid cells in the lung. *Mil Med Res*, 3: 25. doi: 10.1186/s40779-016-0093-2.

Lawson, W. E., Crossno, P. F., Polosukhin, V. V., Roldan, J., Cheng, D. S., Lane, K. B., Blackwell, T. R., Xu, C., Markin, C., Ware, L. B., et al. (2008). Endoplasmic reticulum stress in alveolar epithelial cells is prominent in IPF: association with altered surfactant protein processing and herpesvirus infection. *Am J Physiol Lung Cell Mol Physiol*, 294 (6): L1119-26. doi: 10.1152/ajplung.00382.2007.

Lee, J. M., Yoshida, M., Kim, M. S., Lee, J. H., Baek, A. R., Jang, A. S., Kim, D. J., Minagawa, S., Chin, S. S., Park, C. S., et al. (2018). Involvement of Alveolar Epithelial Cell Necroptosis in IPF Pathogenesis. *Am J Respir Cell Mol Biol*. doi: 10.1165/rcmb.2017-0034OC.

Lee, J. S. (2014). The Role of Gastroesophageal Reflux and Microaspiration in Idiopathic Pulmonary Fibrosis. *Clin Pulm Med*, 21 (2): 81-85.

Lehmann, M., Korfei, M., Mutze, K., Klee, S., Skronska-Wasek, W., Alsafadi, H. N., Ota, C., Costa, R., Schiller, H. B., Lindner, M., et al. (2017). Senolytic drugs target alveolar epithelial cell function and attenuate experimental lung fibrosis ex vivo. *Eur Respir J*, 50 (2). doi: 10.1183/13993003.02367-2016.

Lehtonen, S. T., Veijola, A., Karvonen, H., Lappi-Blanco, E., Sormunen, R., Korpela, S., Zagai, U., Skold, M. C. & Kaarteenaho, R. (2016). Pirfenidone and nintedanib modulate properties of fibroblasts and myofibroblasts in idiopathic pulmonary fibrosis. *Respir Res*, 17: 14. doi: 10.1186/s12931-016-0328-5.

Ley, B., Brown, K. K. & Collard, H. R. (2014). Molecular biomarkers in idiopathic pulmonary fibrosis. *Am J Physiol Lung Cell Mol Physiol*, 307 (9): L681-91. doi: 10.1152/ajplung.00014.2014.

Li, F. J., Surolia, R., Li, H., Wang, Z., Kulkarni, T., Liu, G., de Andrade, J. A., Kass, D. J., Thannickal, V. J., Duncan, S. R., et al. (2017). Autoimmunity to Vimentin Is

Associated with Outcomes of Patients with Idiopathic Pulmonary Fibrosis. *J Immunol*, 199 (5): 1596-1605. doi: 10.4049/jimmunol.1700473.

Maher, T. M., Oballa, E., Simpson, J. K., Porte, J., Habgood, A., Fahy, W. A., Flynn, A., Molyneaux, P. L., Braybrooke, R., Divyateja, H., et al. (2017). An epithelial biomarker signature for idiopathic pulmonary fibrosis: an analysis from the multicentre PROFILE cohort study. *Lancet Respir Med*, 5 (12): 946-955. doi: 10.1016/S2213-2600(17)30430-7.

Moeller, A., Gilpin, S. E., Ask, K., Cox, G., Cook, D., Gauldie, J., Margetts, P. J., Farkas, L., Dobranowski, J., Boylan, C., et al. (2009). Circulating fibrocytes are an indicator of poor prognosis in idiopathic pulmonary fibrosis. *Am J Respir Crit Care Med*, 179 (7): 588-94. doi: 10.1164/rccm.200810-1534OC.

Moore, B. B. & Hogaboam, C. M. (2008). Murine models of pulmonary fibrosis. *Am J Physiol Lung Cell Mol Physiol*, 294 (2): L152-60. doi: 10.1152/ajplung.00313.2007.

Murad, S., Tajima, S., Johnson, G. R., Sivarajah, S. & Pinnell, S. R. (1983). Collagen synthesis in cultured human skin fibroblasts: effect of ascorbic acid and its analogs. *J Invest Dermatol*, 81 (2): 158-62.

Nalysnyk, L., Cid-Ruzafa, J., Rotella, P. & Esser, D. (2012). Incidence and prevalence of idiopathic pulmonary fibrosis: review of the literature. *Eur Respir Rev*, 21 (126): 355-61. doi: 10.1183/09059180.00002512.

Neighbors, M., Cabanski, C. R., Ramalingam, T. R., Sheng, X. R., Tew, G. W., Gu, C., Jia, G., Peng, K., Ray, J. M., Ley, B., et al. (2018). Prognostic and predictive biomarkers for patients with idiopathic pulmonary fibrosis treated with pirfenidone: post-hoc assessment of the CAPACITY and ASCEND trials. *Lancet Respir Med*, 6 (8): 615-626. doi: 10.1016/S2213-2600(18)30185-1.

Noble, P. W., Albera, C., Bradford, W. Z., Costabel, U., Glassberg, M. K., Kardatzke, D., King, T. E., Jr., Lancaster, L., Sahn, S. A., Szwarcberg, J., et al. (2011). Pirfenidone in patients with idiopathic pulmonary fibrosis (CAPACITY): two randomised trials. *Lancet*, 377 (9779): 1760-9. doi: 10.1016/S0140-6736(11)60405-4.

Nogee, L. M., Dunbar, A. E., 3rd, Wert, S. E., Askin, F., Hamvas, A. & Whitsett, J. A. (2001). A mutation in the surfactant protein C gene associated with familial interstitial lung disease. *N Engl J Med*, 344 (8): 573-9. doi: 10.1056/NEJM200102223440805.

Noth, I., Zhang, Y., Ma, S. F., Flores, C., Barber, M., Huang, Y., Broderick, S. M., Wade, M. S., Hysi, P., Scuirba, J., et al. (2013). Genetic variants associated with idiopathic pulmonary fibrosis susceptibility and mortality: a genome-wide association study. *Lancet Respir Med*, 1 (4): 309-317. doi: 10.1016/S2213-2600(13)70045-6.

Okuda, R., Matsushima, H., Aoshiba, K., Oba, T., Kawabe, R., Honda, K. & Amano, M. (2015). Soluble intercellular adhesion molecule-1 for stable and acute phases of idiopathic pulmonary fibrosis. *Springerplus*, 4: 657. doi: 10.1186/s40064-015-1455-z.

Oldham, J. M., Ma, S. F., Martinez, F. J., Anstrom, K. J., Raghu, G., Schwartz, D. A., Valenzi, E., Witt, L., Lee, C., Vij, R., et al. (2015). TOLLIP, MUC5B, and the Response to N-Acetylcysteine among Individuals with Idiopathic Pulmonary Fibrosis. *Am J Respir Crit Care Med*, 192 (12): 1475-82. doi: 10.1164/rccm.201505-1010OC.

Patel, A. S., Lin, L., Geyer, A., Haspel, J. A., An, C. H., Cao, J., Rosas, I. O. & Morse, D. (2012). Autophagy in idiopathic pulmonary fibrosis. *PLoS One*, 7 (7): e41394. doi: 10.1371/journal.pone.0041394.

Peljto, A. L., Zhang, Y., Fingerlin, T. E., Ma, S. F., Garcia, J. G., Richards, T. J., Silveira, L. J., Lindell, K. O., Steele, M. P., Loyd, J. E., et al. (2013). Association between the

MUC5B promoter polymorphism and survival in patients with idiopathic pulmonary fibrosis. *JAMA*, 309 (21): 2232-9. doi: 10.1001/jama.2013.5827.

Peng, R., Sridhar, S., Tyagi, G., Phillips, J. E., Garrido, R., Harris, P., Burns, L., Renteria, L., Woods, J., Chen, L., et al. (2013). Bleomycin induces molecular changes directly relevant to idiopathic pulmonary fibrosis: a model for "active" disease. *PLoS One*, 8 (4): e59348. doi: 10.1371/journal.pone.0059348.

Poletti, V., Ravaglia, C. & Tomassetti, S. (2014). Pirfenidone for the treatment of idiopathic pulmonary fibrosis. *Expert Rev Respir Med*, 8 (5): 539-45. doi: 10.1586/17476348.2014.915750.

Prasse, A., Probst, C., Bargagli, E., Zissel, G., Toews, G. B., Flaherty, K. R., Olschewski, M., Rottoli, P. & Muller-Quernheim, J. (2009). Serum CC-chemokine ligand 18 concentration predicts outcome in idiopathic pulmonary fibrosis. *Am J Respir Crit Care Med*, 179 (8): 717-23. doi: 10.1164/rccm.200808-1201OC.

Raghu, G., Weycker, D., Edelsberg, J., Bradford, W. Z. & Oster, G. (2006). Incidence and prevalence of idiopathic pulmonary fibrosis. *Am J Respir Crit Care Med*, 174 (7): 810-6. doi: 10.1164/rccm.200602-163OC.

Raghu, G., Collard, H. R., Egan, J. J., Martinez, F. J., Behr, J., Brown, K. K., Colby, T. V., Cordier, J. F., Flaherty, K. R., Lasky, J. A., et al. (2011). An official ATS/ERS/JRS/ALAT statement: idiopathic pulmonary fibrosis: evidence-based guidelines for diagnosis and management. *Am J Respir Crit Care Med*, 183 (6): 788-824. doi: 10.1164/rccm.2009-040GL.

Raghu, G., Chen, S. Y., Yeh, W. S., Maroni, B., Li, Q., Lee, Y. C. & Collard, H. R. (2014). Idiopathic pulmonary fibrosis in US Medicare beneficiaries aged 65 years and older: incidence, prevalence, and survival, 2001-11. *Lancet Respir Med*, 2 (7): 566-72. doi: 10.1016/S2213-2600(14)70101-8.

Raghu, G., Rochwerg, B., Zhang, Y., Garcia, C. A., Azuma, A., Behr, J., Brozek, J. L., Collard, H. R., Cunningham, W., Homma, S., et al. (2015). An Official ATS/ERS/JRS/ALAT Clinical Practice Guideline: Treatment of Idiopathic Pulmonary Fibrosis. An Update of the 2011 Clinical Practice Guideline. *Am J Respir Crit Care Med*, 192 (2): e3-19. doi: 10.1164/rccm.201506-1063ST.

Raghu, G., van den Blink, B., Hamblin, M. J., Brown, A. W., Golden, J. A., Ho, L. A., Wijsenbeek, M. S., Vasakova, M., Pesci, A., Antin-Ozerkis, D. E., et al. (2018). Effect of Recombinant Human Pentraxin 2 vs Placebo on Change in Forced Vital Capacity in Patients With Idiopathic Pulmonary Fibrosis: A Randomized Clinical Trial. *JAMA*, 319 (22): 2299-2307. doi: 10.1001/jama.2018.6129.

Rajchgot, J., Stanbrook, M. B. & Anand, A. (2018). Combination Nintedanib and Pirfenidone for Treatment of Idiopathic Pulmonary Fibrosis. *Am J Respir Crit Care Med*. doi: 10.1164/rccm.201805-0954LE.

Richards, T. J., Kaminski, N., Baribaud, F., Flavin, S., Brodmerkel, C., Horowitz, D., Li, K., Choi, J., Vuga, L. J., Lindell, K. O., et al. (2012). Peripheral blood proteins predict mortality in idiopathic pulmonary fibrosis. *Am J Respir Crit Care Med*, 185 (1): 67-76. doi: 10.1164/rccm.201101-0058OC.

Richeldi, L., du Bois, R. M., Raghu, G., Azuma, A., Brown, K. K., Costabel, U., Cottin, V., Flaherty, K. R., Hansell, D. M., Inoue, Y., et al. (2014). Efficacy and safety of nintedanib in idiopathic pulmonary fibrosis. *N Engl J Med*, 370 (22): 2071-82. doi: 10.1056/NEJMoa1402584.

Riteau, N., Gasse, P., Fauconnier, L., Gombault, A., Couegnat, M., Fick, L., Kanellopoulos, J., Quesniaux, V. F., Marchand-Adam, S., Crestani, B., et al. (2010). Extracellular

ATP is a danger signal activating P2X7 receptor in lung inflammation and fibrosis. *Am J Respir Crit Care Med*, 182 (6): 774-83. doi: 10.1164/rccm.201003-0359OC.

Rosas, I. O., Richards, T. J., Konishi, K., Zhang, Y., Gibson, K., Lokshin, A. E., Lindell, K. O., Cisneros, J., Macdonald, S. D., Pardo, A., et al. (2008). MMP1 and MMP7 as potential peripheral blood biomarkers in idiopathic pulmonary fibrosis. *PLoS Med*, 5 (4): e93. doi: 10.1371/journal.pmed.0050093.

Sack, C. S., Doney, B. C., Podolanczuk, A. J., Hooper, L. G., Seixas, N. S., Hoffman, E. A., Kawut, S. M., Vedal, S., Raghu, G., Barr, R. G., et al. (2017). Occupational Exposures and Subclinical Interstitial Lung Disease. The MESA (Multi-Ethnic Study of Atherosclerosis) Air and Lung Studies. *Am J Respir Crit Care Med*, 196 (8): 1031-1039. doi: 10.1164/rccm.201612-2431OC.

Schaefer, C. J., Ruhrmund, D. W., Pan, L., Seiwert, S. D. & Kossen, K. (2011). Antifibrotic activities of pirfenidone in animal models. *Eur Respir Rev*, 20 (120): 85-97. doi: 10.1183/09059180.00001111.

Schiller, H. B., Fernandez, I. E., Burgstaller, G., Schaab, C., Scheltema, R. A., Schwarzmayr, T., Strom, T. M., Eickelberg, O. & Mann, M. (2015). Time- and compartment-resolved proteome profiling of the extracellular niche in lung injury and repair. *Mol Syst Biol*, 11 (7): 819. doi: 10.15252/msb.20156123.

Seibold, M. A., Wise, A. L., Speer, M. C., Steele, M. P., Brown, K. K., Loyd, J. E., Fingerlin, T. E., Zhang, W., Gudmundsson, G., Groshong, S. D., et al. (2011). A common MUC5B promoter polymorphism and pulmonary fibrosis. *N Engl J Med*, 364 (16): 1503-12. doi: 10.1056/NEJMoa1013660.

Selman, M., Pardo, A. & Kaminski, N. (2008). Idiopathic pulmonary fibrosis: aberrant recapitulation of developmental programs? *PLoS Med*, 5 (3): e62. doi: 10.1371/journal.pmed.0050062.

Shi, S., Wu, J., Chen, H., Chen, H., Wu, J. & Zeng, F. (2007). Single- and multiple-dose pharmacokinetics of pirfenidone, an antifibrotic agent, in healthy Chinese volunteers. *J Clin Pharmacol*, 47 (10): 1268-76. doi: 10.1177/0091270007304104.

Sime, P. J., Xing, Z., Graham, F. L., Csaky, K. G. & Gauldie, J. (1997). Adenovector-mediated gene transfer of active transforming growth factor-beta1 induces prolonged severe fibrosis in rat lung. *J Clin Invest*, 100 (4): 768-76. doi: 10.1172/JCI119590.

Simonian, P. L., Roark, C. L., Wehrmann, F., Lanham, A. K., Diaz del Valle, F., Born, W. K., O'Brien, R. L. & Fontenot, A. P. (2009). Th17-polarized immune response in a murine model of hypersensitivity pneumonitis and lung fibrosis. *J Immunol*, 182 (1): 657-65.

Simonian, P. L., Wehrmann, F., Roark, C. L., Born, W. K., O'Brien, R. L. & Fontenot, A. P. (2010). gammadelta T cells protect against lung fibrosis via IL-22. *J Exp Med*, 207 (10): 2239-53. doi: 10.1084/jem.20100061.

Song, J. W., Do, K. H., Jang, S. J., Colby, T. V., Han, S. & Kim, D. S. (2013). Blood biomarkers MMP-7 and SP-A: predictors of outcome in idiopathic pulmonary fibrosis. *Chest*, 143 (5): 1422-1429. doi: 10.1378/chest.11-2735.

Spagnolo, P., Del Giovane, C., Luppi, F., Cerri, S., Balduzzi, S., Walters, E. H., D'Amico, R. & Richeldi, L. (2010). Non-steroid agents for idiopathic pulmonary fibrosis. *Cochrane Database Syst Rev* (9): CD003134. doi: 10.1002/14651858.CD003134.pub2.

Staab-Weijnitz, C. A., Fernandez, I. E., Knuppel, L., Maul, J., Heinzelmann, K., Juan-Guardela, B. M., Hennen, E., Preissler, G., Winter, H., Neurohr, C., et al. (2015).

FK506-Binding Protein 10, a Potential Novel Drug Target for Idiopathic Pulmonary Fibrosis. *Am J Respir Crit Care Med*, 192 (4): 455-67. doi: 10.1164/rccm.201412-2233OC.

Stuart, B. D., Choi, J., Zaidi, S., Xing, C., Holohan, B., Chen, R., Choi, M., Dharwadkar, P., Torres, F., Girod, C. E., et al. (2015). Exome sequencing links mutations in PARN and RTEL1 with familial pulmonary fibrosis and telomere shortening. *Nat Genet*, 47 (5): 512-7. doi: 10.1038/ng.3278.

Sun, N., Fernandez, I. E., Wei, M., Wu, Y., Aichler, M., Eickelberg, O. & A., W. (2015). Pharmacokinetic and pharmacometabolomic study of pirfenidone in normal mice tissues using high mass resolution MALDI-FTICR-mass spectrometry imaging. *Histochemistry and Cell Biology*.

Sun, N., Fernandez, I. E., Wei, M., Witting, M., Aichler, M., Feuchtinger, A., Burgstaller, G., Verleden, S. E., Schmitt-Kopplin, P., Eickelberg, O., et al. (2018). Pharmacometabolic response to pirfenidone in pulmonary fibrosis detected by MALDI-FTICR-MSI. *Eur Respir J*. doi: 10.1183/13993003.02314-2017.

Tang, Y. W., Johnson, J. E., Browning, P. J., Cruz-Gervis, R. A., Davis, A., Graham, B. S., Brigham, K. L., Oates, J. A., Jr., Loyd, J. E. & Stecenko, A. A. (2003). Herpesvirus DNA is consistently detected in lungs of patients with idiopathic pulmonary fibrosis. *J Clin Microbiol*, 41 (6): 2633-40.

Tashiro, J., Rubio, G. A., Limper, A. H., Williams, K., Elliot, S. J., Ninou, I., Aidinis, V., Tzouvelekis, A. & Glassberg, M. K. (2017). Exploring Animal Models That Resemble Idiopathic Pulmonary Fibrosis. *Front Med (Lausanne)*, 4: 118. doi: 10.3389/fmed.2017.00118.

Togami, K., Kanehira, Y. & Tada, H. (2013). Possible involvement of pirfenidone metabolites in the antifibrotic action of a therapy for idiopathic pulmonary fibrosis. *Biol Pharm Bull*, 36 (10): 1525-7.

Travis, W. D., Costabel, U., Hansell, D. M., King, T. E., Jr., Lynch, D. A., Nicholson, A. G., Ryerson, C. J., Ryu, J. H., Selman, M., Wells, A. U., et al. (2013). An official American Thoracic Society/European Respiratory Society statement: Update of the international multidisciplinary classification of the idiopathic interstitial pneumonias. *Am J Respir Crit Care Med*, 188 (6): 733-48. doi: 10.1164/rccm.201308-1483ST.

Tzouvelekis, A., Herazo-Maya, J. D., Slade, M., Chu, J. H., Deiuliis, G., Ryu, C., Li, Q., Sakamoto, K., Ibarra, G., Pan, H., et al. (2017). Validation of the prognostic value of MMP-7 in idiopathic pulmonary fibrosis. *Respirology*, 22 (3): 486-493. doi: 10.1111/resp.12920.

van den Blink, B., Dillingh, M. R., Ginns, L. C., Morrison, L. D., Moerland, M., Wijsenbeek, M., Trehu, E. G., Bartholmai, B. J. & Burggraaf, J. (2016). Recombinant human pentraxin-2 therapy in patients with idiopathic pulmonary fibrosis: safety, pharmacokinetics and exploratory efficacy. *Eur Respir J*, 47 (3): 889-97. doi: 10.1183/13993003.00850-2015.

Vandamme, T. F. (2014). Use of rodents as models of human diseases. *J Pharm Bioallied Sci*, 6 (1): 2-9. doi: 10.4103/0975-7406.124301.

Wang, Y., Zhao, X., Zhong, J., Chen, Y., Liu, X. & Wang, G. (2006). Simple determination of pirfenidone in rat plasma via high-performance liquid chromatography. *Biomed Chromatogr*, 20 (12): 1375-9. doi: 10.1002/bmc.708.

Washko, G. R., Hunninghake, G. M., Fernandez, I. E., Nishino, M., Okajima, Y., Yamashiro, T., Ross, J. C., Estepar, R. S., Lynch, D. A., Brehm, J. M., et al. (2011). Lung volumes

and emphysema in smokers with interstitial lung abnormalities. N *Engl J Med*, 364 (10): 897-906. doi: 10.1056/NEJMoa1007285.

Wollin, L., Wex, E., Pautsch, A., Schnapp, G., Hostettler, K. E., Stowasser, S. & Kolb, M. (2015). Mode of action of nintedanib in the treatment of idiopathic pulmonary fibrosis. *Eur Respir J*, 45 (5): 1434-45. doi: 10.1183/09031936.00174914.

Wynn, T. A. & Vannella, K. M. (2016). Macrophages in Tissue Repair, Regeneration, and Fibrosis. *Immunity*, 44 (3): 450-462. doi: 10.1016/j.immuni.2016.02.015.

Yokoyama, A., Kondo, K., Nakajima, M., Matsushima, T., Takahashi, T., Nishimura, M., Bando, M., Sugiyama, Y., Totani, Y., Ishizaki, T., et al. (2006). Prognostic value of circulating KL-6 in idiopathic pulmonary fibrosis. *Respirology*, 11 (2): 164-8. doi: 10.1111/j.1440-1843.2006.00834.x.

Zhao, Y. D., Yin, L., Archer, S., Lu, C., Zhao, G., Yao, Y., Wu, L., Hsin, M., Waddell, T. K., Keshavjee, S., et al. (2017). Metabolic heterogeneity of idiopathic pulmonary fibrosis: a metabolomic study. *BMJ Open Respiratory Research*, 4 (1). doi: 10.1136/bmjresp-2017-000183.

Acknowledgments

The work compiled in this thesis becomes a reality only with the help and support of many. It takes a village! Thanks God for showing me the right path, putting me at the right time, with the right people, and giving me the endurance to climb the ladder even higher.

To Prof. Dr. Oliver Eickelberg, this work would have not being possible without your guidance, support and constant advice, from the first until the last day.

I would like to thank Prof. Dr. Jürgen Behr and the committee members, for evaluating my work and participating in my PhD examination.Special thanks go to all collaboration partners and co-authors of the manuscripts part of this thesis.

I am deeply grateful to all of those from the “Eickelberg lab” that came, left, and stayed through all these years, with whom I had the pleasure to work, learn, live and laugh. For the fun and support, deep thanks go to Kathy and Natalia; as well as to Gerald and Claudia. Especial thanks go to Kathy and Adrian for the editing and proofing, even last minute. I owe deep thanks to Daniela, Constanze, Katharina and Markus for the technical assistance during the long days of animal work. It is a great pleasure to thank my team, Flavia and Daniela for sharing all those years of work together and the new members of the growing crew Dibora, Ivette and Valeria. Special thanks to PD Dr. Anne Hilgendorff for her support in the endeavors to come.

Nobody has been more important to me in pursuing my career than my family. To my parents, they developed on me the thirst for learning, and showed me that perseverance and endurance comes from passion. Most importantly, to Malte for being unconditional, keeping me up and supporting every step I take, and of course, to my best gifts, Aleph and Quentin who taught me the true value of life.